12-2009

Live-Load Test and Computer Modeling of a Pre-Cast Concrete Deck, Steel Girder Bridge, and a Cast-in-Place Concrete Box Girder Bridge

Leonardo A. Pockels
Utah State University

LIVE LOAD TEST AND COMPUTER MODELING OF A PRE-CAST CONCRETE DECK STEEL GIRDER BRIDGE AND A CAST-IN-PLACE CONCRETE BOX GIRDER BRIDGE

by

Leonardo Pockels

A thesis submitted in partial fulfillment
of the requirements for the degree

of

MASTER OF SCIENCE

in

Civil and Environmental Engineering

Approved:

_____	_____
Dr. Paul Barr	Dr. Marvin Halling
Major Professor	Committee Member
_____	_____
Dr. James Bay	Dean Byron R. Burnham
Committee Member	Dean of Graduate Studies

UTAH STATE UNIVERSITY
Logan, Utah

2009

ABSTRACT

Live-Load Test and Computer Modeling of a Pre-Cast Concrete Deck, Steel Girder Bridge, and a Cast-in-Place Concrete Box Girder Bridge

by

Leonardo Pockels, Master of Science

Utah State University, 2009

Major Professor: Dr. Paul Barr
Department: Civil and Environmental Engineering

The scheduled replacement of the 8th North Bridge, in Salt Lake City, UT, presented a unique opportunity to test a pre-cast concrete deck, steel girder bridge. A live-load test was performed under the directions of Bridge Diagnostic Inc (BDI) and Utah State University. Six different load paths were chosen to be tested. The recorded data was used to calibrate a finite-element model of this superstructure, which was created using solid, shell, and frame elements. A comparison between the measured and finite-element response was performed and it was determined that the finite-element model replicated the measured results within 3.5% of the actual values.

This model was later used to obtain theoretical live-load distribution factors, which were compared with the AASHTO LRFD Specifications estimations. The analysis was performed for the actual condition of the bridge and the original case of the bridge, which included sidewalks on both sides. The comparison showed that the code over predicted

the behavior of the actual structure by 10%. For the original case, the code's estimation differed by as much as 45% of the theoretical values.

Another opportunity was presented to test the behavior of a cast-in-place concrete box girder bridge in Joaquin County, CA. The Walnut Grove Bridge was tested by BDI at the request of Utah State University. The test was performed with six different load paths and the recorded data was used to calibrate a finite-element model of the structure. The bridge was modeled using shell elements and the supports were modeled using solid elements. The model was shown to replicate the actual behavior of the bridge to within 3% of the measured values.

The calibrated model was then used to calculate the theoretical live-load distribution factors, which allowed a comparison of the results with the AASHTOO LRFD Specifications equations. This analysis was performed for the real conditions of the bridge and a second case where intermediate diaphragms were not included. It was determined that the code's equations estimated the behavior of the interior girder more accurately for the second model (within 10%) than the real model of the bridge (within 20%).

(196 pages)

ACKNOWLEDGMENTS

This investigation was possible thanks to the funding provided by the Utah Transportation Center, through Utah State University. I wish to thank UTC for their financial support. I would also like to give very special thanks to Dr. Paul Barr for allowing me to be part of this research study and for guiding me in the creation of this thesis. His assistance, encouragement, and patience helped me stay motivated and focused throughout the entire process.

I would also like to thank Dr. Marvin W. Halling and Dr. James A. Bay of my graduate committee for their support, assistance, and review of this thesis. I also wish to thank Bridge Diagnostics Inc for providing me with all the information regarding the live-load test performed on the two studied bridges.

Finally I would like to give special thanks to the Dominican Republic Government for granting me a full scholarship and allowing me to obtain a master of science degree in structural engineering, at one of the most recognized universities in this field in the USA.

Leonardo A. Pockels

CONTENTS

Page

LIST OF TABLES

LIST OF FIGURES

CHAPTER 1

INTRODUCTION

1.1 Context

A bridge is a typical structure that is designed to support the traffic loads of vehicles that transit through it. In the designing process of a particular bridge, the engineer has to come up with an efficient structure capable of resisting the live load imposed to it, as well as any present dead load. The dead loads are relatively easy to determine for each member of the structure, since they only depend on the material properties of every structural component on the bridge.

On the other hand, the quantification of the maximum response due to an imposed live load is very complicated to determine. It depends on numerous factors related to the geometric properties of the bridge, the number of girders and structural properties of every component. This complex situation forces the designer to use certain simplifications in the design process. Using a code based equation to estimate the actual behavior of the structures is one of these simplifications. Code based equations were developed to estimate the maximum live load response that will affect every member of the bridge. These equations are very simply to use, but in most cases lead to a greatly overdesigned structure.

Another alternative that could be used in the design of a particular bridge is the implementation of a finite-element analysis. This approach tends to provide more accurate values for the design process. The only problem is that it takes a large amount of time to perform compared to the calculations using the code based equations. Another

disadvantage is that it may reflect some inaccuracy if the final conditions of the bridge are not being taken into consideration in the model elaboration.

This research study focused on the determination of the accuracy of the AASHTO LRFD Specifications (2006) and AAHSTO Standard Specifications (1996) equations applied to a pre-cast concrete deck, steel girder bridge and a cast-in-place concrete box girder bridge. This analysis was done by developing a three-dimensional finite element model from both structures. Theoretical live-load distribution factors were calculated using these models and were compared with the code based calculations. The accuracy of the finite-element models were established by replicating a live-load test that was performed on every structure, and comparing the calculated results with the measured data.

1.2 Live-Load Distribution Factor

The distribution factor is defined as the ratio of the maximum response of an interior or exterior bridge girder over the maximum response of a single, simply supported beam, subjected to the same live load. According to the AASHTO distribution factor method, an individual bridge girder is to be idealized as 1-D beam, and its maximum response, subjected to trucks loads, can be obtained using elementary beam theory. Depending on the load location and bridge geometric properties, each bridge girder will carry different portions of the live load. In order to estimate the lateral distribution of the imposed live load in every girder, two different approaches have been proposed as a result of many studies, the AASHTO Standard Specifications (1996) and the AASHTO LRFD Specifications (2006).

The AASHTO Standard Specifications (1996) is one of the simplest procedures among all the code-based distribution factor equations. However, it usage is limited since it was derived on studies based in non-skewed, simply supported, two-lane bridges. Additionally, it does not differentiate between exterior girders and interior girders. The AASHTO LRFD Specifications (2006) were developed as a result of an intensive research on many different bridges. This study considered many important parameters that were not included in the Standard Specifications such as girder stiffness, span length, girder spacing, continuity and skew. Despite this extensive study, the accuracy of these procedures remains uncertain, since the accuracy of these equations to predict moment distribution for any type of bridge is still questionable. This is why a research study is necessary to investigate the accuracy of these equations on the two type of bridges mentioned in this study.

1.3 Research Objectives

Many goals were intended to be accomplished based on the studies performed on the two bridges. These research objectives are summarized in the following:

- Obtain and analyze experimental data from a live-load test of the two bridges, in order to determine and understand the structural behavior and boundary conditions of a pre-cast concrete deck, steel girder bridge and a cast-in place concrete box girder.
- To create finite-element models that can accurately replicate the real structural behavior of the studied structures. The finite-element models (FEM) needed to be calibrated using the results from the live-load tests.

- To get familiar with the basic steps of a modeling process and estimate the large effort that implies the creation of a finite-element model for complicated structures, such as the two studied bridges.
- To determine theoretical values of live-load distributions factors using the calibrated finite-element models.
- To evaluate the accuracy of the live-load distribution factors equations from AASHTO LRFD Specifications, as they are applied to the two studied bridges. This evaluation will be done by comparing the theoretical values from the models with the calculated values from the code.

1.4 Scope and Organization

The research project was organized and presented in five chapters. Chapter 2 presents a summary of previous studies where a finite-element model was created in order to develop an equation that could estimate the live-load distribution factors or simply to determine the maximum load that a particular bridge would carry.

Chapter 3 presents a detailed description of the 8th North Bridge. It describes the live-load test that was performed on this structure and presents an analysis of the results that were obtained from it. It also outlines the procedure used in the development of the finite-element analysis for this structure and explains how the results from the live-load test were used to calibrate this model. This chapter also describes the AASHTO Standard Specifications (1996) and The AASHTO LRFD Specifications (2006) equations that are used to estimate the live-load distribution factors on a particular bridge. Finally it

presents a detailed comparison between the theoretical values obtained from the finite-element analysis and the calculated values from the code based equations.

Chapter 4 discusses the live-load test that was performed on the Walnut Grove Road undercrossing. It starts by presenting a very detailed description of this structure. It also describes how the live-load test was performed and how the recorded data was analyzed. This chapter also describes the procedure used to create a finite-element model that could accurately replicate the behavior of this type of structure. Finally, theoretical live load distribution factor values of this bridge were obtained through the FEM and were compared with the code based equation results. The accuracy of these equations was evaluated in this comparison.

Finally, Chapter 5 summarizes the results presented in this study and the conclusions that were elaborated through the examination of these results.

CHAPTER 2

LITERATURE REVIEW

In many previous studies, researches have had to utilize a finite-element method either to obtain an equation that could predict the load distribution factors of different types of bridges, or simply to determine the maximum load that a specific bridge could carry. These researches have found this type of method to be very accurate when used properly. Chapter 2 presents a briefly descriptions of some of this studies, in which a finite-element analysis had to be performed in order to accomplish the goals of the investigation. Each article explains the process by which the finite-element analysis was conducted, and how the results obtained from this process were used to complete the research with a significant success.

2.1 Chajes, Mertz, and Comander (1997)

The authors of this article explain how the load limitation that has been posted on many bridges in the United States tends to underestimate the actual load carrying capacity for those bridges. According to the authors, one way of determining the actual load capacity of any bridge is to conduct an experimental live-load test. The authors concentrate on demonstrating how this experimental live-load test can be used to create a simple, but accurate, numerical bridge model and how this model can subsequently be used to determine the load carrying capacity of the tested bridge. The focus bridge that was studied and analyzed in this paper is a steel girder and slab bridge located in Delaware. It has three, simply-supported spans, with nine steel girders.

In order to measure the bridge's capacity, the authors conducted a nondestructive field test, using what is called a diagnostic test. Their intention was to place a specific load, close to the predetermined bridge's capacity, at different locations along the bridge and then measure the response. After the load test, the researches used the measured response to create and develop a finite-element model, which would later be used to estimate the maximum allowable load for the bridge.

To measure the bridge's response to the applied load, reusable strain gages were applied to the bridge to gather the data. Since the larger, middle span controlled the maximum moment, only this span was instrumented. The transducers were attached to all girders at mid-span and in between the end of the girder and the first diaphragm. This latter instrumentation position was done to some selected girders. Most of the transducers were attached to the top and bottom flanges of the beam. There were 32 strain gages in total. All these gages were connected to a digital data acquisition system, which recorded all the changes in strains caused by the loading applied to the bridge. The truck used to impose the load had a total weight of 223 kn, which was closed but didn't exceed the rated posting of 231 kn. Three different paths were marked along the width of the bridge, indicating the place where the truck's wheel would be driven along. The truck was driven along each path twice and the strain was recorded at every longitudinal location of the truck along the bridge.

As reported by the authors, the measured data was used to create a finite-element model (FEM). The model had the same characteristic as the bridge in terms of beam's spacing, type of girders and diaphragms, and dimension of the concrete deck. Despite the fact that the beams were simply supported, the measured data showed that some bearing

restraint was being developed at the supports. To account for this the boundary conditions were set as pin-and-roller, including some rotational springs. The loads were applied at 11 locations along the three paths. For all 33 cases, the analytical responses were computed and compared with the measured responses. The percent of error was about 7.9%, which demonstrates the accuracy of the model and its capacity of estimating the actual load capacity on the bridge.

The tested bridge was originally designed as a non-composite structure, with simply supported spans; however, the finite-element model showed that the beams were acting compositely with the concrete deck and that there was some restraint at the supports. Accordingly, it was clear that the actual rating of the bridge would be higher than that posted before. After analyzing the bridge, the authors concluded that the real posted rating would range from 1.38 to 2.55, which is considerably higher than the actual posted rating. Therefore, they concluded that the actual posting levels on the bridge were not required.

2.2 Hughs and Idriss (2006)

In this paper the authors focused on the evaluation of the shear and moment live load distribution factor of a prestressed concrete box-girder bridge located in Las Cruces, New Mexico. The bridge had five spans, and each span had six, spread box prestressed concrete girders with a height of 1.37 m. The girders were designed to act as simply supported with a non-composite dead load, and continuous and composite with live load.

The moment and distribution factors were obtained by performing a live load test with fiber optic sensors attached inside the girders. These results were later used to prove the accuracy of the finite-element model of the bridge, which would be used to obtain the moment and shear distribution factors due the AASHTO design truck. After the data was obtained from the model, the authors compared their results with the AASHTO standard specifications and the AASHTO LRFD bridge specifications.

For the instrumentation program of the bridge, fiber optic sensors were used throughout the bridge. These sensors were only installed in the first span of the bridge because they wanted to obtain the necessary data to compare the actual structural behavior of the bridge with finite-element model. Each sensor contained two types of optical fiber; one type would measure the structural deformation while the other would measure the deformation due to temperature changes. These sensors were accommodated in two different configurations: the parallel topology, for measuring bending moments, and the crossed topology, for measuring shear. After the live-load test was performed, the recorder data was compared with the calculated values using the finite-element model in order to confirm the model's accuracy.

The finite-element model described in this paper was developed using the structural analysis software SAP2000. This analytical model represented the girders as frame elements and the deck with shell elements. The composite behavior was modeled by placing rigid links between the girders and deck. The girders were divided into small sections of about 1 foot long. The deck was also divided into small sections of 1 foot long by 0.867 feet wide. The truck that was used for the live load test was a dump truck with three axles and a total weight of 252.2 KN. The truck was placed at different

predetermined locations and an analysis was performed at each load location. Once the predicted distribution factors were obtained using the finite-element model, they were compared with those obtained from the live load test to realize that they were very close to the measured values. In addition to this, the finite-element model was found to be conservative, which makes it more appropriate to use it for prediction of the maximum distribution factors using the AASHTO test truck.

After applying the AASHTO design truck into the finite-element model, the results were compared with the AASHTO standard specifications equations and the AASHTOO LRFD specifications. According to the author's conclusions, the standard specifications predictions for distribution factors varied from highly unconservative, when used with interior girders, to highly conservative, when used with exterior girders. The LRFD specifications predictions were accurate with interior girders and conservative with exterior girders. That is why the authors concluded that the LFRD specifications are the best options for calculating the distribution factors for interior girders in comparison to the standard specifications; however, for the exterior girders, both are adequate, although too conservative.

2.3 Mabsout, Tarhini, Frederick, and Kesserwan (1998)

This paper describes the study of the influence of continuity on moment distribution factors based on the analysis of 78 different bridges. In order to perform the analysis, a finite-element model was created for every bridge. All bridges selected for this study had some common characteristics: two spans of equal length, two lanes, straight deck and girders, and had steel girders acting as a composite structure with the deck. Results were later compared with the new equation proposed by Zokaie in the NCHRP Project 12-26, which includes a single modification to account for continuity. The finite-element results were also compared with the formula proposed by AASHTO Standard (1996).

The main purpose of this investigation was to determine the accuracy of the formulations proposed by Zokie to account for continuity in any type of bridge. His equation seemed to represent the actual distribution factor on any single span bridge. However, for a multi-span bridge, the author felt his predictions did not give the same impression.

According to previous investigations, only the girders spacing and the span length were found to significantly affect the distribution factors. This is the reason why only these two parameters were modified during this study. Basically, all the bridges had a constant width, around 30 ft, with a deck thickness of 7.5 in. The point loads, simulating two HS20 design truck's axles, were located in such a way that the interior girders would receive more live load than the exterior girders. The two trucks were separated by a distance of 4 feet and were assumed to be running in the same direction.

For the finite-element model, two different programs were used in the analysis, SAP90 and ICES STRUDL II. For the SAP90 model, the concrete slab was modeled as a shell element and the girders as frame elements, where the centroid of the girders coincided with the centroid of the deck. The ICES STRUDL II program was used to model the concrete slab as a solid eigth-nodes element, and the web and flanges as shell elements.

After the results were studied, the researchers found that the AASHTO Standard (1996) load distribution factors were less conservative than the formulation proposed by Zokaie, when the span length was less than 60 feet and the girder spacing was less than 6 feet. However, for longer spans and girder spacings, the AASHTO Standard (1996) was more conservative and the equation proposed by Zokaie was closer to the analytical results. Therefore, the authors concluded that a factor of 5% must be applied when using the NCHRP Project 12-26 equation for both, positive and negative moment, and a 15% reduction factor should be applied when using the AASHTO Standard (1996) formulation.

2.4 Barr, Yanadori, Halling, and Womack (2007)

This paper describes the process by which a live-load test was performed to a horizontally curved, steel girder bridge. It also explains how the results obtained from the test were used to create a finite-element model of the bridge. This finite-element model was later used to determine the maximum bending moments, positive and negative, and the moment distribution factors of the bridge. These values were compared with those calculated according to the V-load method. The curved bridge presented in this study was a three span, continuous bridge, which had been designed as a non-composite structure.

The bridge deck had a thickness of 8 inches, and a width of 42.3 feet. It was supported by five steel girders separated by a distance of 8 feet 10 inches.

For the live-load test, two dump trucks were used to apply the live load into the bridge. These trucks were driven along three different longitudinal paths, which were predetermined by the researchers. The first path was located at 1.43 feet from the outside part of the exterior girder #1.The second path was determined at a distance of 3 feet on the inside of the girder #3. The last path was selected at a distance of 1.4 feet from girder #5. The response was measured in every case by placing strain gauges on every steel girder at various locations and configurations. Around 48 reusable strain gauges were used in 136 different instrumentations locations. In order to estimate the strong bending moment at least two gauges were used at every instrumentation location.

The finite-element model used to analyze the horizontally curved bridge was created using the computer program SAP2000. In this model, shell elements were used to represent the bridge deck, the web and flanges of the steel girders, the vertical stiffener and the diaphragms. The nodes for the shell element were located at the centroid of the element being modeled. Because of the curved condition of the bridge, the nodes of the concrete deck and steel girder were placed radially along the mesh in angles of 0.166 degrees. The web and flanges were divided into two elements. Different frame elements were placed between the concrete deck nodes and the steel girders nodes in order simulate the connection. The properties of these frame elements were varied in order to calibrate the model and adapt the results to the live-load test results.

In order to determine the accuracy of the finite-element model, the wheel loads, simulating the dump trucks used in the live load test, were applied at intervals of 2 feet. The response of the model was analyzed at each interval. These results were then compared with the results obtained from the live-load test, which quantified the accuracy of the model. Once the model was shown to accurately predict the bridge behavior, it was then used to determine the maximum positive and negative bending moment on the bridge. Moment distribution factors were also investigated. In order to do so, different combinations of the AASHTO HS-20 truck were placed on the model. The results were compared with V-load test calculations.

According to the researcher's findings, the V-load method was determined to be unconservative for positive moments with a difference of about 6.8% for exterior girders and 8.3% for interiors girders. For the negative moments, the V-load-method was shown to be conservative for the interior girder, with a difference of 16.1 %, and unconservative for the exterior girder on the inside of the curve, with a difference of 12 %. Finally, the AASHTO distribution factors for the interior girder were found to be conservative, with a difference of 25 %, for the positive moment and 14 % for the negative moment. For the exterior girder, the AASTHO Standard Specifications were conservative with only a 5% of difference, except for the positive moment, which was 14% conservative compared with the finite-element results.

2.5 Chen and Aswad (1996)

This paper presents a description of a general analysis procedure for predicting the live load distribution factor on simply-supported bridges. This procedure is used to verify the accuracy of the Load and Resistance Factor Design (LRFD) distribution factor

formulas when applied to prestressed concrete bridges made with I girders or spread box beams. The primary concern with these equations was that they were developed by analyzing typical bridges with the same span length, which was approximately 48 feet. This span length is considered to be short compared to actual present day bridges (80 to 90 ft).

The major goal of this study was to compute the distribution factors for many slab and beam bridges that cover a big part of real-life situations for I-beams and spread box girders bridges. A total of ten different I-beam bridges and six spread box beam structures were covered in this study. The spacing between girders varied from 8 feet to 10.5 feet. The span length ranged from 90 to 140 feet.

The finite-element model of the bridges was created by using ADINA 1991. A four node shell element with a constant thickness was used to represent the concrete slab. The composite behavior of the slab with the beams was represented by connecting the center of the slab with the center of the beam using rigid links. All beams were modeled as simply supported beams by placing rollers at one end and pinned supports at the other end. For the loading analysis, an HS-20 truck was applied to the model by placing point loads that represented the axle loads from the truck. In addition to the truck load, a lane load was also taken into consideration.

After analyzing many models with different span lengths and beam spacing, the authors found that finite-element models of bridges with large span-to-depth ratios may reduce the mid-span moments by 18% to 23% for interior beams, and by 4-12 % for exterior beams, when compared to the LRFD simplified method. Finally, the authors stated that the exterior-girder capacity should be at least equal to the interior-girder

capacity. This is because the distribution factors for the exterior girders predicted by the analysis were usually larger than the ones for the interior girder. Another reason is that the exterior-girder carries more of load due to the increased stiffness of the parapet.

2.6 Sennah and Kennedy (1999)

This paper presents a very detailed study performed over a huge number of composite steel, concrete multi-cells, box-girder bridges. These types of bridges have very efficient transverse load distribution due to the excellent torsional stiffness, which is provided to the composite cross section by the box girders. That is the main reason why these bridges types are considered very economical and are being used in many more bridge deck constructions. However, the design process part becomes very narrow and complicated, because of the lack of simpler and more accurate analytical methods that may be able to describe the behavior of these structures. This is why this paper focuses on the development of equations that can precisely estimate the moment and shear distribution factors for these bridge types.

The main objective of this paper is to conduct a parametric study on these types of bridges in order to determine what parameters are most influential on the load distribution factors. The parameters that were taken into consideration were the number of cells, span length, cross-bracings and number of lanes. These parameters were studied one by one using various finite-element models and the result were used to deduce equations for moment and shear distribution factors.

Approximately, 120 simply-supported bridges were used in this study, with span lengths that ranged from 20 to 100 meters. The number of cells ranged from 1 to 4 for a one lane, from 1 to 7 for two lanes, form 3 to 9 for three lanes and from 4 to 9 for four lanes. All these cases were analyzed using a representative finite-element model. However, before considering using the finite-element model in those structures, an experimental study had to be conducted in order to calibrate the computer model. That is why a composite, concrete deck-steel bridge model with three cells was constructed and tested under several static load conditions. The results were later used to improve the analytical model of the bridge.

The program used to create the analytical models was ABAQUS. The deck was modeled using a four-node shell element with six degrees of freedom in each node. The steel webs, steel bottom flanges and end diaphragms were modeled using the same procedure. The steel top flanges, cross bracings and top chords were modeled using three-dimensional, two-node beam element. In order to establish the simply supported conditions on the bridges, rollers were placed at one end of the bridge, while hinges were placed at the other end. A beam constraint element was used to connect the shell nodes of the concrete slab with the beam nodes from the top flanges.

After analyzing the bridge models, the authors observed that the number of cells affected the moment and shear distribution factors. In addition, they also observed that the span length played an important role. For longer bridges, the moment distribution factor decreases for the central girders and increases for the exterior girders. In addition, it was observed that by increasing the number of cells, the moment distribution factor decreases. It was also noted that by increasing the number of lanes, the moment

distribution factor was also increased. The same behavior was observed in the shear distribution factor. As a result, the authors concluded that these three parameters have a significant impact in determining the maximum moment in each girder. Therefore they included these factors to deduce the expressions for computing the moment and shear distribution factors. Finally, the authors concluded that the use of these proposed equations would lead to a more accurate and economical design.

CHAPTER 3

A COMPARISON OF LIVE-LOAD DISTRIBUTION FACTORS FOR THE I-15/8th NORTH BRIDGE

In this chapter a detailed description of a study that was performed on the 8th North Bridge near Salt Lake City will be presented. This study primarily consisted of creating a very precise finite-element model (FEM) of the 8th North Bridge in order to analyze and determine the locations at which the maximum moments would occur along each girder. The model was developed and calibrated by comparing its behavior with the recorded data that was taken from a live-load test performed on this bridge by Bridge Diagnostic Inc (BDI). By creating the analytical model, maximum design moments were obtained. These calculated design moments could then be compared with predicted moments obtained from the AASHTO LRFD Specifications. The comparison was the primary focus of the study.

Chapter 3 is divided into seven sections, where each section describes a single aspect of the investigation. In Section 3.1, a very extensive description of the bridge being studied is presented. Section 3.2 describes every detail related to the live load test performed on the 8th North Bridge. Section 3.3 describes the assembly of the finite-element model, the type of elements that were used to represent the structural components, and what type of boundary conditions were used to simulate the actual supports on the bridge. Section 3.4 presents the results obtained from the live-load test. Section 3.5 reviews the different equations provided in the AASHTO LRFD Specifications to estimate the live-load distribution factors on the exterior and interior

girders. Section 3.6 describes how the finite-element model was used to determine the moment distribution factors. Finally, Section 3.7 shows and describes a comparison between the FEM live-load distribution factors and the AASHTO LRFD calculated values.

3.1 Bridge Description

The 8th North Bridge is located at the 800 North Street overcrossing of the I-15 freeway, in Salt Lake City, Utah. It has a slightly curved shape, which is very appropriate for the geometric conditions of the road, as can be seen in Fig 3.1. The bridge is owned by the Utah Department of Transportation (UDOT), and was designed to support two opposing traffic lanes. In fall of 2007, the reinforced concrete deck was removed due to the deterioration that had accumulated over the many years that had been in service, and was replaced with pre-cast concrete deck panels.

Fig 3.1 Aerial view of the 8th North Bridge.

Figure 3.1 shows an aerial view of the concrete bridge prior to the placement of the pre-cast concrete panels. The old concrete deck was totally removed, as it is shown in this picture. This type of replacement was UDOT's first experience with pre-cast concrete deck panels. Within two years of the deck replacement, the entire bridge was scheduled to be replaced due to the Beck Street reconstruction project. This unexpected replacement provided a unique opportunity to study the performance of a pre-cast, concrete deck panel system after two years of service.

Most of the bridges that are currently built use a straight contour, which makes the design and construction process easier. However, sometimes the situations will dictate where the bridge owner is required to adapt the bridge shape to the geometry of the highway, as was the case of the 8th North Bridge. This tends to complicate the analysis and design of the structure, because the behavior of this type of structures is less understood and more assumptions are required, thus making the design process more difficult. This dilemma and the fact that the bridge was programmed to be replaced were the main reasons why this bridge was chosen to be studied.

Figure 3.2 shows a picture from the 8th North Bridge, taken from the I-15 Freeway. In this figure it can be noticed that there is some deterioration on the steel girders. The 8th North Bridge passes over the I-15 Freeway and it is supported by three pier caps. The curved shape of the bridge is also appreciated in this picture.

Fig 3.2 8th North Bridge view from I-15 Freeway.

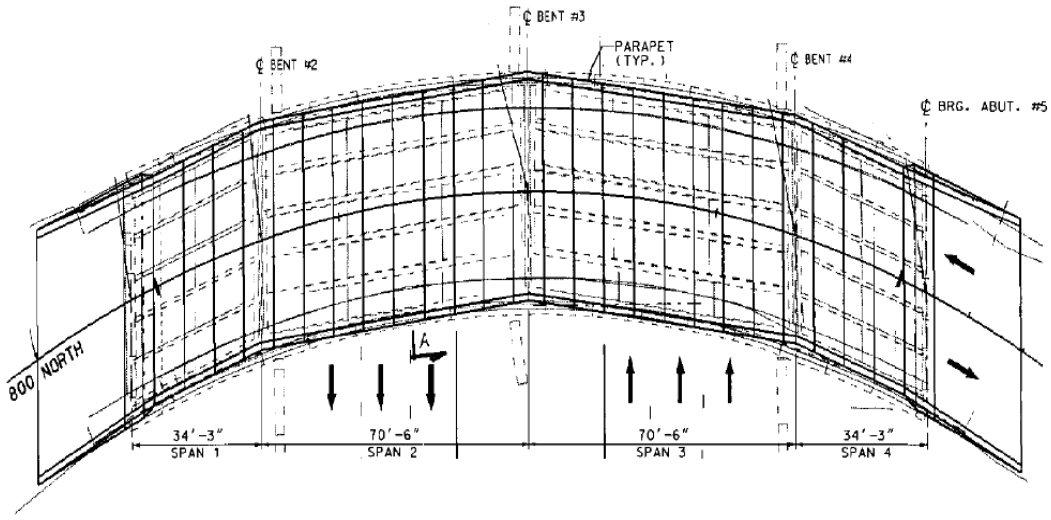

Fig 3.3 Bridge girder layout.

A plan view of the bridge is shown in Fig. 3.3.The bridge was designed as a four span bridge with some degree of continuity. The first and last span had the same length of approximately 36 feet and 7 inches long, while the second and third spans were 70 feet and 8 inches long. As a consequence, the bridge had a total length of about 215 feet. Based on the elevation view of the original bridge, the concrete deck was designed to have a horizontal curve. However, this was only true for the concrete deck because, as we can see in Figure 3.3, the girders were placed and designed as straight elements from one support to another.

The orientation of the girders was modified at every support in order to adapt the structural elements to the shape of the concrete deck. The superstructure could not be treated as a typical curved girder bridge, thus some assumptions were required in order to model and analyze the structure. These assumptions will be further discussed in Section 3.3.

The 8th North Bridge overpass was designed to carry two, 12-foot wide lanes of traffic, with two equal shoulder widths of 8 feet and 5 inches. As shown in Fig 3.4, the total width of the bridge is 43 feet and 8 inches. This total width includes the two barriers which were 1 foot 5 inches wide at the base and were placed at both edges of the roadway. These barriers were constructed on site, following the specifications given in Fig 3.5.

Another important aspect of this bridge that must be emphasized is the presence of a 5-foot wide side walk that had a thickness of 9 inches. This particular element is not commonly used in these types of bridges, and therefore was not taken into consideration

on the equations to calculate the load distribution factors that are presently used in the AASHTO LRFD Specifications. This sidewalk member was constructed in situ along with the concrete deck and the barriers, which would indicate that the system may behave as a composite structure with the concrete deck. Fig 3.6 shows more details of the curb.

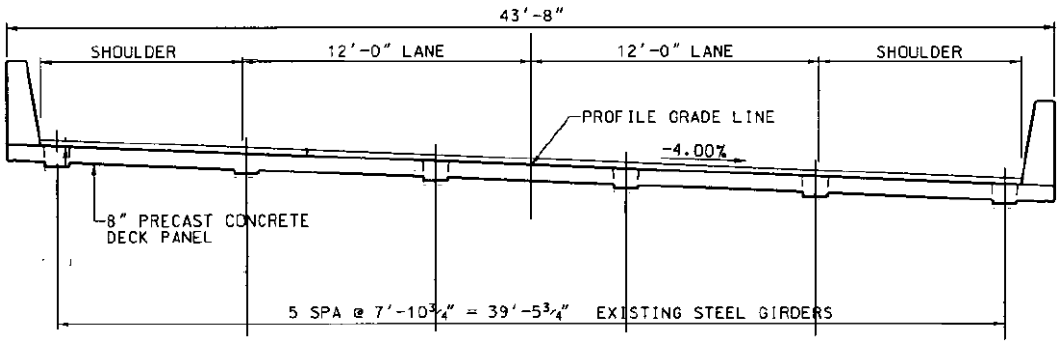

Fig 3.4 Bridge cross section.

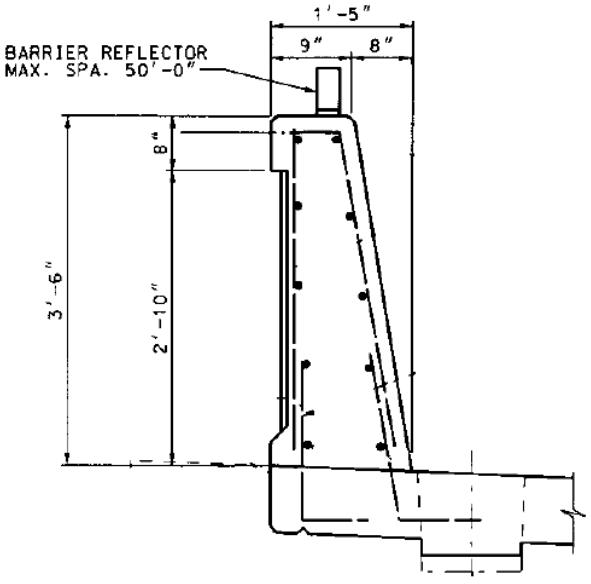

Fig 3.5 Barrier specifications.

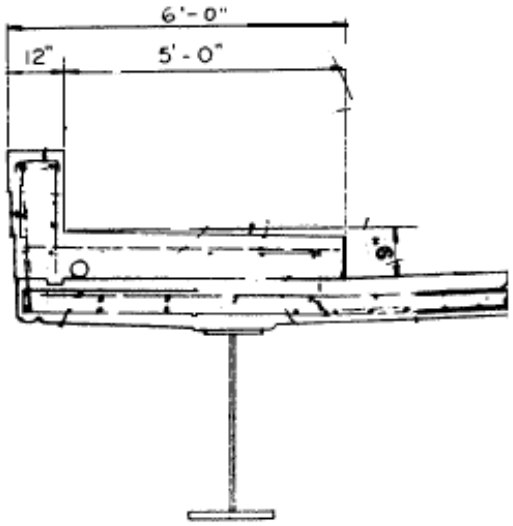

Fig 3.6 Curb details.

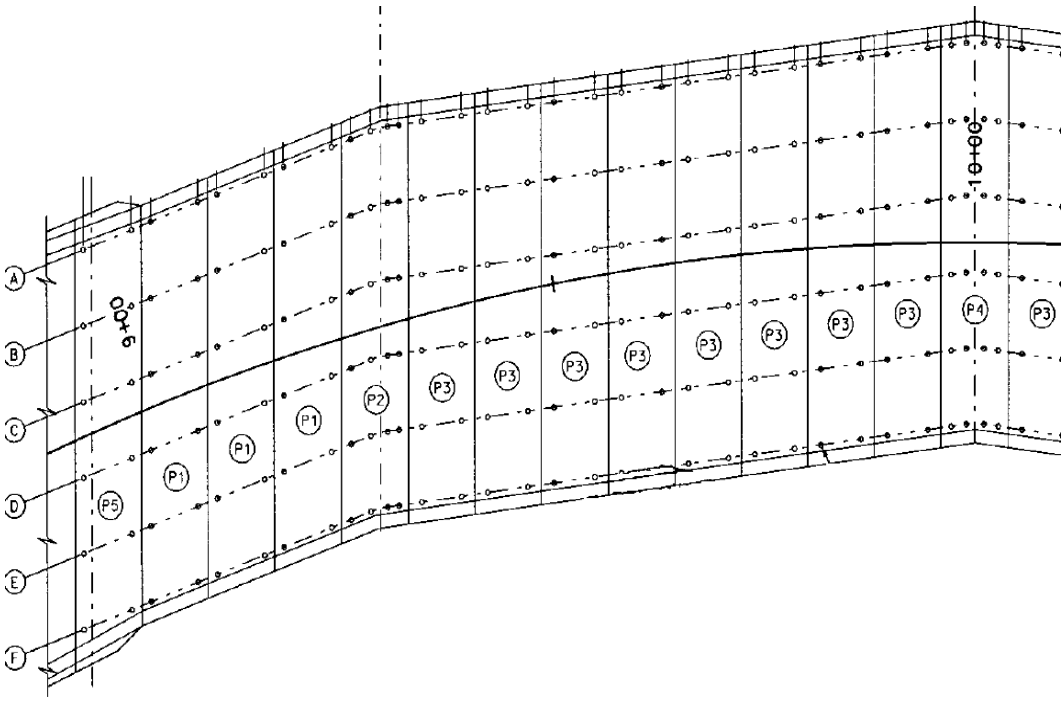

Fig 3.7 Pre-cast concrete panel lay out plan.

Before its reconstruction, the old bridge deck was designed using the Interstate Alternate Loading or HS-44, in accordance with the AASHTO Specifications of 1973. The concrete deck had a specified compressive strength of 3000 psi, with Grade 36 reinforcing steel, and a constant thickness of 7.5 in. The new concrete-bridge deck had a specified compressive strength of 4000 psi, with a modulus of elasticity of approximately 3600 ksi. It was reinforced with Grade 60 steel, and with reinforcements than ranged from #4 to #6 bars. The new pre-cast reinforced concrete deck had a constant thickness of 8 inches, and the curb element was not included, as can be shown on Figure 3.8.

In the picture shown below, an actual view of the new concrete deck is shown. As it can be seen, two opposing traffic lanes are being supported by the pre-cast concrete panel deck. It can also be noticed that the sidewalk has been removed in the reconstruction process, thus affecting the structural behavior of the bridge.

Fig 3.8 Barriers and concrete deck on the 8th North Bridge.

As previously mentioned, the new concrete deck was built using different sizes of pre-cast concrete panels. Fig 3.7 shows the layout of the pre-cast concrete panels on the bridge deck. The steel reinforcing of these panels varied in size and distribution according to its location. These concrete panels were connected using a female-to-female deck joint filled with non-shrink grout, in combination with some metal plates and shear studs .These deck joints were thought to transmit shear and flexion from one panel to the other. Figure 3.9 shows some details of the deck joints used in this structure.

At the abutments, the panels were connected using compression joints. These joints were created with the solo purpose of sealing those unions between two adjacent concrete panels, and not for structural purposes, as one might think. Figure 3.10 shows some details of the connection of the compressive joint.

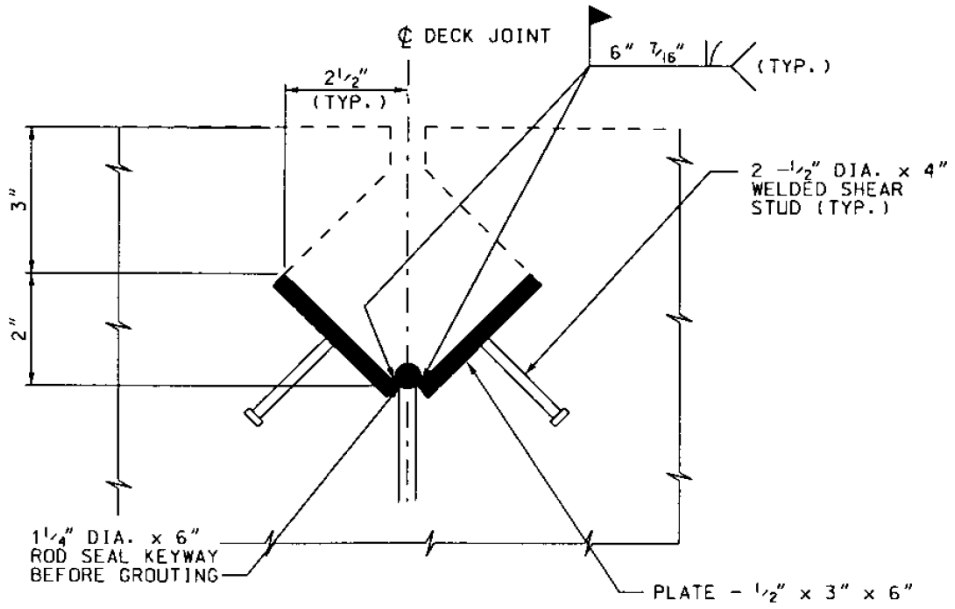

Fig 3.9 Detail of a deck joint.

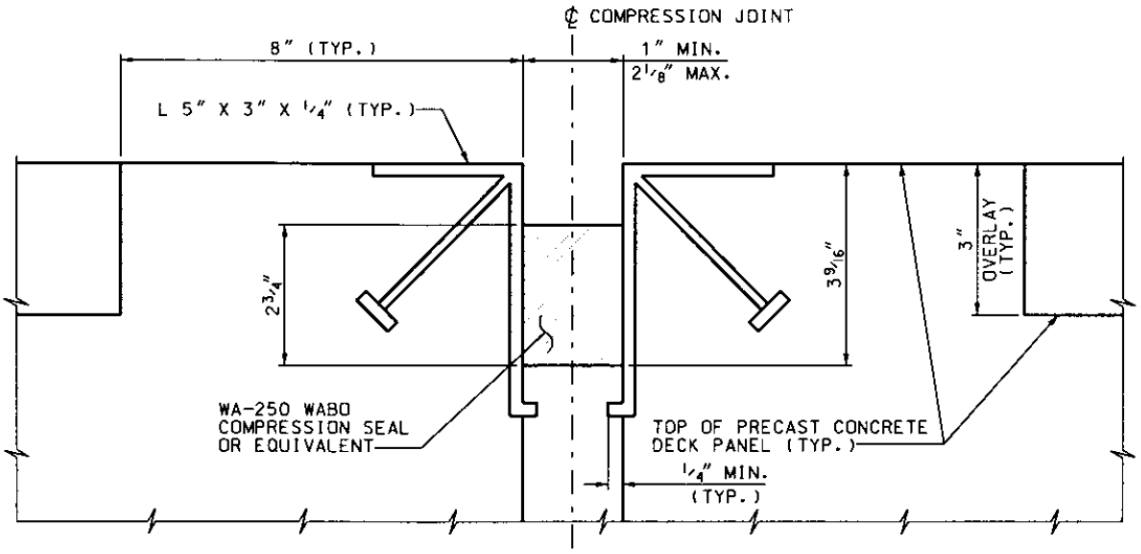

Fig 3.10 Detail of a compressive joint.

Each span of the 8th North Bridge has a total of six continuous steel girders that supported the concrete deck. The girders were spaced at a constant distance of 7 feet and 43/4 inches. An A-36 structural steel was used in the fabrication of the girders. Each girder was designed according to Allowable Stress Design principles with an allowable stress of 20 ksi.

These beams did not come from any specified w-shapes or any other shape, but were built up sections constructed using different types of plates that were welded together. A filler type, ¼" weld, on both sides, was used to connect the individual plates in order to form a single structural element. As a result, a single beam would have the same web and flange size as the remaining five; however, the flange size varied along the length of the girder. For instance, as shown in Figures 3.11 and 3.12, the plate's sizes used in the structural members of Span 1 differ from those used in Span 2.

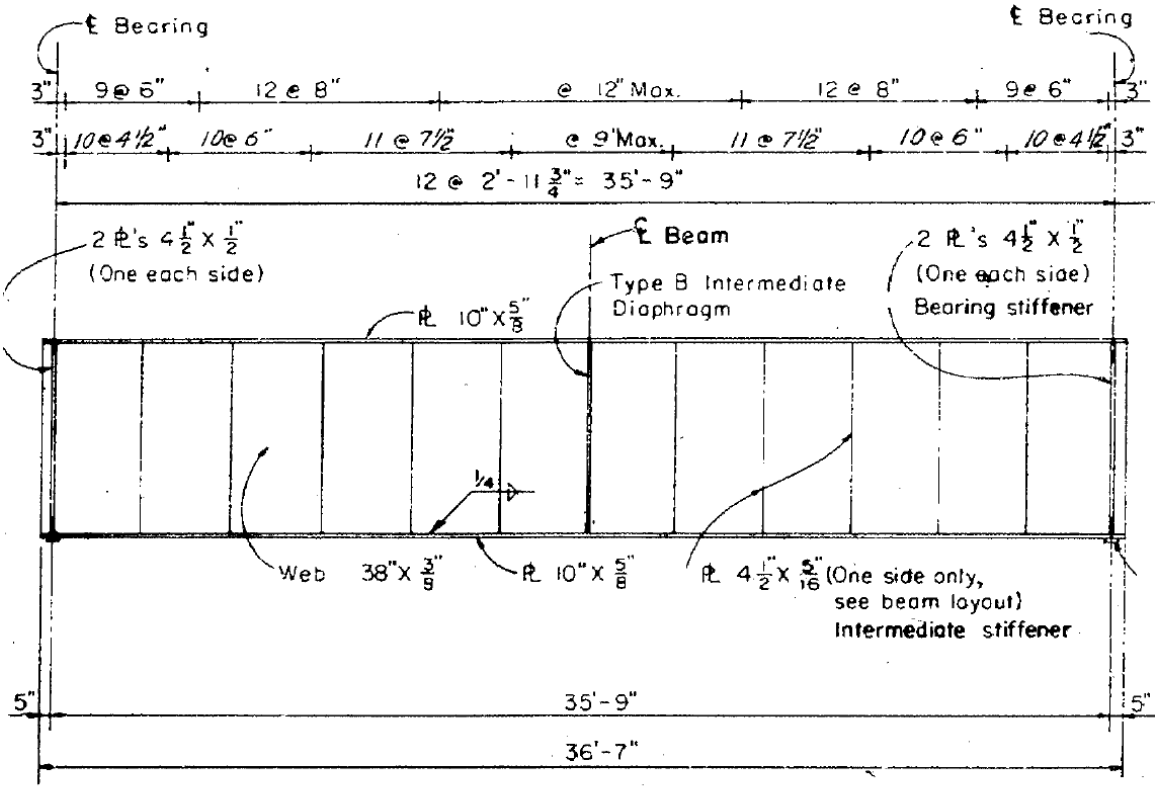

Fig 3.11 Span 1 girder details.

In Span 1, a 10”x5/8” plate was used for the flanges and a 38” x 3/8” plate was used for the web. The length of the span was designed to be approximately 38 feet long with a horizontal inclination of about 19 degrees and 37 seconds, which can be appreciate in Figure 3.3. Another important fact that is shown in Fig 3.10 is the presence of some web and bearing stiffeners.

These elements were used to add more load bearing resistance at critical load points to prevent web crippling. A 4 ½” x 5/16” plate was used as a web stiffener and two 4 ½” x 1/2” plates, on each side, as a bearing stiffener.

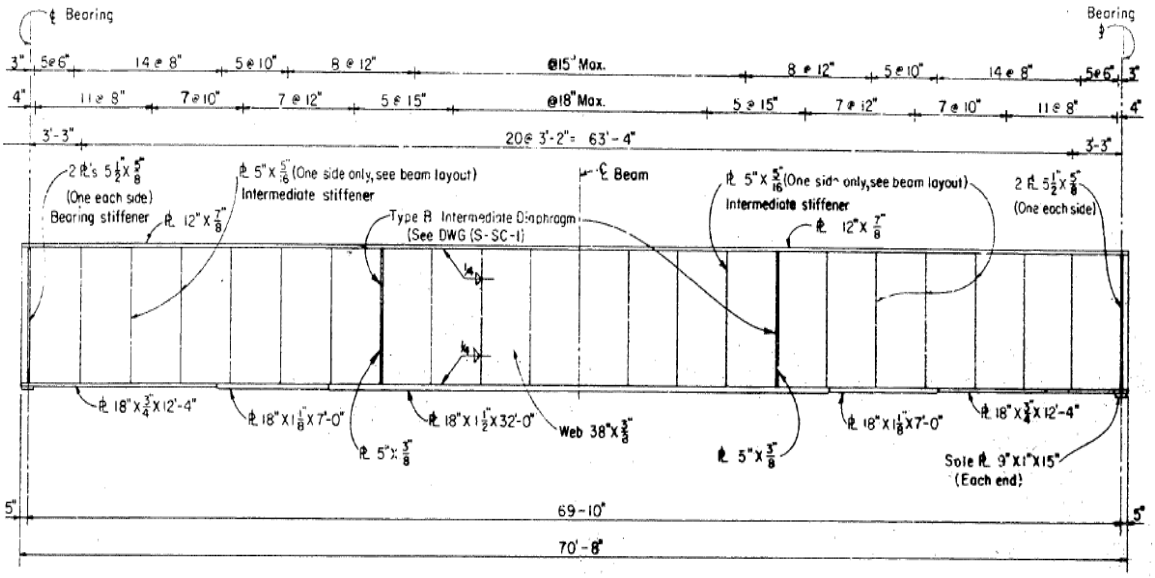

Fig 3.12 Span 2 girder details.

The girders of Span 2 had a total length of approximately 71 feet and a horizontal inclination of seven degrees and seven minutes. As shown in Fig 3.12, the web and the top flange sizes were constant, but the bottom flange changed along the span length. The web had a height of 38 inches and a thickness of 3/8 inches, as in the first span. The top flange had a width of 12 inches and a thickness of 7/8 inches. At the bottom of the flange, things were slightly more complicated.

From the beginning of the second span to a distance of twelve feet and 4 inches from the support, the bottom flange has a width of 18 inches and a thickness of ¾ inches. Between that point and seven more feet, the bottom flange changes its thickness to 9/8 inches. Finally, from the end of the last segment to the mid-span of the beam, around 16 feet, the thickness of the bottom flange increases to one and a half inches. The rest of the beam has the same format starting from the other end. In the second span, the presence of some web and bearing stiffener were used as well. In this case, two different plates were

used as web stiffeners, a 5” x 5/16” plate and a 5” x 3/8” plate. For the bearing stiffener, two plates of 5.5” x 5/8 were used. For more stiffeners details, refer to Figure 3.12

Despite being pre-cast, the concrete-deck was designed to act compositely with the steel girders. In order to accomplish this composite condition, shear studs were placed at many locations along the length of the girders. These shear studs had a diameter of 7/8 inches and a length of six inches. They were placed in groups of three shear studs per block-outs, and transversally spaced every three and a half inches in Spans 1 and 4, and four and a half inches in Spans 2 and three. Fig 3.13 shows more details concerning the shear studs distribution. The block-outs were specially constructed to make the bond between the shear studs and the concrete panels possible. Table 3.1 specifies the number of block-outs per girders in every concrete panel, and the spacing between them. Figure 3.3 shows the number of the pre-cast panels that are mentioned in Table 3.1

Table 3.1 Concrete Panel Block Out Locations

Pre-Cast Concrete Panel	Numer of Block-outs per girder	Space Between Block-Outs
Panel #1	7	1'- 2 1/4"
Panel #2 A	2	1'- 2 1/4"
Panel #2 B	4	1'- 2 1/4"
Panel #3	5	1'- 7 1/4"
Panel #4 A	2	1'- 7 1/4"
Panel #4 B	2	1'- 7 1/4"
Panel #5	5	1'- 2 1/4"

Figure 3.14 shows an example of the shear Block layout at a pre-cast concrete panel. In this case, the distribution of the shear blocks along panel number 3 is presented. As showed in Table 3.1, this specific panel has five blocks per girder.

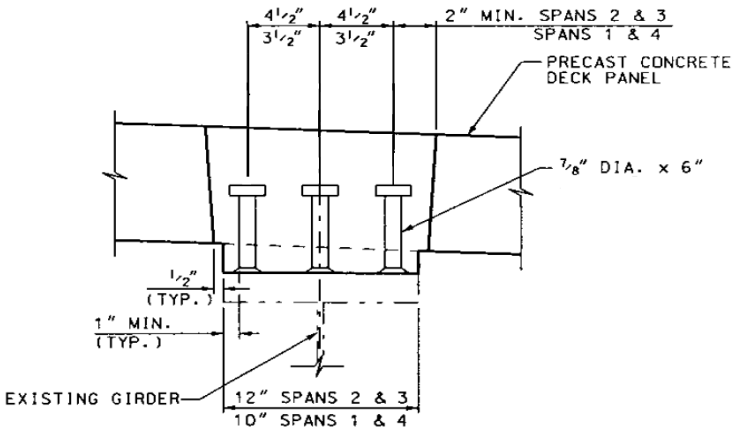

Fig 3.13 Shear stud detail.

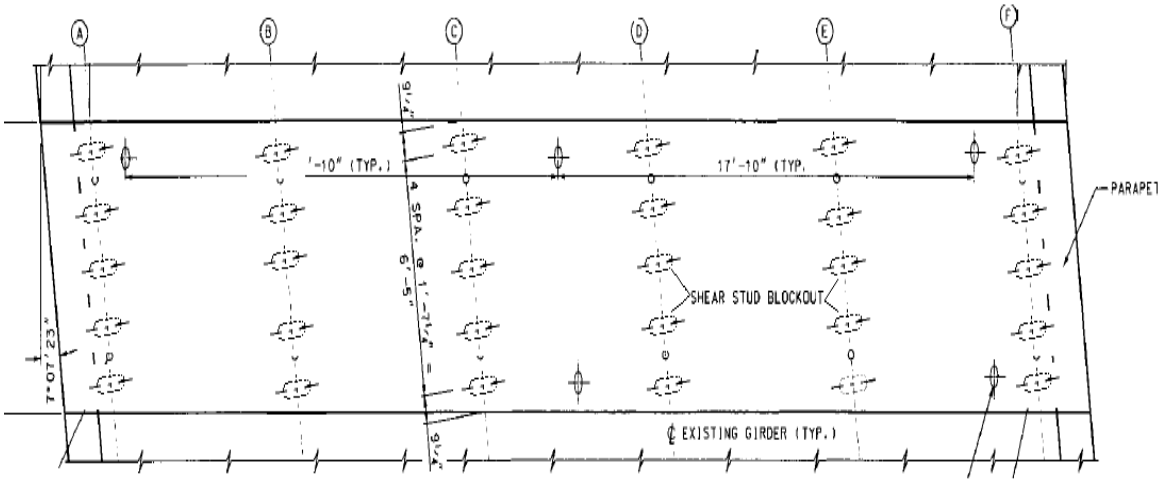

Fig 3.14 Panel P3 shear block layout.

The superstructure was supported by three pier caps, which were placed at every bent of the bridge. These structural elements are made of one horizontal member, acting as a beam, and two vertical elements, that functioned as columns. The pier caps had a height of four feet and a width of three feet, and had a clear span of 24 feet and nine inches. The pier caps were designed to carry the weight of the six girders placed on top of them plus the deck and the live load. The columns had a dimension of four feet long and three feet wide, and were supported by a nine foot by nine foot pile cap. These pile caps were 3 foot-3 inches thick, and were supported with five concrete piles. Fig 3.15 shows the structural details of the pier caps.

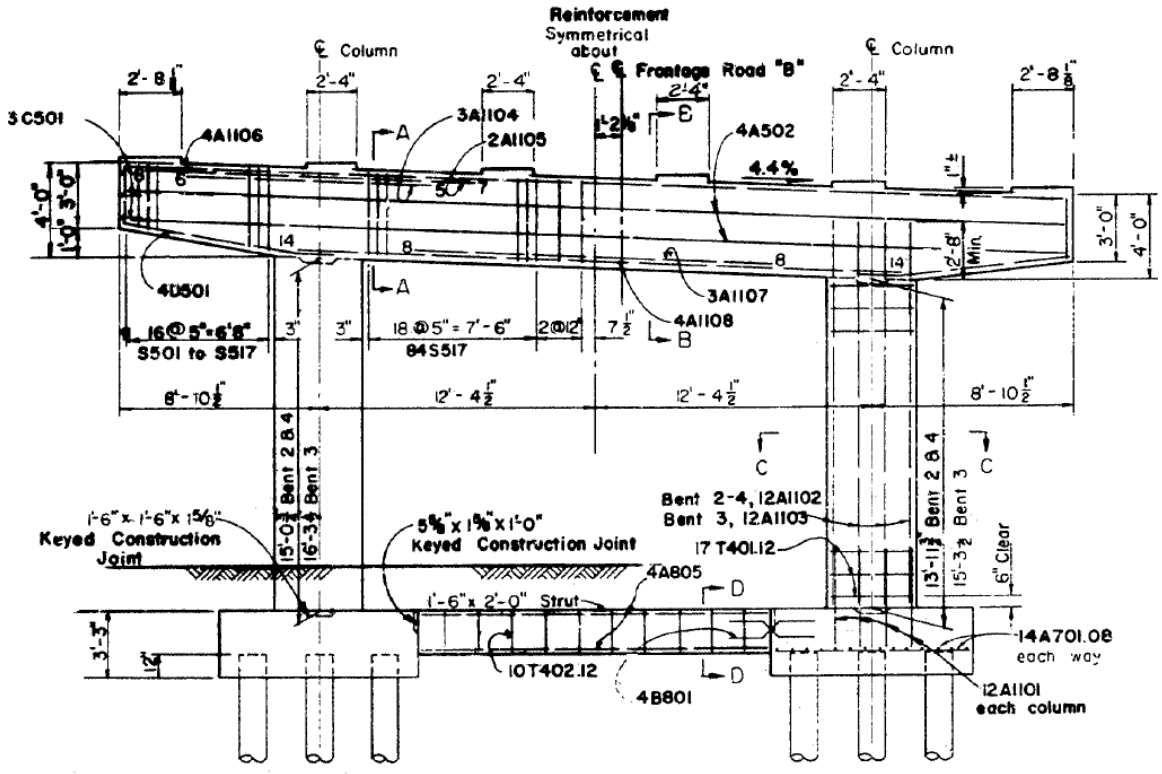

Fig 3.15 Pier cap detail.

3.2 Live Load Test

In June of 2009, Bridge Diagnostic Inc (BDI) performed a live-load test on the 8th North Bridge with the purpose of measuring the structural behavior of the bridge before its demolition. The live-load test results would later be used to develop and calibrate a finite-element model that could accurately determine the load ratings of the bridge.

This test consisted of driving a truck load along six different load paths, and measure the response of the super structure by recording the strains and deflection produced at previously determined locations. The change in strain was measured in 57 different locations on the bridge by placing a strain gage at each point of interest. The deflections were recorded in 6 different locations, one for each girder .These spots were closed to the mid-span of the second span. In order to record these deflections, LVDT sensors were employed. Both, the LVDT and strain gages were assigned a code name that would help

Fig 3.16 Part of the BDI structural testing system**.**

indentify and locate every measured data on the bridge. Figures 3.17 and 3.18 show an example of the strain gages and LVDT sensors used for this test.

Fig 3.17 Typical strain gage used in the live load test.

Fig 3.18 Typical LVDT sensor used in the live load test.

The strain gages were spread out over the structure and placed at six different locations. These locations are shown in Figure 3.19. As can be shown, the response of the superstructure was intended to be measure close to the end of the bridge, Section AA, close to the abutments, Section CC, DD and FF, and at the mid-span of the two spans, Section BB and EE. In the first span, Section AA is located at 4 feet and 4 inches from the end support while Section CC is located at 7 feet and 3 inches from the pier support. Section BB was placed at 1foot and 6 inches from the mid-span. In the second span, Section DD was placed at 8 feet and 2 inches from the pier support and Section FF at 8 feet and 2 inches from the central pier. Section EE was placed at the mid-span of the second span. This particular section contained all the LVDTs used in this test.

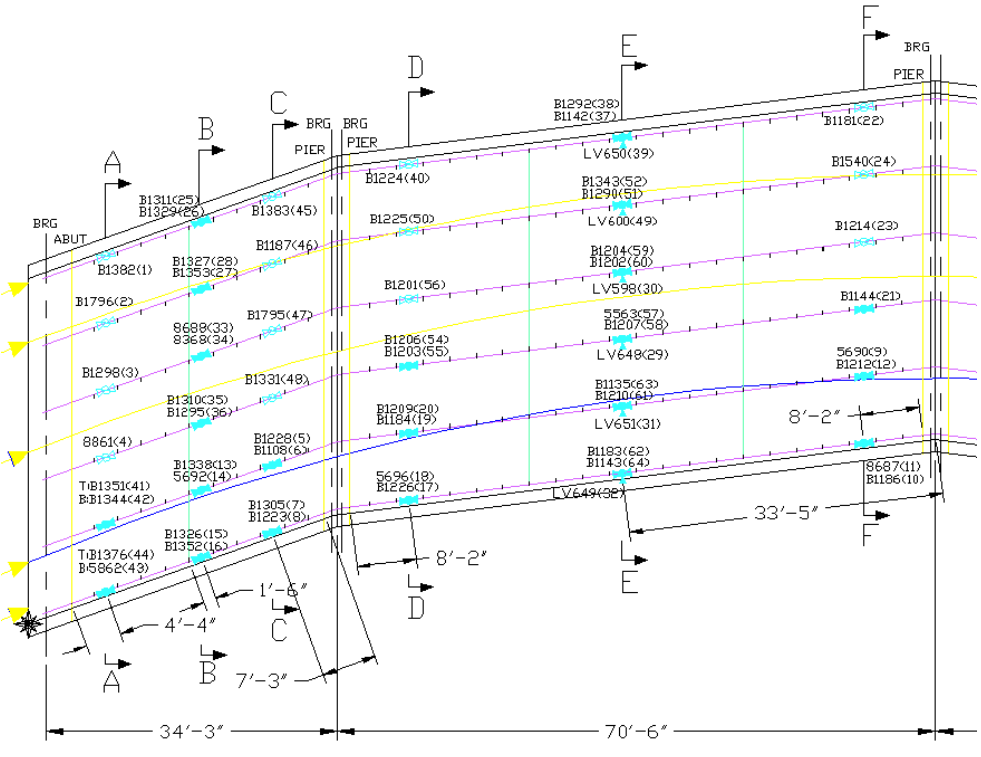

Fig 3.19 Instrumentation plans of strain gages and LVDTs. (Courtesy of BDI).

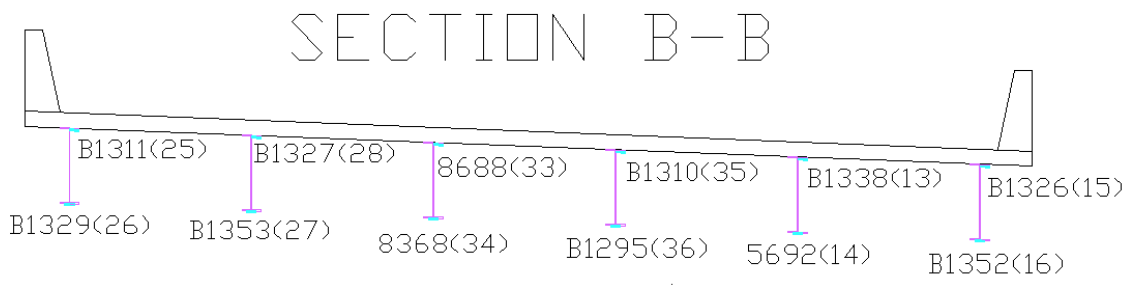

Fig 3.20 Location of strain gages at section BB. (Courtesy of BDI).

Figure 3.20 shows how the strain gages were distributed at cross Section BB. As can be seen, the strain gages were placed at the top and bottom of the steel girders. The reason why sensors were placed in this configuration is because it facilitates the calculation of the neutral axis in the composite section. The calculation of the neutral axis is very important because it allows the determination of whether or not the steel girders are acting compositely with the concrete deck.

Before the test was started, a point of reference was selected on the bridge. This is very important because it helps determine the truck position on the bridge in relation to the measured data. The point of reference chosen for the test was at the southwest corner of the bridge, in the interior side of the bridge, along the compressive joint. Figure 3.21 shows the location of this reference point on the bridge superstructure.

As previously mentioned, six different loading paths were chosen for this test. According to Figure 3.21 these loading paths were named as Y1(P), Y2(D), Y3(P), Y4(D), Y5(P) and Y6(D). Y5 (P) and Y6 (D) were located at two feet from each barrier as can be observed in Figure 3.21.

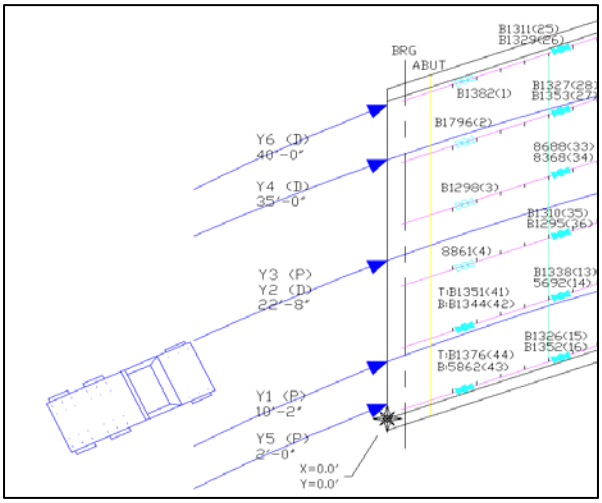

Fig 3.21 "Zero Location" and truck loading paths. (Courtesy of BDI).

These loading paths were chosen with the purpose of obtaining the response of the bridge due to the imposed live load, at the closest location that the wheel loads are allowed to be from the barriers, which is two feet according to the AASHTO code. For the load case Y5, the truck was driven using the passenger-side wheel, while in Y6, the driver-side wheel was used. Load PathsY4 and Y3, located at distance from the zero point of 35 feet and 22 feet and 8 inches, respectively, also used the driver-side wheel. Y1 and Y2 used the passenger-side wheel and were located at 22 foot-8 inches and 10 foot-2 inches, respectively, from the reference point.

For this live-load test, a semi-static test and a high speed test was conducted. The semi-static test was performed by driving the truck at and average speed of 5 mph. This test simulated the application of statics loads on the bridge. The data for this test was recorded at sample rate of 40 Hz. The high-speed load test was performed at an average speed of 50 mph. This test was performed with the purpose of measuring the behavior of the structure due to a dynamic load. This data was recorded at a sample rate of 100 hz.

Fig 3.22 Double truck test.

For the semi-static test, a single truck test was performed on paths Y5 and Y6, while two different trucks were used at the same time for the other paths. This was done to increment the respond of the superstructure and obtain larger strains measures at the point of interest. Figure 3.22 shows the two trucks used in this test, placed in loading paths Y4 and Y3. The position of the trucks was recorded at every test through the employment of a magnificent device called auto-clicker. This useful tool would be described with more details in Section 4.2.

The trucks used in this test were three-axle dump trucks, with similar dimensions. These dimensions can be fully appreciated in Figure 3.23. The front axle had an average width of 6 feet and 10 inches with a measured weight of 18,820 pounds for truck #1 and 16,400 pounds for truck #2. The two rear axles had an average width of 7 feet and three inches with a total weight of 38,120 pounds for truck #1 and 38,700 pounds for truck number two. The front and rear axles were separated by a distance of 17 feet and 4 inches. The two rear axles were separated by 4 feet and 7 inches. Figures 3.24 and 3.25 show a picture from the truck #1 and #2, respectively.

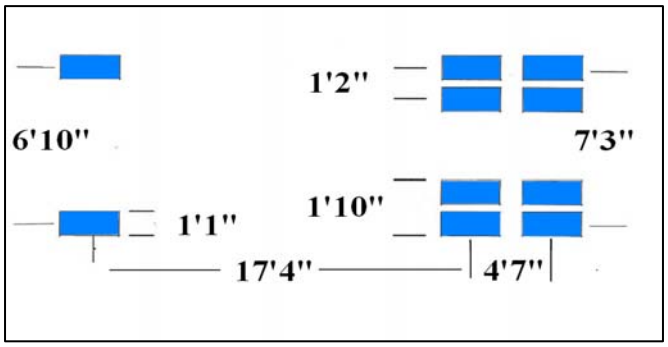

Fig 3.23 Test truck footprint.

Fig 3.24 Truck #1.

Fig 3.25 Truck #2.

The live-load test data was used to determine if the concrete deck was acting compositely with the steel girders. As a result, the recorded strain from strain gages that were placed at the top and bottom of interior girders, at section EE, were examined and an associate neutral axis was obtained at every position of the loading truck. The calculated neutral axis for the second span sections, using an effective width of 94.75 inches for the concrete, was found to be 33.66 inches, measured from the bottom of the girder. The neutral axis of the girders alone was found to be 14.13 inches. It is believed that the actual neutral axis should lie between these two values. Figure 3.26 shows the variation of the neutral axis according to truck position. As can be observed the calculated values are closer to neutral axis of the composite section, represented by the red line, than the neutral axis for the steel girder acting by itself, represented by the blue line. This demonstrates that the structure behave compositely with the steel girders.

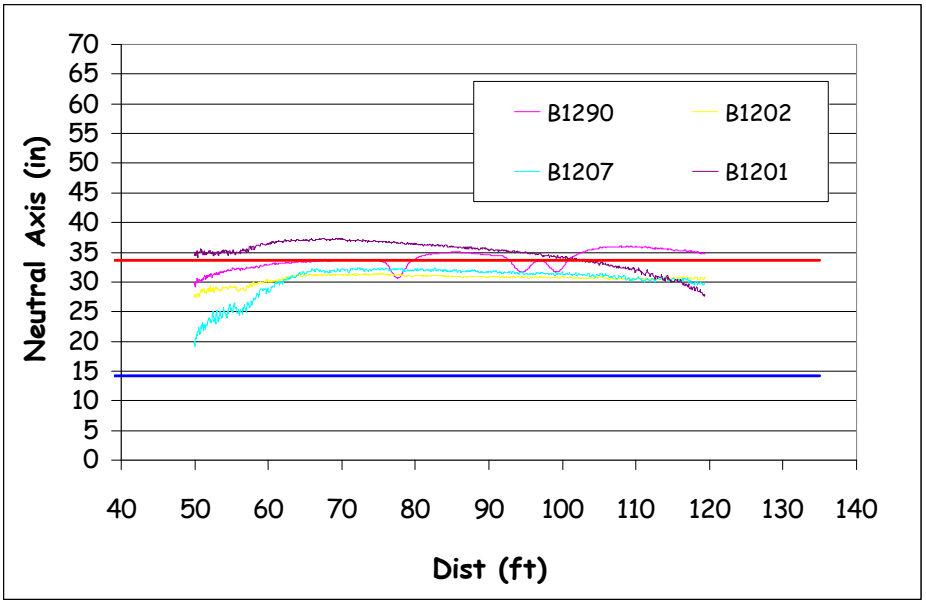

Fig 3.26 Location of neutral axis (Test Y6).

3.3 Finite-Element Model

Two finite-element models were used to replicate the 8th North Bridge. These models were created using the computer program SAP2000. This program requires that the material properties, (such as the modulus of elasticity and compressive strength), and the geometric properties, (such as the cross-sectional area and moment of inertia), be input for every element.

For the first model, the steel girders, concrete deck and barriers were all incorporated into the model. Shell elements were used for the concrete deck, while frame elements were used to model the steel girders. Solid elements were used to model the barrier. The first model represents the actual condition of the bridge without including the sidewalk elements.

The second model focused the conditions of the structure before the deck replacement, by including the sidewalk element into the modeling. Shell elements were used to represent the curb. As in the first model, the steel girders were represented with frame elements and the concrete deck was modeled using shell elements. The main purpose of the second model was to represent a condition where the curb elements were included, and determine the effect of this element in the behavior of the structure. These two types of models were taken into consideration in order to quantify the influence of the added stiffness and change in lane location on the moment distribution factors for the exterior and interior girders. This comparison will be shown in Section 3.6.

3.3.1 Elements representation

Figure 3.27 shows a 3D representation of the frames elements used in the finite-element modeling of the bridge girders. As shown in Figure 3.27, a two-node frame element was selected to represent the steel girders of the bridge. This particular type of element allows the generation of any cross sectional shape that is required, from a simple rectangular form to any difficult w-shape or H-shape. The engineer only needs to input the appropriate dimensions, and the program will calculate the cross-sectional area, moment of inertia, and other properties.

The selection of a frame element to model the steel girders was based on a combination of accuracy and simplicity. The process was first started by modeling a simply-supported beam, composed of a steel girder with a concrete slab placed on top of it. The steel girder and concrete deck were both modeled using shell elements for model 1. After the shell model was constructed, a second model was created using frame elements to represent the steel girders.

A comparison of these two models showed that the second model (frame girders elements) resulted in deflections and stresses that were as close to the exact solution as the more detailed model (shell girder elements). Many other models were created by changing the boundary conditions and beam spacing, but in every single case, frame elements produced comparable results and was therefore chosen due to its simpler geometry.

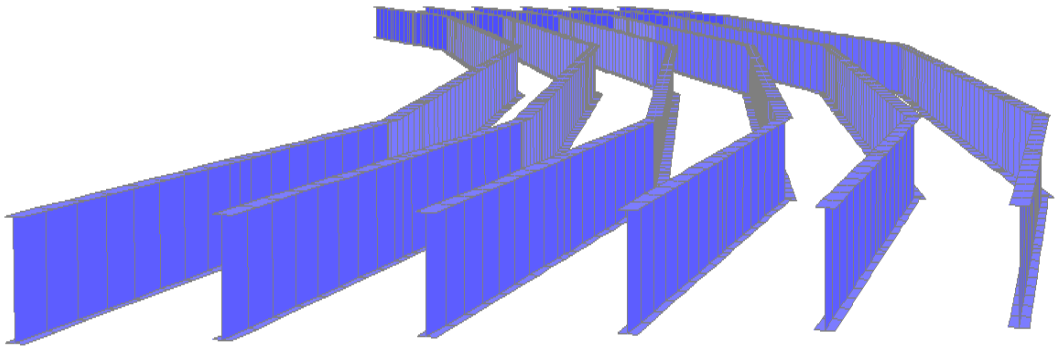

Fig 3.27 Steel girders 3-D FEM representation.

As described in Section 3.1, the flanges and webs for the steel girders varied for the first and second spans. As a result, four different frame elements had to be created. The frame elements were created in SAP2000 by changing the dimensions of the web and flanges.

The first span had a total length of 36 feet and 4 5/8 inches. The frame elements on this span were divided into seventeen segments with equal length of 25.68 inches. This element was denoted as SPAN1 when defining all the frame elements in SAP. The second span had three different types of frame elements, which were distributed symmetrically with respect of the midpoint of the span. The first type had a total length of 148 inches and was divided into five segments of 24.36 inches, one segment of 11.67 inches and one segment of 14.53 inches. These were denoted as SPAN2-12.

The second frame had a length of 6 feet and 11 inches. This second frame element was divided into three equal length segments, 24.36 inches, and one segment of 9.82 inches. This section was defined as SPAN2-7.

Finally, the last frame had a total length of sixteen feet and three inches, which was divided into eight segments and was denoted as SPAN2-32. Figure 3.28 shows more closely the distribution of the four types of frame elements used to model the steel girders. This representation goes from one end of the bridge up to midpoint of the second span.

The concrete deck was modeled using four-node, thick-shell elements. It was decided to use a thick element over a thin element because the mesh used in this model created elements with a ratio of the thickness to the larger length larger than the recommended value of 0.1 for thin elements. The shell element has the ability to combine the out of plane deformation (beam behavior) of plate, with the in-plane deformation (membrane behavior) of a plane stress/strain element. This characteristic makes it the ideal element to represent the behavior of the concrete deck. The thickness, material types and nodal locations are the only inputs required to create a shell element.

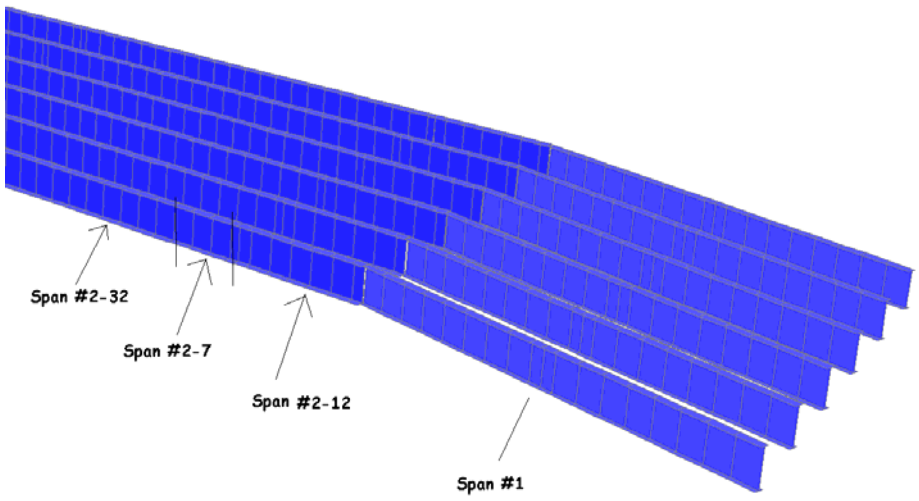

Fig 3.28 Frame element segments.

The concrete deck was broken up into four rectangular elements. These elements had the same orientation and length as the girders below them. For instance, the first span had a horizontal inclination of approximately nineteen degrees and the second span had approximately seven degrees. These two values corresponded with those from the girders below the concrete deck. Figure 3.29 shows a plan view of the different rectangular elements that were used to model the concrete deck of the bridge.

The four spans of rectangular shell elements were subsequently divided into smaller elements. The modeling criteria used to divide the various spans into smaller elements was the same criteria used for the steel girders. For example, the shell elements of the first span were longitudinally divided into smaller segments of 25.68 inches and the second span into elements of 24.36 inches. Laterally, these elements were divided according to the loading case that was being analyzed. The load-distribution factors are analyzed based on how many traffic lanes the bridge can provide and what girder, (exterior or interior), is being considered for the analysis.

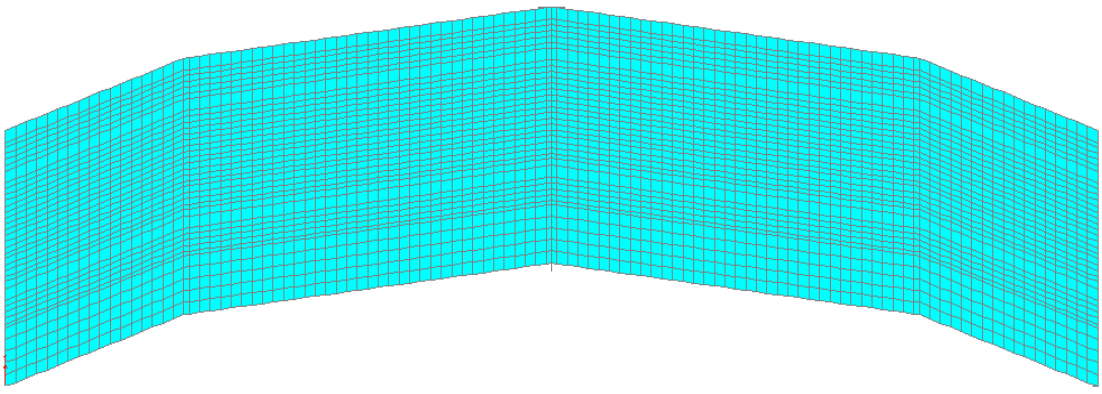

Fig 3.29 Concrete deck finite element representation.

Depending on the load case being studied, the truck's wheels will be applied at different locations, which will be explained in more detail in Section 3.5. Since the main intention was to apply the simulated truck's wheel loads onto the corresponding shell nodes, the shell elements nodes had to coincide with the truck's wheels positions by changing the nodes distribution for each case. In all cases, the shell elements aspect ratio did not exceed the recommended value of four.

Since the steel girders had different web thickness in many sections, the centroid of some elements didn't coincide in the same plane. For instance, Span #1 had an eccentricity of 25.375 inches, while Span 2-32, Span 2-7 and Span 2-12 had eccentricities of 31.985 inches, 29.89 inches and 27.12 inches respectively. As a consequence, the frame elements nodes were placed at different distance bellow the shell element nodes, leaving a discontinuity between frames elements of different eccentricity, as shown in Figure 3.30. This modeling issue will be later discussed in the following pages.

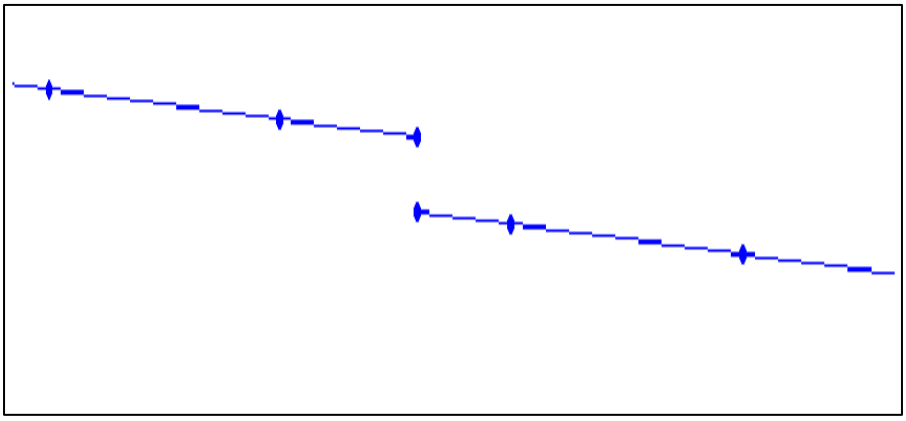

Fig 3.30 Discontinuity of the frames elements due to change in eccentricity**.**

The barriers were modeled using solid elements in SAP. The selection of the solid elements was due to the irregular shape that the barrier element presents. The solid elements were longitudinally divided according to the longitudinal distribution of the deck mesh. Laterally, it was divided into two segments of equal length. The total height of 42 inches was divided into segments of 10.50 inches. The bottom nodes of the barrier elements were placed at a distance of 4 inches from the deck's nodes, which simulates the exact condition of the barriers on top of the concrete deck. Figure 3.31 shows a typical cross section of the bridge including the barrier elements.

After the frame elements for the steel girders, the shell elements for the concrete deck and the solid elements for the barriers were applied the model, the next step was to determine how these three structural elements would be connected so they would behave as a composite member. With the use of embedded shear studs, the bridge superstructure was designed to behave compositely, where no sliding between the concrete deck and the girders was allowed.

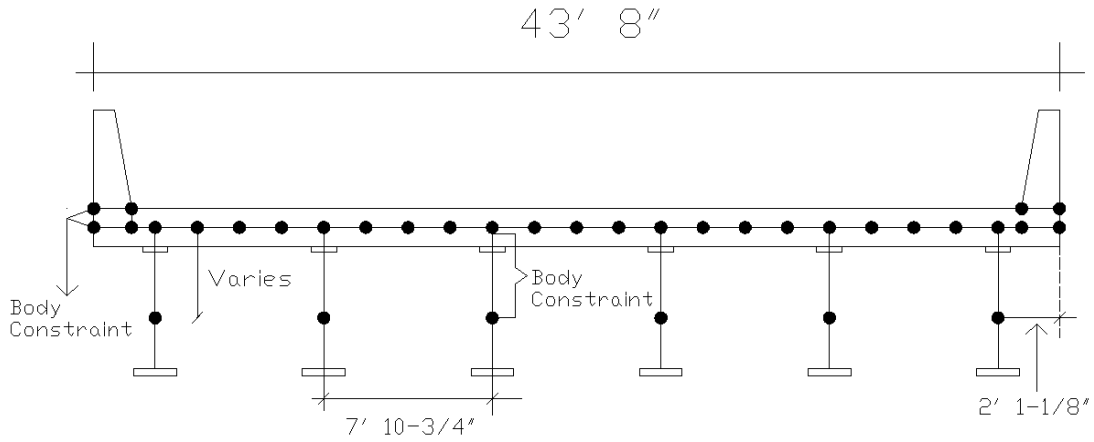

Fig 3.31 Typical cross section of the 8th North Bridge model.

Also, the barrier was cast at the same time as the pre-cast concrete panel, creating a monolithic concrete structure. These conditions had to be replicated in the finite-element model. After evaluating many different options, it was decided to use an internal SAP member called a Body Constraint. A body constraint causes all of its constrained joints to move together as a three-dimensional rigid body. As a result, all degrees of freedom at each connected joint experience the same displacement.

Figure 3.32 shows graphically how a body constraint behaves. All the nodes are working as a rigid body by maintaining the alignment between them, in spite of the loading conditions. This condition clearly represents the behavior of a cross section that remains plane after bending deformation occurs, which is an assumption that is assured in the beam theory.

Approximately 1,670 body constraints were used in this model, constraining every pair of nodes that were located within a specified range. A range of 32 inches was used to combine the deck mesh with the frame elements, while 4 inches and 8.5 inches were used for the concrete barrier and the curb element, respectively. The body constraint was also used to combine the frame elements that presented some discontinuity due to the change in eccentricity. For this purpose, a range of 3 inches was used.

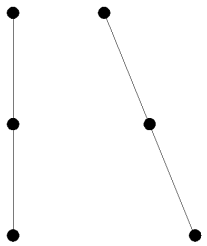

Fig 3.32 Body constraint behavior.

The second finite-element model was created in order to include the effects of the sidewalk component into the analysis. As it has been discussed in the previous section, the sidewalk was poured simultaneously with the concrete deck, creating a monolithic structure without any cold joints. Therefore it is believed that this component would have had a tremendous effect on the load-distribution factor, since it might add more rigidity to the exterior girder. This would result in a larger moment for the exterior girder and relative smaller moments for the interior girder, compared to those obtained from the analysis without the sidewalk. In addition, and maybe more important, the sidewalk alters the loading locations for the bridge deck.

The sidewalk element was modeled using four-node shell elements. The sidewalk's nodes were placed at a distance of 8.5 inches from the deck nodes, as can be observed in Figure 3.33. The sidewalk had a thickness of nine inches, in addition to the eight inches of the concrete deck. The overall width of each element was 72 inches, which was later divided into three smaller segments of 24 inches each, as can be seen in Figure 3.33.

The sidewalk shell elements had the same structural characteristics as the deck elements, except for the thickness. Nevertheless, since they were created in different meshes, they had to be connected by means of a body constraint. In total, 840 body constraints were used to connect the sidewalk mesh with the deck mesh. These body constraints were created by connecting every single pair of nodes located within a distance of 8.5 inches. Figures 3.34 and 3.35 show a graphical representation of the bridge, including the sidewalk element.

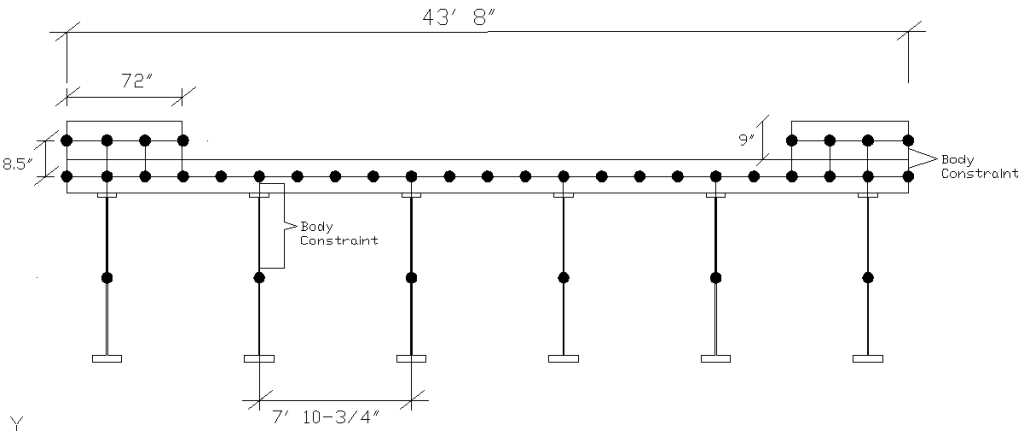

Fig 3.33 Typical cross section of a model including the curb.

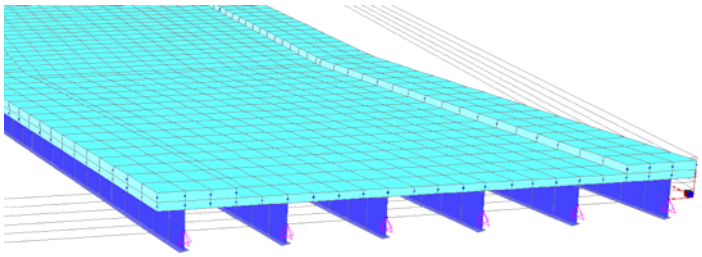

Fig 3.34 3-D View of the modeling of the bridge with the curb.

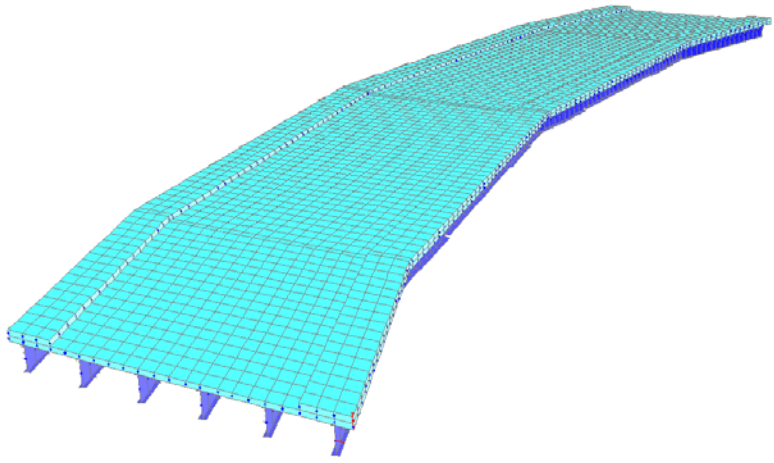

Fig 3.35 3-D view of the model.

3.3.2 Boundary conditions

The pier caps, columns and beams, which supported the bridge, were not explicitly modeled because they were considered to be very rigid in comparison to the other structural elements. Instead, the boundary conditions were modeled by placing rigid vertical supports at the end of each span, and horizontal springs in the X and Y local directions. These horizontal springs were assigned initial values, which were varied until the response of the structure matched the results obtained from the live load test. Figure 3.36 shows an example of the application of the support and horizontal springs in the FEM.

One particular characteristic of the 8th north bridge is that the concrete panels were not continuous over the location of the pier caps, as is shown in Figure 3.37, but presented some kind of discontinuity. As previously described, these concrete panels were connected through compressive joints, which are basically used to prevent the water from going down to the supports structures.

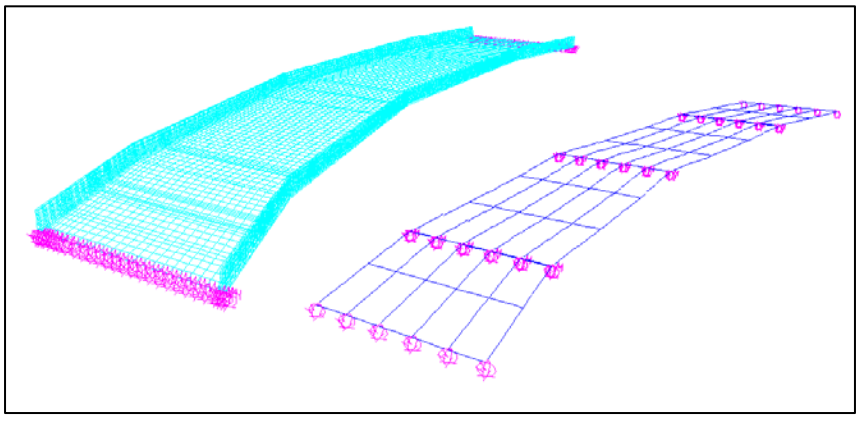

Fig 3.36 Vertical supports and horizontal springs in the FEM.

.

Fig 3.37 Supports at the pier caps.

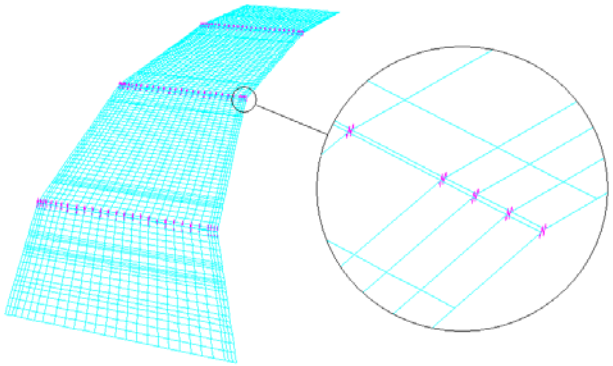

Fig 3.38 Representation of link elements on the FEM model.

So, in order to model this connection of the concrete panels, two-node link elements were chosen to represent this condition. These link elements were assigned initial stiffness values, which were varied accordingly to the calibration process of the model. Figure 3.38 shows the application of these elements into the model. Moreover, it can also be noted from figure 3.37 that the steel girders were not continuously connected over the pier caps. This particular condition was also taken into consideration in the FEM by

simply separating the nodes at the pier locations, so that there would not be any connection between frame elements of different spans.

3.3.3 Truck load and loading path description

The three-axle dump trucks used for the live-load test of the 8th North Bridge were represented in the FEM as a two-axle truck by combining the two rear axle into one. This was done to simplify the modeling process and the application of the live loads into the model. As a result, the simulated truck was composed of two axles separated by an average distance of 235.5 inches and an average width of 78 inches. Figure 3.39 shows an example of how the geometric dimensions of the test truck were incorporated into the model. The wheel loads produced by the trucks were represented as point loads and were placed accordingly to the geometry of the trucks.

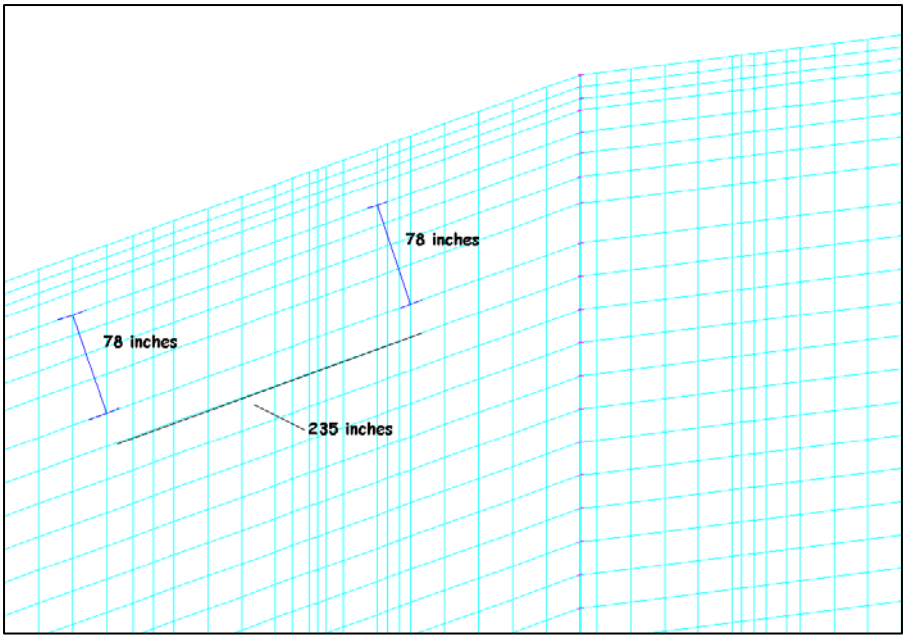

Fig 3.39 Loading truck dimensions in the FEM.

For the finite-element analysis only one loading path, Y6 path, was used to calibrate the model. However, the accuracy of the model to replicate other loading paths will be demonstrated in the following pages. The simulated truck was longitudinally placed at different positions along loading path Y6. For each position, the model was run and the results were recorded. These results would later be used for comparison with the data obtained from the live load test.

Approximately 123 different positions were evaluated along path Y6. Y6 was selected among the other loading paths because it was the easiest to locate on the concrete deck and because its trajectory was parallel to the orientation of the bridge spans. Because of this last characteristic, highly distorted elements were avoided in the concrete deck mesh. Figure 3.40 shows the trajectory of the test truck along the Y6 path was adapted into the finite-element model.

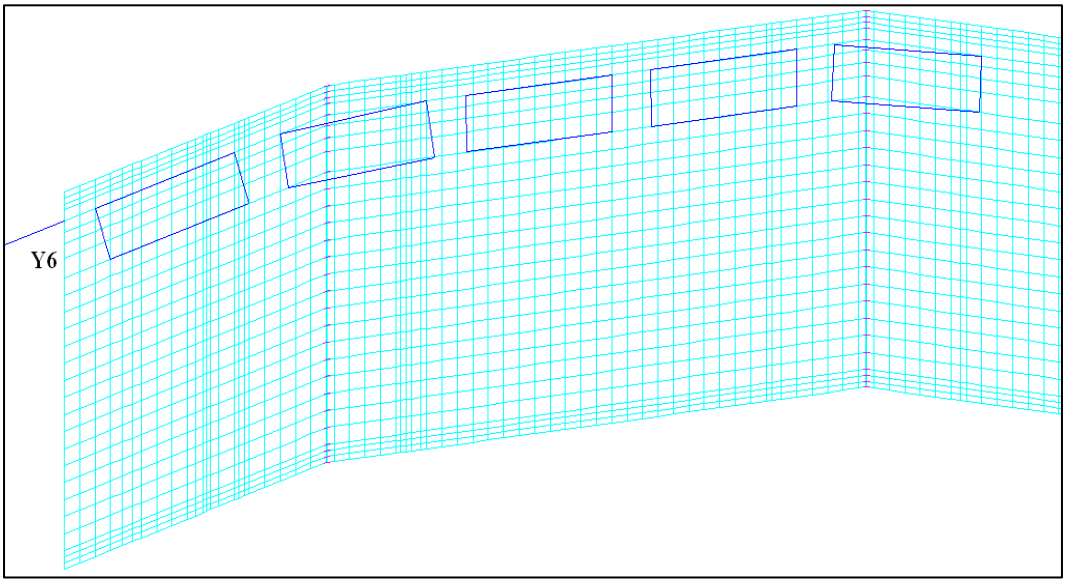

Fig 3.40 Y6 Loading path in the FEM.

3.4 Comparison of FEM and Live-Load Test results

In the creation process of the finite-element model, 15 different locations were chosen for the comparison between the FEM and the live-load test results. These 18 locations represented 9 strain gages and 6 LVDTs used in the 8th North Bridge test, which were placed underneath the steel girders. The strain gages used in this comparison were located in sections AA, BB and DD, while the LVDTs belonged to section EE. Figure 3.41 presents the locations of these strain gages on the FEM. These sensors were selected because they were easy to locate on the FEM and because they gave a good idea of the behavior of the bridge at the beginning and at the mid-span of every span on the bridge, as can be noticed from Figure 3.41.

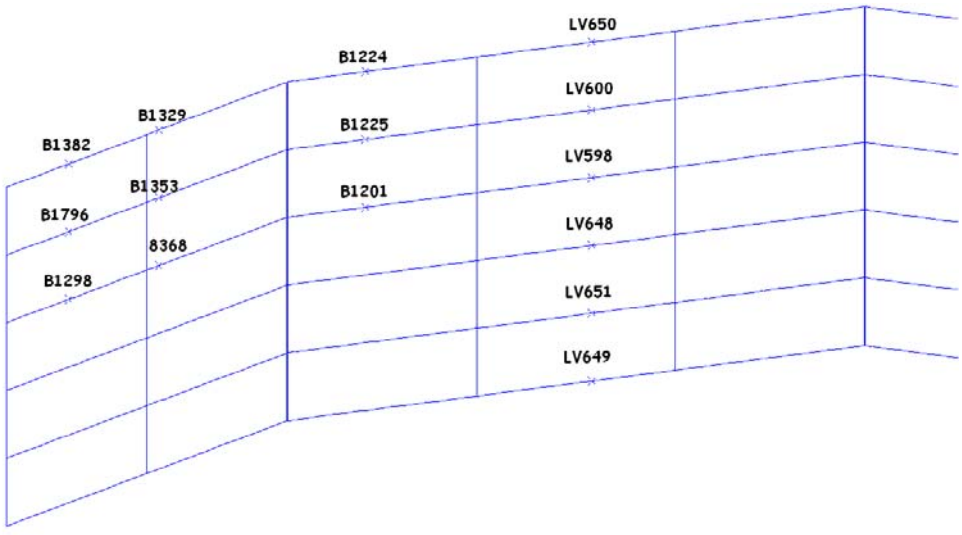

Fig 3.41 Y6 Location of sensors and LVDTs used in the FE analysis.

The LVDTs deflections obtained in the live load test were directly compared with the results recorded in the computer program. This was possible due to the fact that in SAP2000 the displacements can be directly recorded from any specific point of the model.

On the other hand, the comparison between the strain gages measurements recorded during the live-load test and the FEM result was not that easy to perform, since the strain measures can not be recorded directly from the FEM results. These strains measures were calculated using a different approach. Two different approaches were taken into consideration in this issue.

The first approach consisted in recording the X and Y global displacements from the nodes of the concrete mesh that were placed above the strains gages location, and the nodes from the steel girders at those locations. These global displacements were then converted into local displacements according to the orientation of the spans in the model.

An associate strain was calculated by dividing the local displacements by the longitudinal length of the segment that contained the specific node. As a result, the strains at the centroid level of the concrete deck and steel girder would be obtained. However, the strains from the selected sensors were measured at the bottom of the steel girders, not at the centroid. This situation was resolved by calculating these strains using similar triangles. Figure 3.42 shows a better representation of this approach.

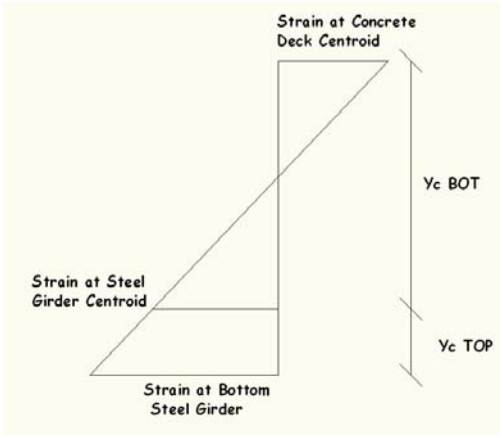

Fig 3.42 Triangular strain distribution at the composite section.

The second approach consisted in using the internal forces of the frame elements, obtained from the finite-element analysis, to calculate the strains at the bottom of the steel girders. These forces combined, axial force and moment produced a stress at the bottom of the frame element that was later converted into strain by simply dividing the stress by the modulus of elasticity of the steel girders. The two approaches generated similar results. The second approach was chosen since it was the easiest to compute among the two options.

The calculated strains and deflections for the different locations were plotted against the truck's position in the model and were directly compared with the live-load test results. Initial variation between the FEM and the live load test results were observed. The deflections of the LVDT data were used to calibrate the model. Initial values of the spring and link elements properties were varied until FEM results were closely matched with the live-load test results. Table 3.2 shows the final values of these parameters. Finally, the strain data from the strain gages were compared with FEM results to prove

the model's accuracy. Figures 3.43 through 3.54 show all the plots that were generated in the analysis.

Table 3.2 Elements Final Values

	Element Stiffness	
	X-local	Y-local
Link Elements	10 kip/in	0
Hor. Spring Girders End Support	11,000 kip/in	0
Hor. Spring Girders Interior Support	50 kip/in	50 kip/in
Hor. Spring Deck	1,000 kip/in	1,000 kip/in

-LVDTS

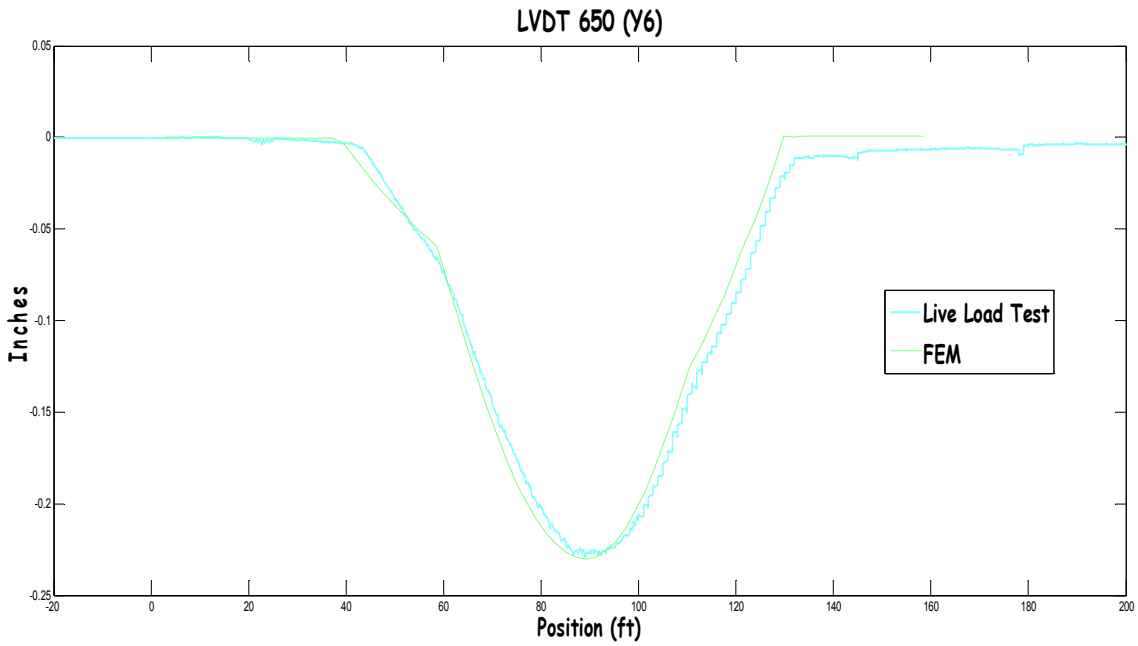

Fig 3.43 Comparison between FEM and load test (LVDT 650).

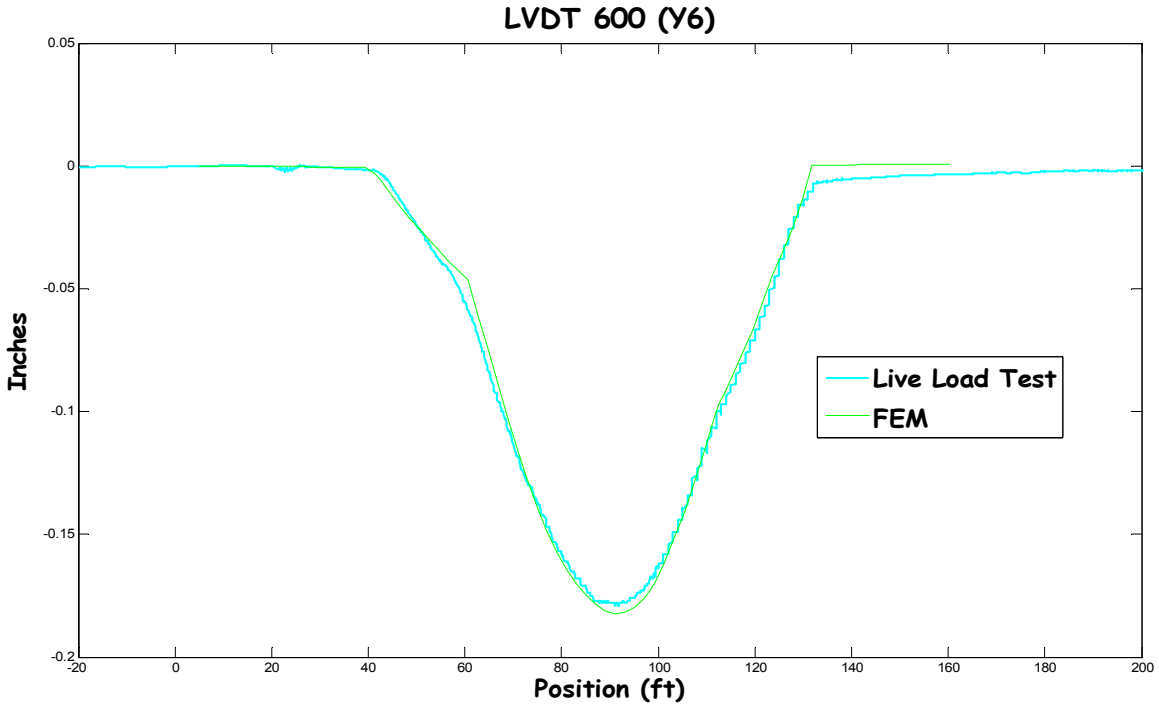

Fig 3.44 Comparison between FEM and load test (LVDT 600).

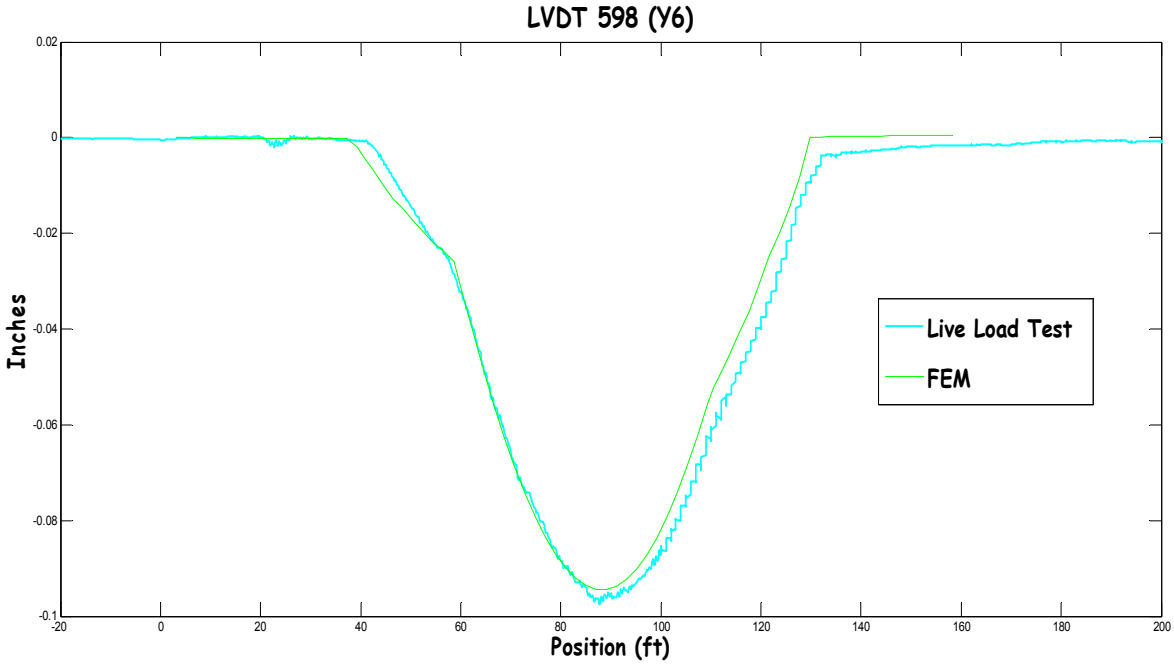

Fig 3.45 Comparison between FEM and load test (LVDT 598).

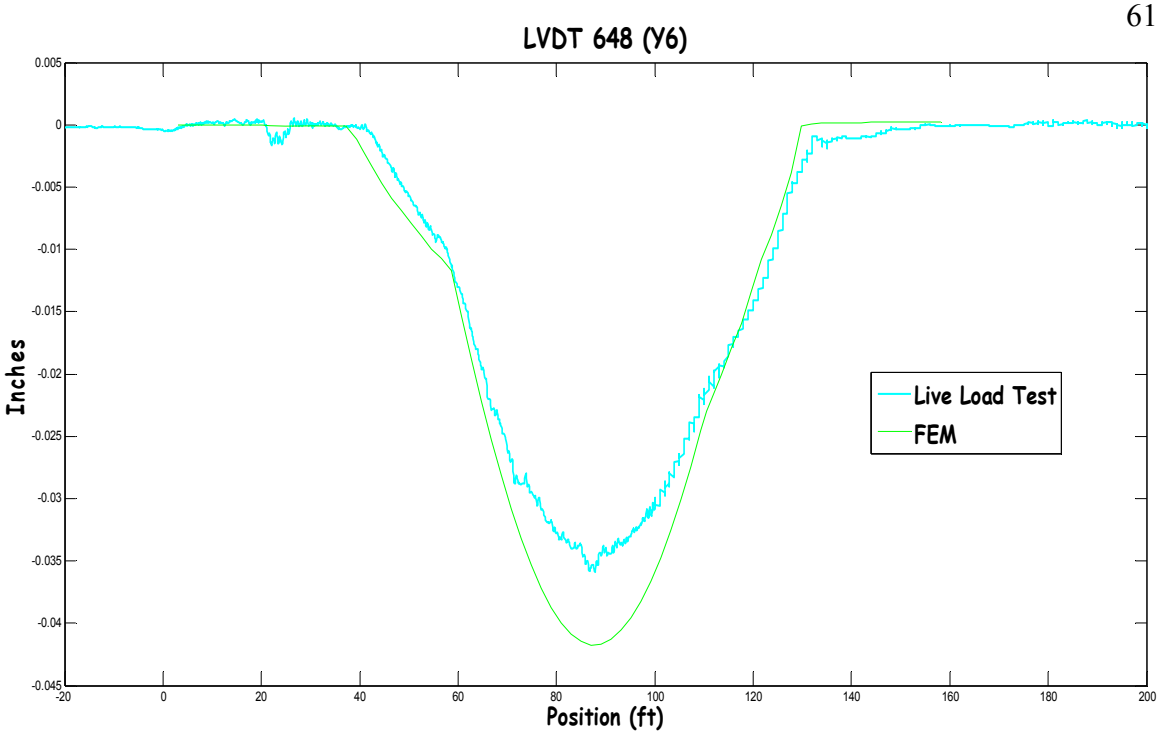

Fig 3.46 Comparison between FEM and load test (LVDT 648).

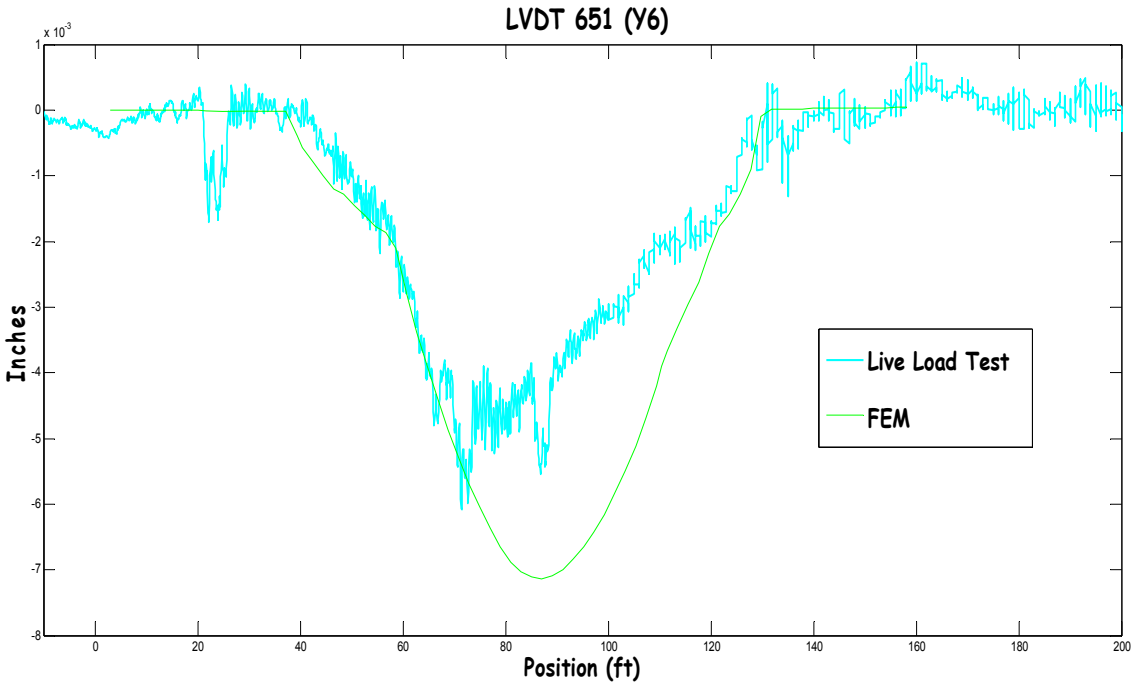

Fig 3.47 Comparison between FEM and load test (LVDT 651).

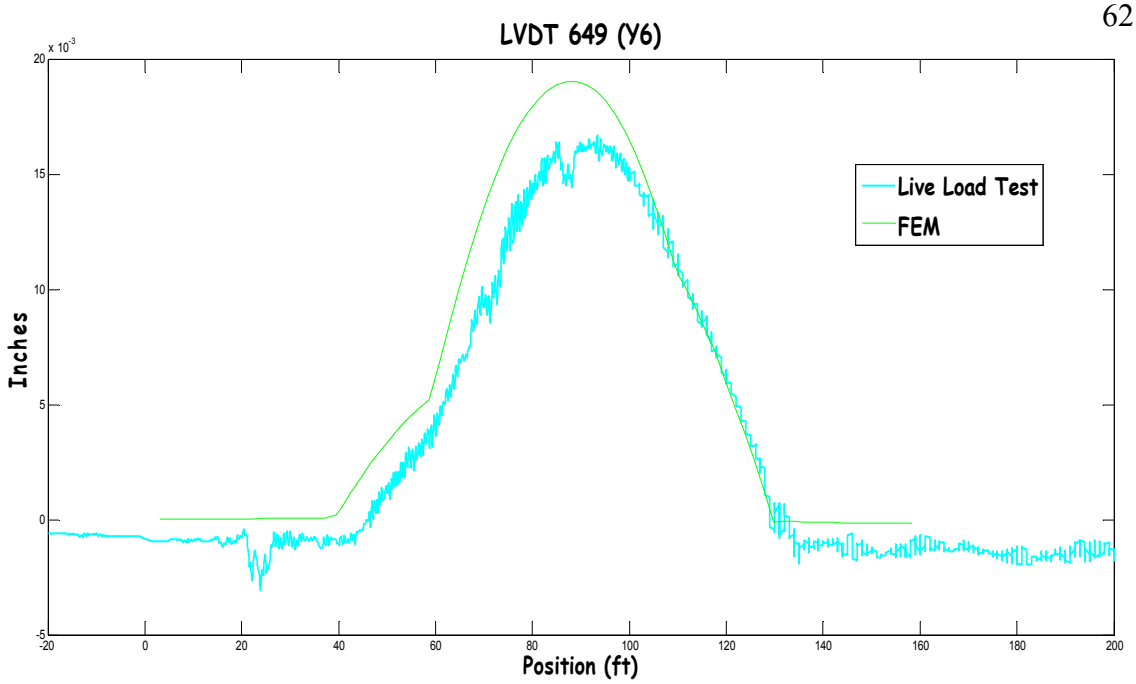

Fig 3.48 Comparison between FEM and load test (LVDT 649).

-Section AA

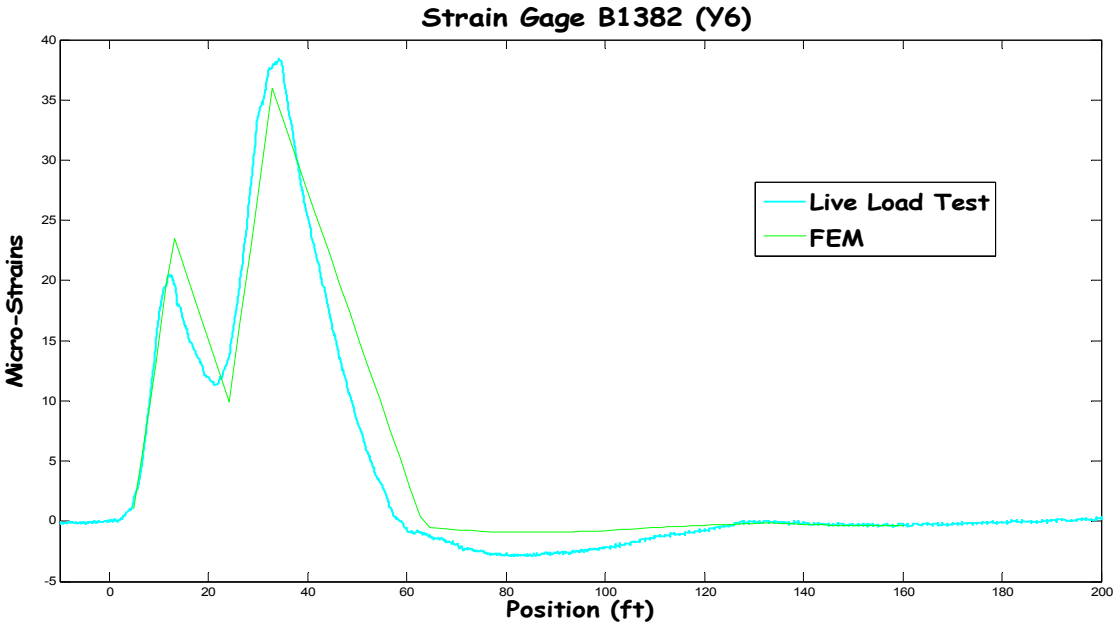

Fig 3.49 Comparison between FEM and load test (Strain GageB1382).

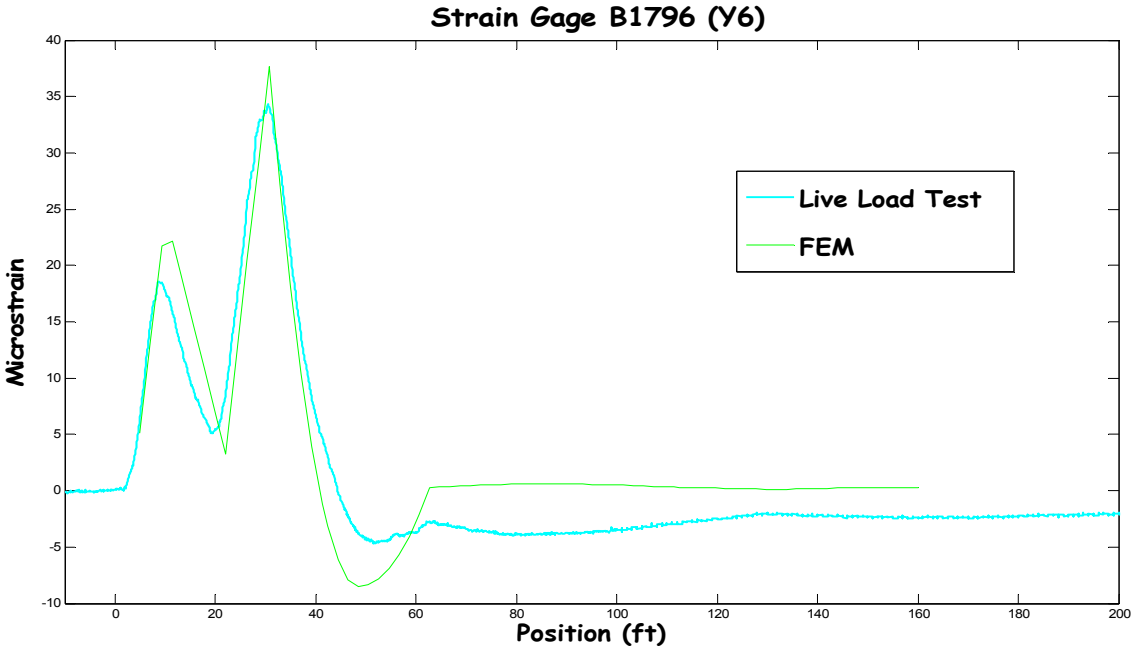

Fig 3.50 Comparison between FEM and load test (Strain Gage B1796).

-Section BB

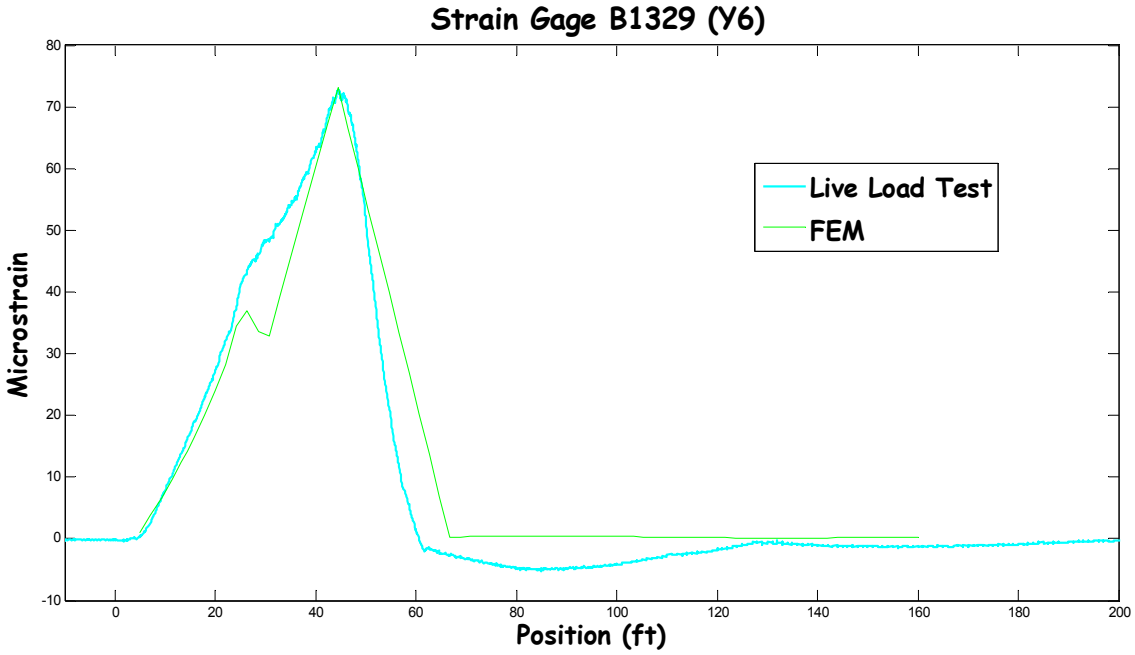

Fig 3.51 Comparison between FEM and load test (Strain Gage B1329).

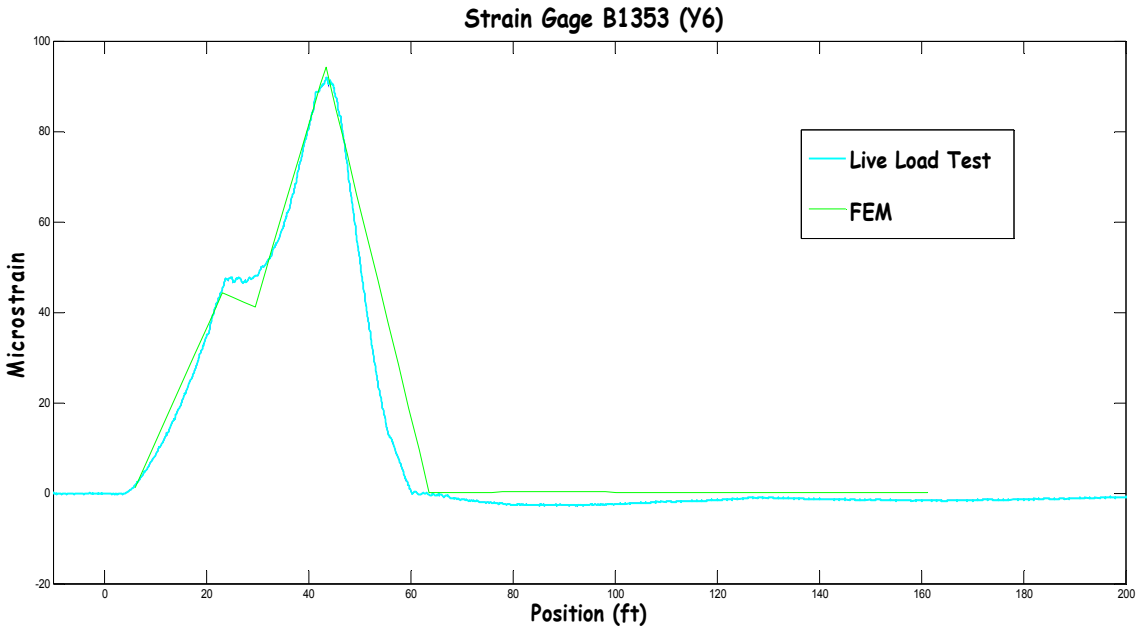

Fig 3.52 Comparison between FEM and load test (Strain Gage B1353).

-Section DD

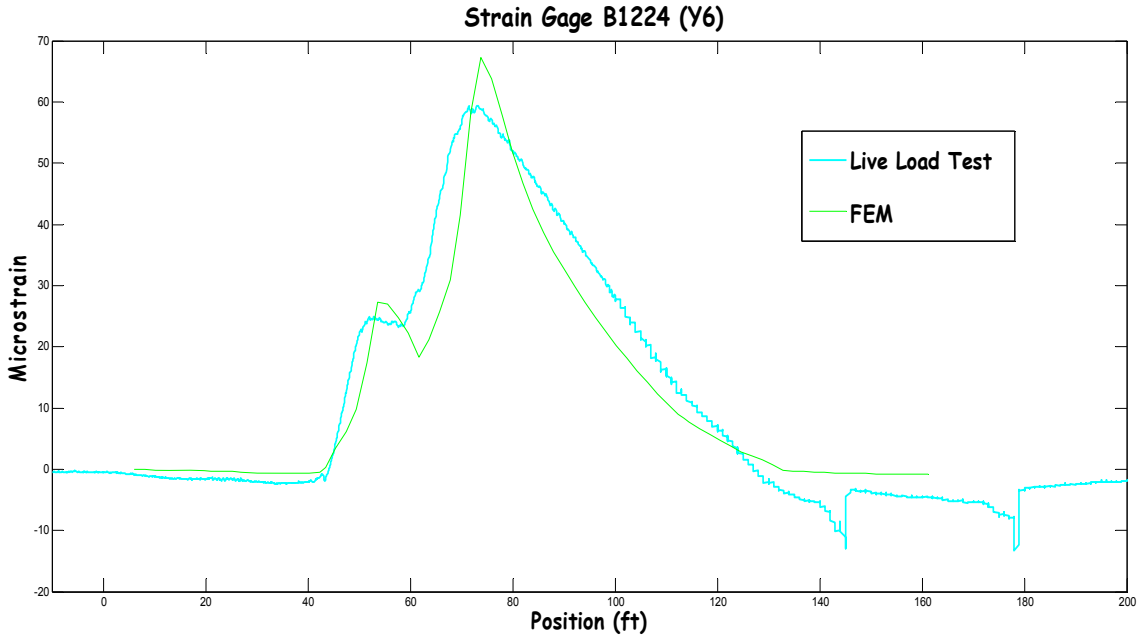

Fig 3.53 Comparison between FEM and load test (Strain Gage B1353).

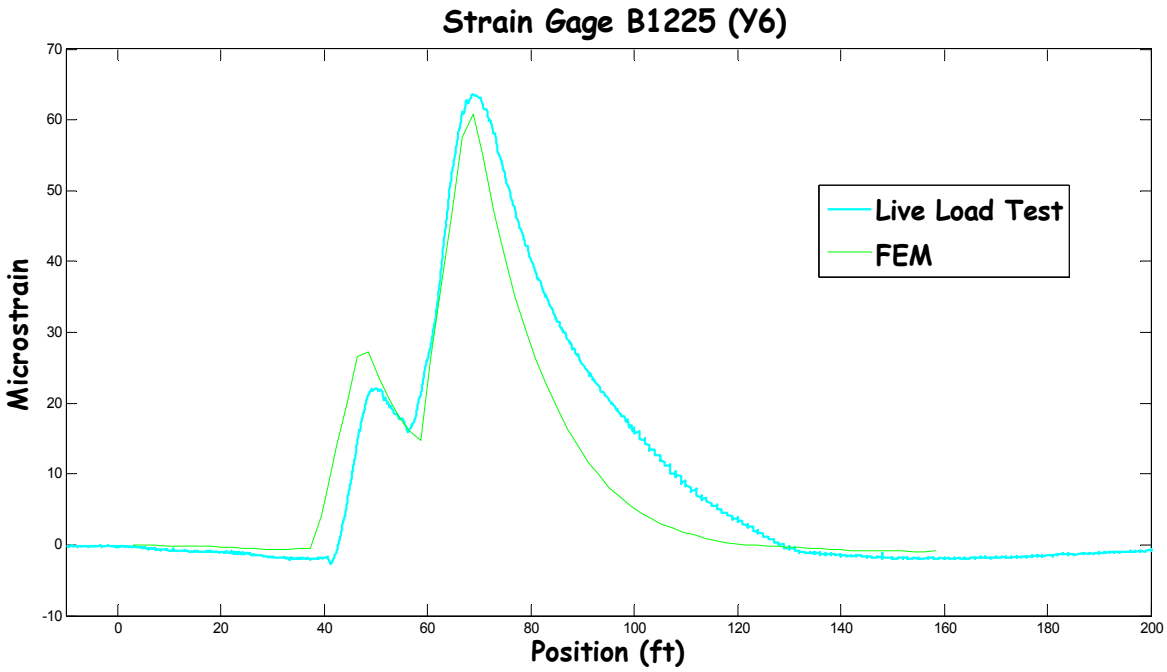

Fig 3.54 Comparison between FEM and load test (Strain Gage B1353).

As can be observed in Figures 3.43 through 3.54, the response obtained from the finite-element model was very close to that recorded from the live-load test. In terms of displacements, the FEM produced results that were closer to the live-load test, while the strain results were still close to the actual response. This is because the LVDTS measures were the one used for the calibration process of the model, while the strains in the selected points were plotted just for merely comparison. In all cases, the strains were either matched or overestimated by the FEM.

Another comparison between the FEM and the live-load test was performed by plotting the deflections and strains values from both cases against each other. A linear best fit line was created to quantify how close finite-element model replicate the actual behavior of the superstructure. Figure 3.55 and 3.56 show these comparisons.

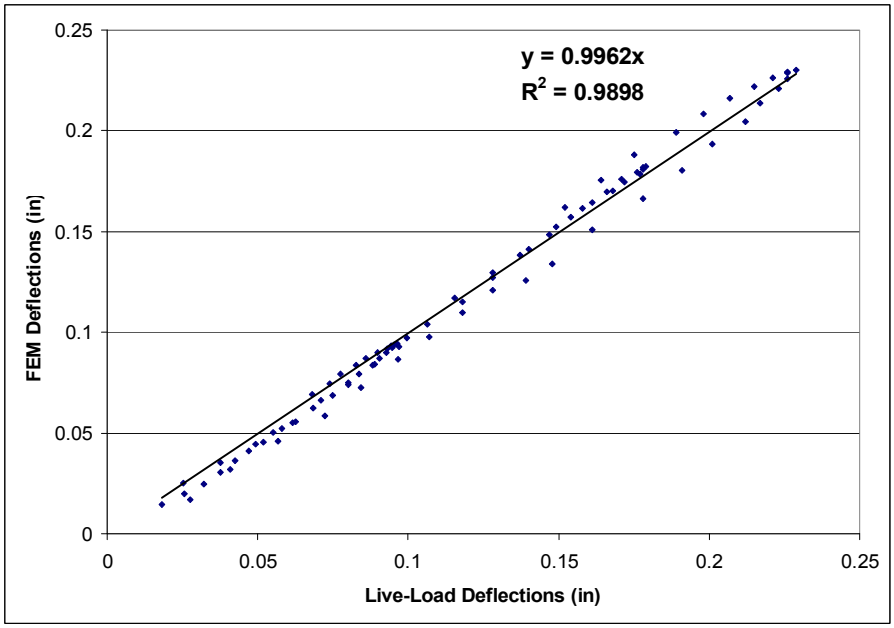

Fig 3.55 Deflection values from all LVDTS.

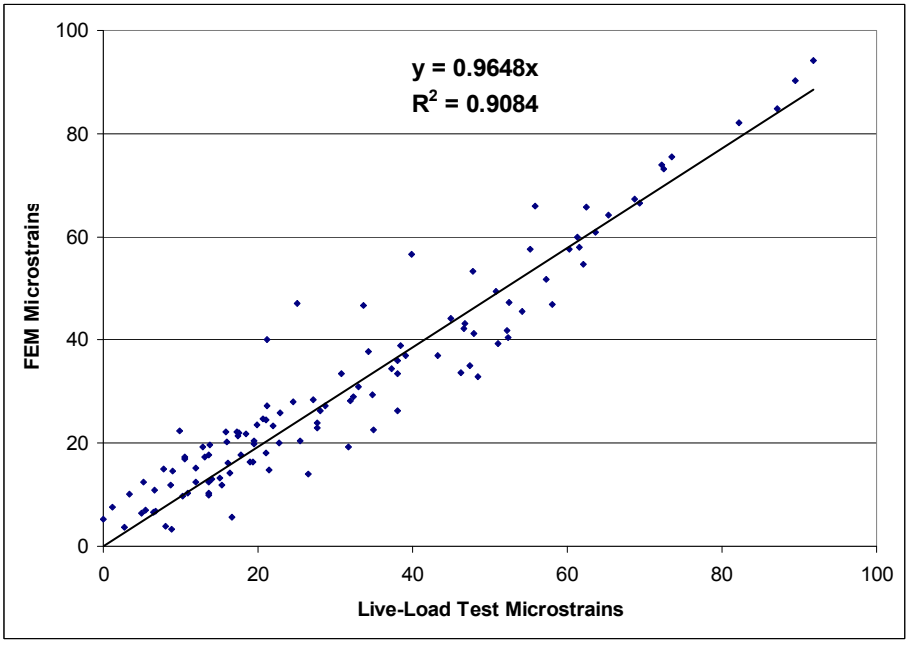

Fig 3.56 Strain values from Sections BB, AA and DD.

In Figure 3.55 it can observed how the deflections obtained from the FE model correlate with those obtained from the live-load test. In this figure the best fit line has a slope of 0.9962, which means that the FE deflections are within the 0.38% of the actual deflections. It can also be noted from the figure that the correlation factor, R^2, has a value of 0.9898, which shows a very good correlation between the FEM and the load test.

Figure 3.56 shows the comparison between the calculated strains from the FEM and those obtained from the live-load test. The best fit line from this figure presents a slope of 0.9648, meaning that the data from the FEM is within 3.52% of the actual strains. The R^2 value on this figure was computed on 0.9084, which denotes a good correlation between the two data. The difference between the results from both figures is expectable since the finite element method is more accurate for the evaluation of displacements.

Another comparison was analyzed to verify the accuracy of the finite-element model. The transversal distribution of the FEM moments over the width of the 8th North Bridge was compared to that from the load test. The maximum moments from both results were plotted for each girder and compared in a graph. Figures 3.57 and 3.58 show these comparisons. Figure 3.57 presents the moment distribution across Section EE. It can be observed from this figure that the calculated moments for all the girders either matched or exceed the measured values of the live-load test. The maximum measured moment was within 3% of the finite-element moment. Figure 3.58 shows the moment distribution across Section BB. The maximum computed moment exceeded in 5% the maximum measured moment, as can be appreciated in this figure.

Figures 3.59 through 3.62 show a similar comparison using the load paths Y1 and Y3. As can be observed from these figures, the finite-element model either matched or exceeded the measured values. The maximum measured moment was within 4% of the finite-element model, for both cases. Figures 3.63 and 3.64 present the same comparison using the displacements recorded in the live-load test for Y1 and Y3. It can be observed that the FE displacements are very close to the measured displacements (within 4%).

According to the longitudinal and transverse comparison between the finite-element model results and the live-load data, it has been shown that the computer model used in this analysis has the ability to accurately replicate the structural behavior of the 8th North Bridge due to any imposed live load. There fore, this model is considered to be adequate and will be used to determine load distribution factors.

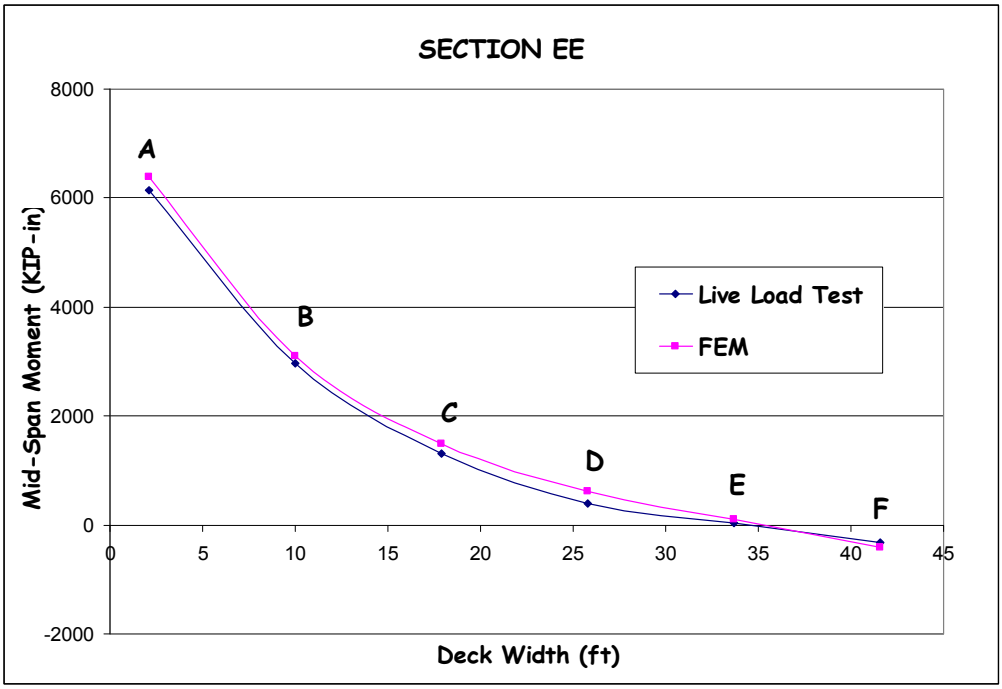

Fig 3.57 Transverse comparison between FEM and live-load test for Y6 (Section EE).

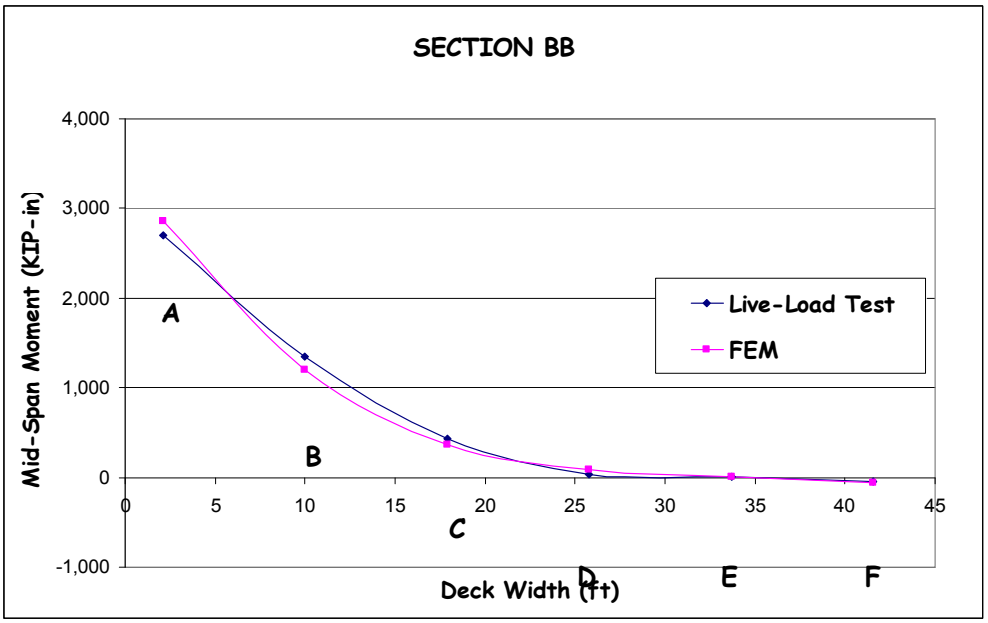

Fig 3.58 Transverse comparison between FEM and live-load test for Y6 (Section BB).

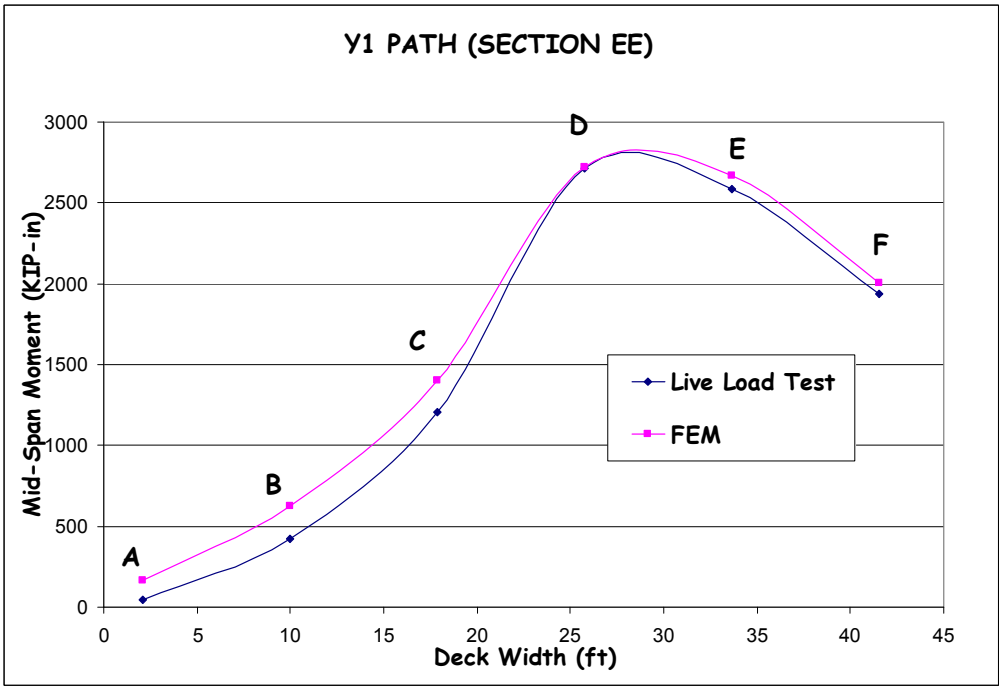

Fig 3.59 Transverse comparison between FEM and live-load test for Y1 (Section EE).

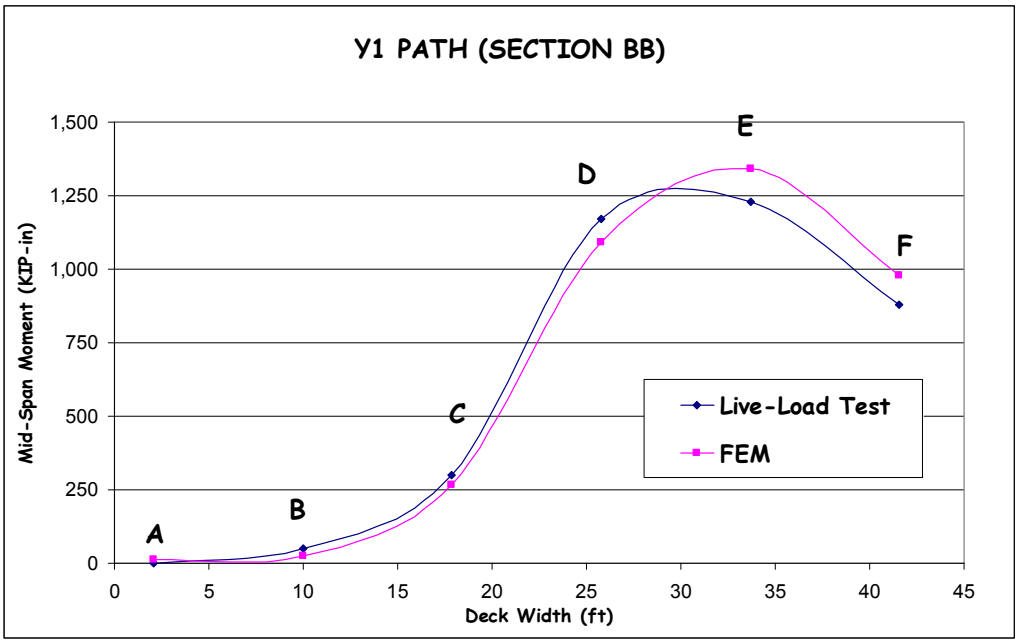

Fig 3.60 Transverse comparison between FEM and live-load test for Y1 (Section BB).

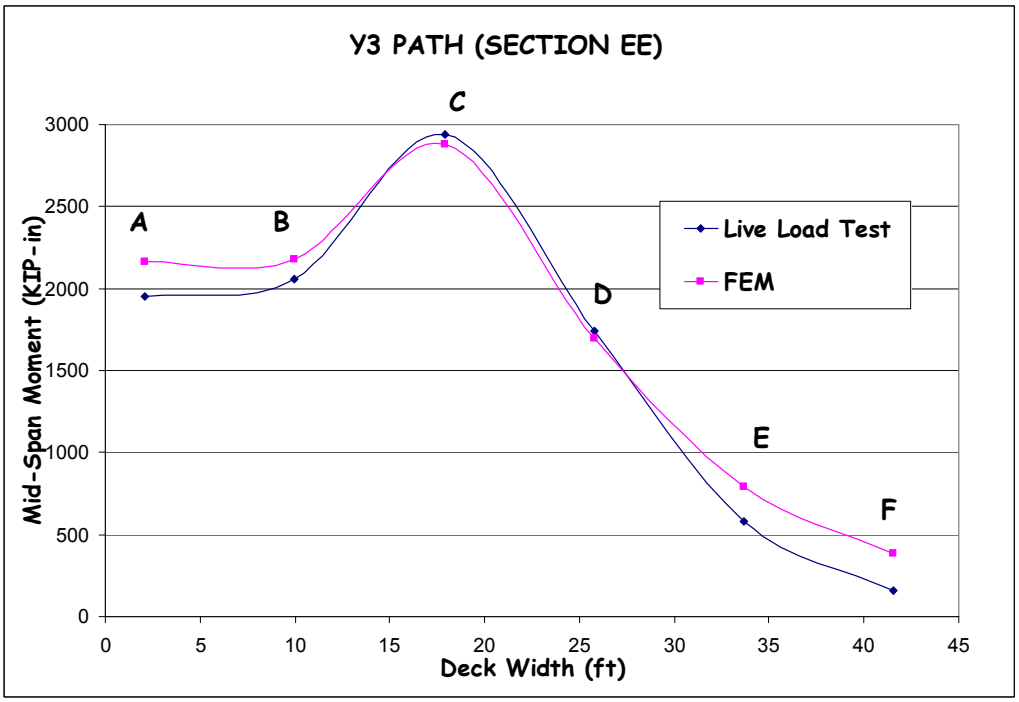

Fig 3.61 Transverse comparison between FEM and live-load test for Y3 (Section EE).

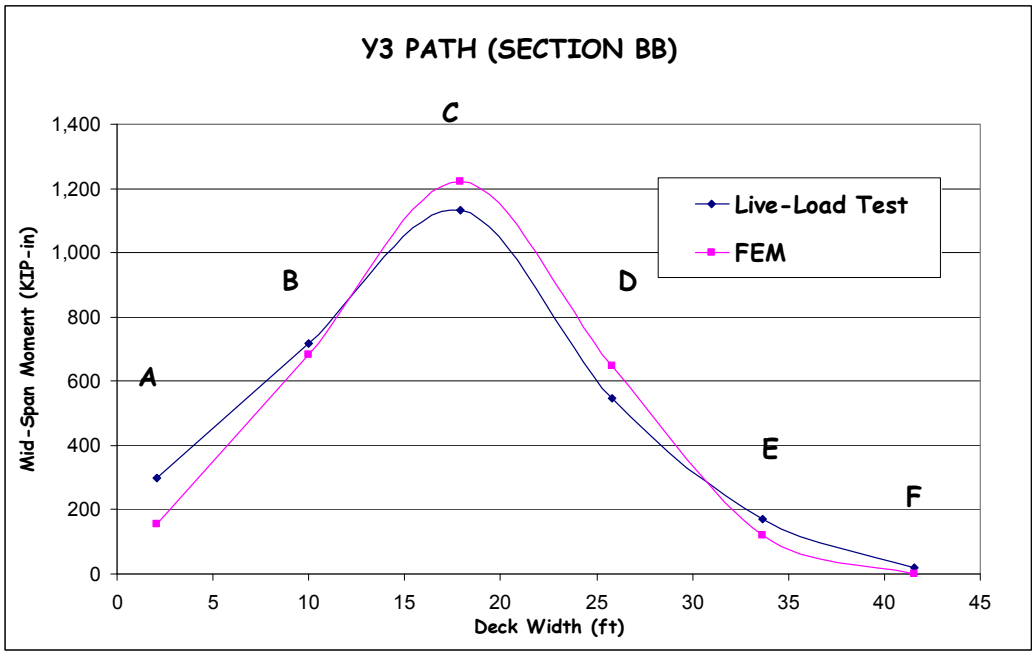

Fig 3.62 Transverse comparison between FEM and live-load test for Y3 (Section EE).

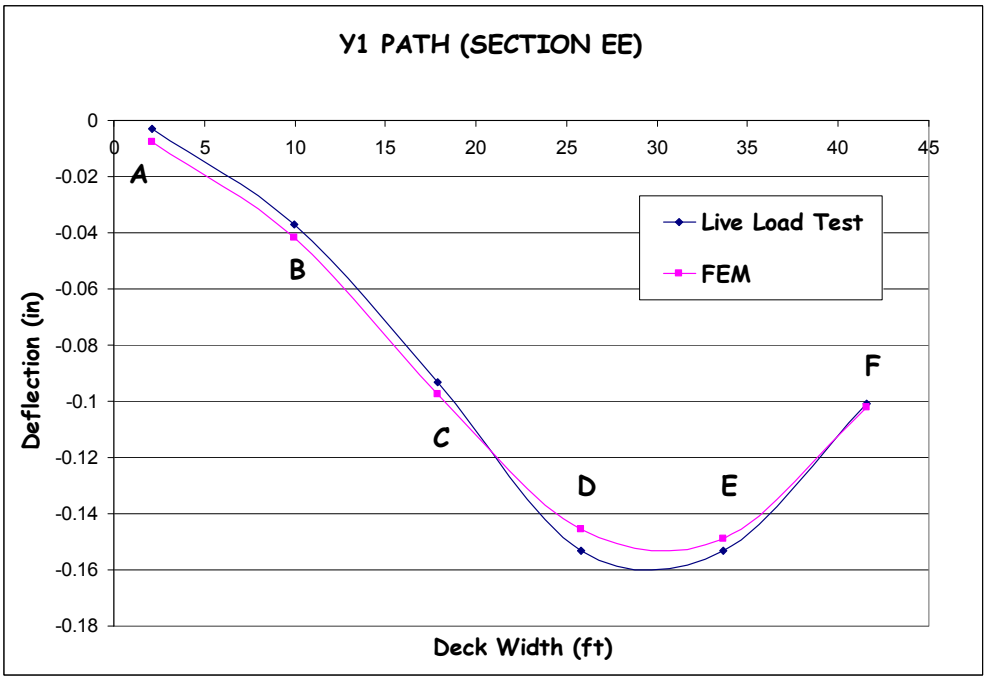

Fig 3.63 Transverse comparison between FEM and live-load test using deflections (Y1).

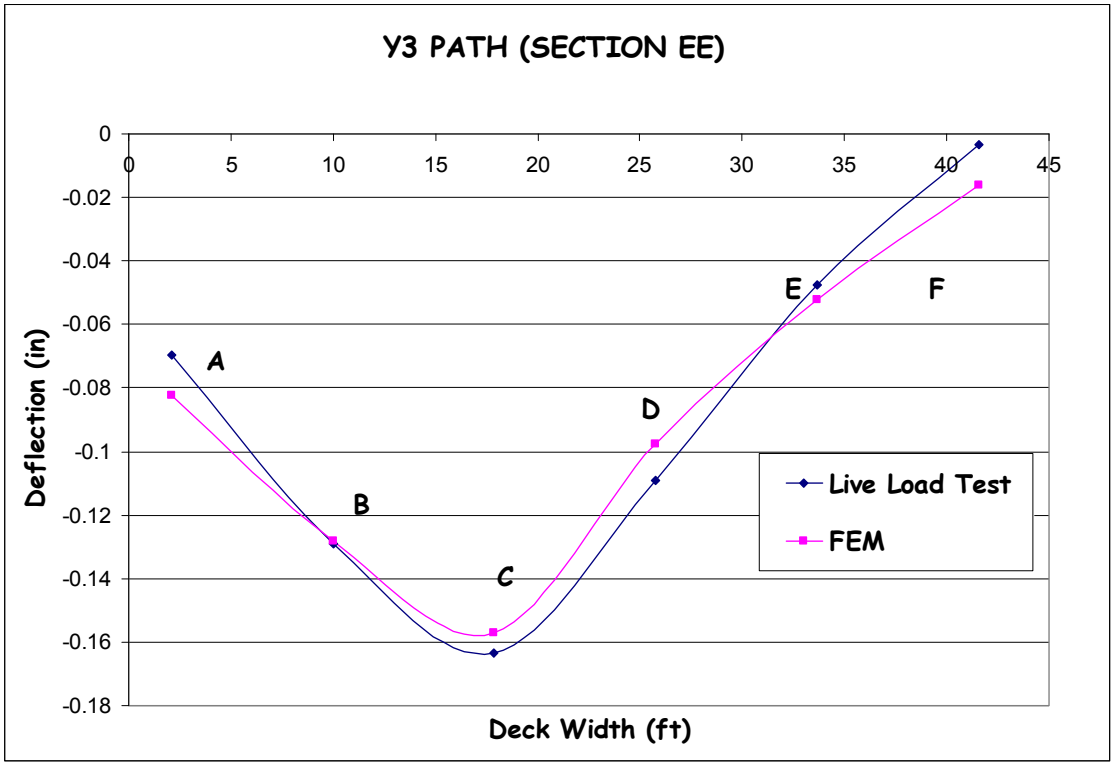

Fig 3.64 Transverse comparison between FEM and live-load test using deflections (Y3).

3.5 Live-Load Distribution Factor

The accurate estimation of the response of a bridge subjected to the effects of traffic live loads is a critical issue in the design process. The most accurate means to obtain this response may be obtained by modeling the bridge using a finite-element program. However, this process requires considerable effort and time from the designer. As a result, simpler methods have been developed to estimate the respond of the bridge, and design of its structural components.

According to the AASHTO LRFD distribution factor method, first an individual bridge girder can be idealized as 1-D beam, and its maximum response, subjected to truck loads, can be obtained using elementary beam theory. The influence that the entire bridge has on the individual beams is then obtained by multiplying the maximum response of the 1-D beam by a corresponding distribution factor. The distribution factor is defined as the ratio of the maximum response of an interior or exterior bridge girder over the maximum response of a 1-D beam, subjected to the same live load. At any longitudinal location of the live load, each bridge girder will carry portions of the live load, depending on the load location and the bridge geometric properties.

Many studies have been performed on a considerable number of bridges, using a finite-element analysis and live-load tests, with the sole purpose of developing equations that accurately estimate the value of the live load distribution factors. Two different approaches have been proposed as a result of those studies, the AASHTO Standard Specifications (1996) and the AASHTO LRFD Specifications (2006). The latter

specification is a major change from the AASHTO Standard Specifications and is the most commonly used among the bridge designers.

3.5.1 AASHTO Standard Specifications (1996)

This method is considered the simplest procedure among all the code-based distribution factor equations. The equations used in this method were obtained as a result of investigations performed by Westergaard (1930) and Newmark et al (1948). As a result, the live load distribution factors for a concrete bridge, supported with four or more steel or concrete girders and subjected to two or more traffic lanes loads, can be calculated using Equations 3.1 and 3.2, which are shown below:

1-when $S \leq 6$ feet:

$$DF = \frac{S}{5.5} \tag{3.1}$$

2-When $6\,feet < S < 14\,feet$:

$$DF = \frac{S}{(4 + .25S)} \tag{3.2}$$

where : (S= gider spacing)

These equations were derived on studies based only in non-skewed, simply supported, two-lane bridges, which limit its use to this type of bridges. In addition, it does not differentiate between exterior girders and interior girders. Unlike the AASHTO LRFD Specifications (2006), this method does not include an internal multilane reduction factor and does not provide a separate equation for the distribution factor for shear.

3.5.2 AASHTO LRFD Specifications (2006)

The AASHTO LRFD Specifications (2006) were created as a result of an intensive research program performed on bridges listed in the National Bridge Inventory File (NBIF), using finite-element models. This study was funded by the NCHRP, and considered many important parameters that were not included in the Standard Specifications such as girder stiffness, span length, girder spacing, continuity and skew. According to AASHTO LRFD Table 4.6.2.2.2b-1, the moment distribution factor for an interior girder of a non-skewed bridge is calculated using Equations 3.3 and 3.4 shown below.

-For one design lane loaded:

$$DFM_I^{ns} = 0.06 + \left(\frac{S}{14}\right)^{0.4}\left(\frac{S}{L}\right)^{0.3}\left(\frac{K_g}{12Lt_s^3}\right)^{0.1} \qquad (3.3)$$

-For two or more design lanes loaded:

$$DFM_I^{ns} = 0.075 + \left(\frac{S}{9.5}\right)^{0.6}\left(\frac{S}{L}\right)^{0.2}\left(\frac{K_g}{12Lt_s^3}\right)^{0.1} \qquad (3.4)$$

where:

DFM_I^{ns} = Interior Girder Distribution Factor for Moment of non-skewed bridges

S = Girder Spacing (ft)

L = Span Length (ft)

t_s = Slab Thickness (in.)

K_g = Longitudinal Stiffness Parameter (in^4)

$= n(I + Ae_g^2)$

n = modular ratio of girder to concrete deck material

I = moment of inertia of girder (in^4)

A = cross sectional area of girder (in^2)

e_g = distance from c.g. of girder to c.g of deck (in.)

There are some requirements that have to be met in order to be able to use these equations. Table 3.3 lists a detailed description of these requirements. Moreover, these equations inherently include a multiple presence factor, which is intended to take into account the possibility of the presence of multiple trucks on the bridge at the same time. These factors are represented in Table 3.4.

Table 3.3 Requirements for Equation 3.3 and 3.4

Spacing	3.5 <= S <= 16
Thickness	4.5 <= Ts <=12
Length	20 <= L <= 240
NO. of Beams	Nb>= 4

Table 3.4 Multiple Presence Factors

No. of Design Lanes	**Multiple Presence Factor**
1	1.2
2	1
3 or more	0.9

The distribution factor for an exterior girder with two or more design lane loaded can be calculated by applying a correction factor to Equation 3.4. This correction factor is shown in Equation 3.5.

$$DFM_E^{ns} = (e) \times DFM_I^{ns} \tag{3.5}$$

where:

DFM_E^{ns} = Exterior girder distribution factor for moment of non-skewed bridges

e = exterior girder correction factor for moment

$$= 0.77 + \frac{d_e}{9.1}$$

d_e= distance between the center of exterior beam and the interior edge of curb or traffic barrier (ft) valid for $-1.0 \le d_e \le 5.5$

The AASHTO LRFD Specifications also provides a modification factor to account for the effect of skew in the calculation of the distribution factors. This modification factor is represented by Equation 3.6, which is shown below.

$$DFM_I^{skew} = (sk) \times DFM_I^{ns} \tag{3.6}$$

where:

DFM_I^{skew} = Interior girder distribution factor for moment of skewed bridges

sk = skew correction factor for moment

$$sk = 1 - \left[0.25 \left(\frac{k_g}{12Lt_s^3} \right)^{0.25} \left(\frac{S}{L} \right)^{0.5} \right] \times (\tan\theta)^{1.5} \tag{3.7}$$

θ = skew angle where $30^0 \leq \theta \leq 60^0$

The moment distribution factor for an exterior girder can be calculated by multiplying Equation 3.6 by the exterior correction factor (e).

3.5.3 The Lever Rule

The lever rule is an important tool that is used to calculate the distribution factor for exterior girders when the bridge is loaded with a single design truck. This is a very useful tool, for example, when the requirements of Equations 3.3 and 3.4 are not met and another method is required. Figure 3.65 shows a representation of a free body diagram used to calculate the shear and moment distribution factor for an exterior girder, using the lever rule.

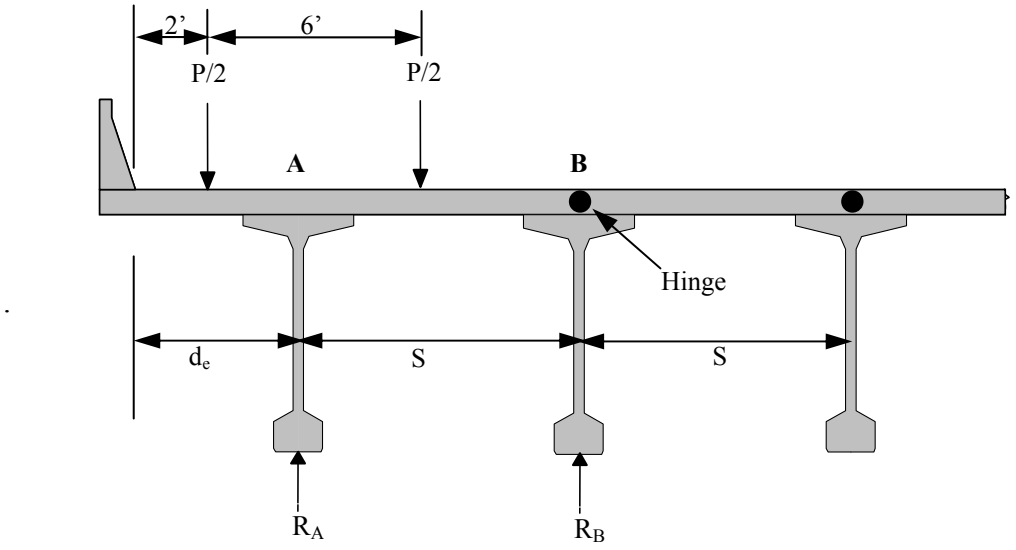

Fig 3.65 Lever Rule free body diagram.

As can be seen in Figure 3.65, a hinge has been placed at the top of every girder in order to make the analysis a lot simple.

According to Figure 3.65, the reaction Ra is obtained by taking a moment about point B. This results in an expression to obtain the value of the reaction at A, which is calculated using Equation 3.8, shown below.

$$R_A = \frac{P(S + d_e - 5)}{S} \tag{3.8}$$

This expression allows the designer to determine the fraction of the truck load P that is carried by the exterior girder. This fraction represents the moment and shear distribution factor for the exterior girder and is shown as Equation 3.9. Notice the presence of the multiple presence factor of 1.2, for a single loaded lane bridge.

$$DFM_E^{One-lane} = \frac{1.2 \times (S + d_e - 5)}{S} \tag{3.9}$$

where:

$DFS_E^{one-lane}$ = Exterior girder DFS for single lane loaded bridge

S = Girder spacing (ft)

d_e = Overhang distance (ft)

3.6 Finite Element Analysis (FEA)
Distribution Factors

The load distribution factors can also be calculated using a finite-element approach, which is considered to be more accurate than the approximate equations described in the previous sections. In order to do so, the load position that produces the maximum moment has to be determined before any analysis can be performed. This critical load location is obtained by analyzing the bridge initially as a 1-D single beam and placing the respective live loads at the position where the maximum moment is produced.

The AASHTO Standard and LRFD Specifications for Highway Bridges specifies that a HS-20 type truck should be positioned along the length of the bridge for the purpose of determining the loading critical location. A drawing of an HS-20 truck is shown in Figure 3.66. The HS-20 truck shown has three axles, separated by a distance of fourteen feet. The second and third axles have a total weight of 32,000 pounds each, while the first axle only supports 8,000 pounds. Every axle is comprised of two wheels, separated by 6 feet, and each wheel shares exactly half of the total load of the axle where they are located.

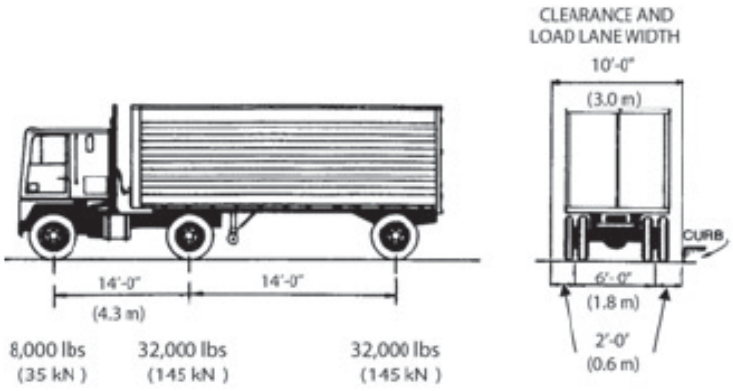

Fig 3.66 AASHTO-approved live loading specifications for standard HS20 trucks.

Initially, every span of the bridge was modeled as an independent 1-D beam. The HS20 truck loads were placed along the length of the 1-D beam and the maximum moments were obtained for every case. The program used for this analysis is called Dr. Beam. This program allows the user to run any desired load across the length of the beam, presenting, at the same time, the variation of the moment curve due to the change of position of the loads being displaced. It also allows the user to generate a moment envelope, which holds the maximum response of the beam at any location.

As shown in Figure 3.67, the bridge moment envelope has a maximum positive moment response, which is obtained by placing the truck at a critical load location along the length of the beam. The critical load location obtained from Dr. Beam was applied to the finite-element model. Many locations were evaluated using this initial location as a reference point until the actual critical load location was obtained.

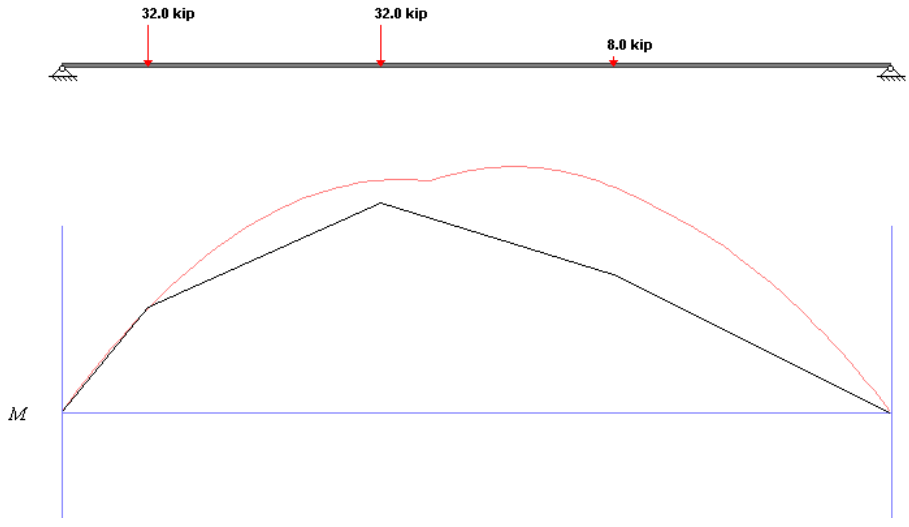

Fig 3.67 Moment envelope produced by the HS-20 truck in a particular span.

The composite behavior response at any location on the bridge deck was obtained by adding together the response of every single element that was located at the desired location. This action was accomplished by grouping all this elements through the group command in SAP2000. This command integrates every selected element into a single group, and combines every response from the group elements into composite response. Different group elements were formed close to the maximum moment response's location provided by Dr. Beam. The truck loads were placed at different longitudinal positions, and each group's total response was recorded. The location where the maximum moment occurred was then determined for the group with the maximum recorded response.

Once the critical load location was determined, the design truck was moved transversally across the width of the finite-element model. According to the AASHTO LRFD Specifications, the design truck cannot be positioned at a distance closer than 2 feet from any curb or barrier, nor it can placed closer than 2 feet from the lane boundary. This means that the closest possible distance between two trucks is 4 feet. The critical transverse position was easily obtained when one loaded lane is analyzed; however, it became more complicated when more than one loaded lane was taken into consideration. According to the AASHTO Specifications, any loaded lane placed on the bridge should have a total width of 12 feet.

As discussed in the previous section, the bridge was analyzed with and without the sidewalk. The inclusion of the sidewalk influenced the location of the critical transversal position. Analyzing the bridge without the sidewalk allowed enough room to place up to three loaded lanes on the bridge, since the remaining space exceeds the 12 feet width per lane required by the AASHTO Specifications. However, by including the sidewalk into the analysis only two loaded lanes could be placed on the bridge. These two scenarios are shown graphically in Figure 3.68.

In every case the truck was systematically moved within each lane at increments of 1foot, until the critical transversal location was found. For the critical single truck case, the truck was placed so that the exterior wheels were at a distance of two feet from the curb or barrier, which ever case applied. For the two or more trucks case, each truck was placed within a design lane and was moved transversely assuming that any truck could not get closer than 2 feet from the edge of the lane.

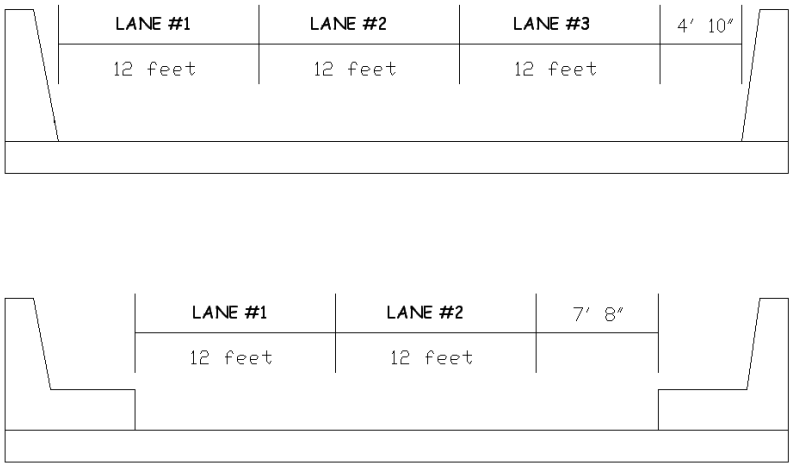

Fig 3.68 Loaded lanes distribution on the bridge deck with and without the curb.

It was also assumed that all the design lanes could be moved together across the width of the bridge. This increased the number of possible combinations that had to be analyzed.

At every truck's position, the girder's maximum moment at the specified location was analyzed and recorded for each girder. This was done by grouping every girder with its corresponding portion of the deck and determining the response of the whole group. The corresponding portion of the deck for each girder goes from half of the spacing between girders on one side, to half of the spacing on the other side. The maximum moment for the interior and exterior girders was then obtained from all the considered cases. With this information, the theoretical load distribution factor was calculated using Equation 3.10.

$$DFM = \frac{M_{max}}{M} \qquad (3.10)$$

where:

DFM = Distribution Factor for Moment

M_{max} = Maximum girder moment considering all possible load locations

M = Maximum Moment calculated using a single beam subjected to a single design truck placed at the critical longitudinal location.

This process was done for the single truck case and the two or more truck case. The maximum distribution factor obtained from all these cases was the one that controlled the moment response, since it contained the maximum moment that the studied girder will theoretical experience.

3.7 Comparison of Distribution Factors

In this section a comparison between the calculated distribution factors using the AASHTO LRFD Specifications (2006), the AASHTO Standard Specifications (1996) and the finite-element analysis performed using Sap2000 will be provided. Section 3.7.1 will present the calculated values obtained using the equations provided in the AASHTO Standard Specifications (2006). Section 3.7.2 will present all the calculations using the AASHTO LRFD Specifications (2006). Section 3.7.3 will show all the loading cases analyzed using the finite-element model and the different load distribution factors obtained as a result of the analysis. Finally, Section 3.7.4 will present a comparison between the results presented in Sections 3.7.1, 3.7.2 and 3.7.3.

3.7.1 AASHTO LRFD Specifications (2006) distribution factors

A distribution factor for the exterior and interior girder will be calculated for each span of the bridge. The analysis will be done both including and excluding the sidewalk. According to Equations 3.3 and 3.4, most of the variables used in these formulas are constant for every case, except for the span lengths, the overhang distance "*de"*, the cross section of the steel girder and the skew angle. These parameters will be calculated for each respective case. Table 3.5 presents a briefly summary of the bridge properties. For the bridge model without the curb de= 0.6771 feet and e = 0.8444. For the bridge model including the curb de= -3.906 feet and e = 0.3407.

Table 3.5 Bridge Girder Properties

S=	7.896 feet	**"A" Span #1=**	26.75 in^2
Es=	29000.00 KSI	**"A" Span #2 @Mid=**	51.75 in^2
Ec=	3605.00 KSI	**"A" Span #2 @ end=**	38.25 in^2
Skew Angle #1 =	19.62 degrees	**Thickness =**	8.00 inches
Skew Angle #2 =	7.12 degrees	**n=**	8.0444
eg Span1=	25.375 in	**Inertia Span #1 =**	6377.32 in^4
eg Span2 @ Mid=	31.986 in	**Inertia Span #2 @ Mid =**	14125.64 in^4
eg Span2 @ End=	27.127 in	**Inertia Span #2 @ End =**	6377.32 in^4

- Span 1

For the first Span, L= 36.340833 feet.

$Kg = = 8.044(6377.32 + 26.75x25.375^2) = \underline{189{,}858.83\ in^4}$

***For one design lane**:

$$DFM_I^{ns} = 0.06 + \left(\frac{7.896}{14}\right)^{0.4}\left(\frac{7.896}{36.34}\right)^{0.3}\left(\frac{189{,}858.83}{12x36.34x8^3}\right)^{0.1} = \underline{0.555}$$

DFM_I^{ns} = **0.555**, for interior girders

For the exterior girders, the lever rule will be used.

$$DFM_E^{One-lane} = \frac{1.2\times(7.896 + 0.6771 - 5)}{7.896} = \mathbf{0.543}$$, for the ext. girders w/o the curb

$$DFM_E^{One-lane} = \frac{1.2\times(7.896 - 3.906 - 2)}{2x7.896} = \mathbf{0.15122}$$, for the ext. girders with the curb

***For two or more design lane**:

$$DFM_I^{ns} = 0.075 + \left(\frac{7.896}{9.5}\right)^{0.6}\left(\frac{7.896}{36.34}\right)^{0.2}\left(\frac{189{,}858.83}{12x36.34x8^3}\right)^{0.1} = \underline{0.724}$$

DFM_I^{ns} = **0.724**, for the interior girders

DFM_s^{ns} = 0.8444 x 0.724 = **0.6113**, for the exterior girders without the curb

DFM_s^{skew} = 0.3407 x 0.724 = **0.2467**, for the exterior girders with the curb

- Span 2

The second span has a length of 71.043 feet. Since the second span has different elements sizes at the mid-span and at the ends, some variables will vary according to the location where they are being used.

Kg, for positive moment $= 8.056(14{,}125.64 + 51.75x31.986^2) =$ 539,534.54 in^4

Kg, for negative moment $= 8.056(10{,}664.55 + 38.25x27.127^2) =$ 263,388.9 in^4

***For one design lane**:

$$DFM_I^{ns} = 0.06 + \left(\frac{7.896}{14}\right)^{0.4}\left(\frac{7.896}{71.043}\right)^{0.3}\left(\frac{539{,}534.54}{12x71.043x8^3}\right)^{0.1} = \mathbf{0.48023}, \text{ for mid-span}$$

$$DFM_I^{ns} = 0.06 + \left(\frac{7.896}{14}\right)^{0.4}\left(\frac{7.896}{53.692}\right)^{0.3}\left(\frac{312{,}224.30}{12x53.692x8^3}\right)^{0.1} = \mathbf{0.505}, \text{ for ends}$$

$DFM_I^{ns} =$ **0.48023**, for the interior girders and positive moment.

$DFM_I^{ns} =$ **0.505**, for the interior girders and negative moment.

-Using the lever Rule:

$DFM_s^{ns} =$ **0.543**, for the ext. girders w/o the curb for positive and negative moment

$DFM_s^{ns} =$ **0.1512**, for the ext. girders with the curb for positive and negative moment

***For two or more design lane**:

$$DFM_I^{ns} = 0.075 + \left(\frac{7.896}{9.5}\right)^{0.6}\left(\frac{7.896}{71.043}\right)^{0.2}\left(\frac{539{,}534.54}{12x71.043x8^3}\right)^{0.1} = \mathbf{0.6641}, \text{ for mid-span}$$

$$DFM_I^{ns} = 0.075 + \left(\frac{7.896}{9.5}\right)^{0.6}\left(\frac{7.896}{53.692}\right)^{0.2}\left(\frac{312{,}224.30}{12x53.692x8^3}\right)^{0.1} = \mathbf{0.68163}, \text{ for ends}$$

$DFM_I^{ns} =$ **0.6641**, for the interior girders and positive moment.

DFM_I^{ns} = **0.68163**, for the interior girders and negative moment. p

DFM_s^{ns} = 0.8444 x 0.6641 = **0.5608**, for the ext. girders w/o the curb and positive moment

DFM_s^{ns} = 0.8444 x 0.68163= **0.576**, for the ext. girders w/o the curb and negative moment

DFM_s^{ns} = 0.3407 x 0.6641 = **0.226**, for the ext. girders with the curb and positive moment

DFM_s^{ns} = 0.3407 x 0.6816= **0.232**, for the ext. girders with the curb and negative moment

3.7.2 AASHTO Standard Specifications (1996) distribution factors

Since these specifications do not distinguish between interior and exterior girders, nor it distinguishes between two different spans, only one single equation was needed for each loading case.

-For one design lane:

Since S > 6 feet,

$$DF = \frac{7.896}{(4 + 0.25x7.896S)} x1.2 = \mathbf{1.586}$$

-For two design lane:

$$DF = \frac{7.896}{(4 + 0.25x.896S)} x1 = \mathbf{1.312}$$

Since these equations are based on half an axle load, they have to be divided by two, so they can be directly compared with the LRFD distribution factor. Therefore, for a design lane the moment distribution factor would be **0.793**, instead of the 1.586. For two design lane load would be **0.661** instead of the value of 1.312. These values were used for both spans, and both the exterior or interior girders.

3.7.3 Calculation of FEA distribution factors

As it was mentioned in the previous sections, the finite-element distribution factors are based on the maximum response that any particular girder might experience during service, due to the presence of traffic. This maximum response might vary between exterior and interior girders, and between the positive and negative moments. This fact makes the process of obtaining the maximum girder response complicated, since a finite-element analysis would have to be performed in every case. Moreover, the calculations of the distribution factors require a 1-D analysis of the bridge as a one-dimensional structure. This analysis was explained in Section 3.6, and its results will be shown in this section.

The maximum load response for each span was determined by positioning the wheel loads along the length of the 1-D bridge, with the help of the software Dr. Beam. For instance, Figure 3.69 shows how the moment envelope was created by running the wheel loads along the beam's length. This envelope was used to obtain the maximum local response in each span. As shown in Figure 3.69, the maximum positive moment that Span 1 would experience, as a 1-D beam, was approximately 3,746 kip-in. This value will be subsequently used to determine the load distribution factors from the Finite-Element Model. Figures 3.70 shows the maximum positive moment for Span 2. It can be observed that these two figures also present the exact location at which the maximum response would occur along the length of the beam. These locations were used in the FEM to estimate a similar location in the model.

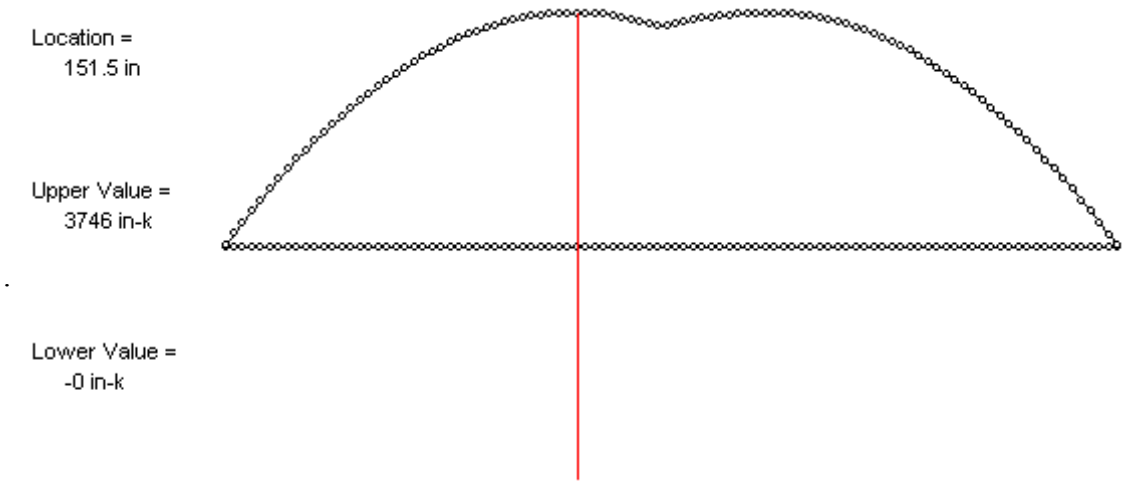

Fig 3.69 Moment envelope that shows the maximum positive moment in Span #1 .

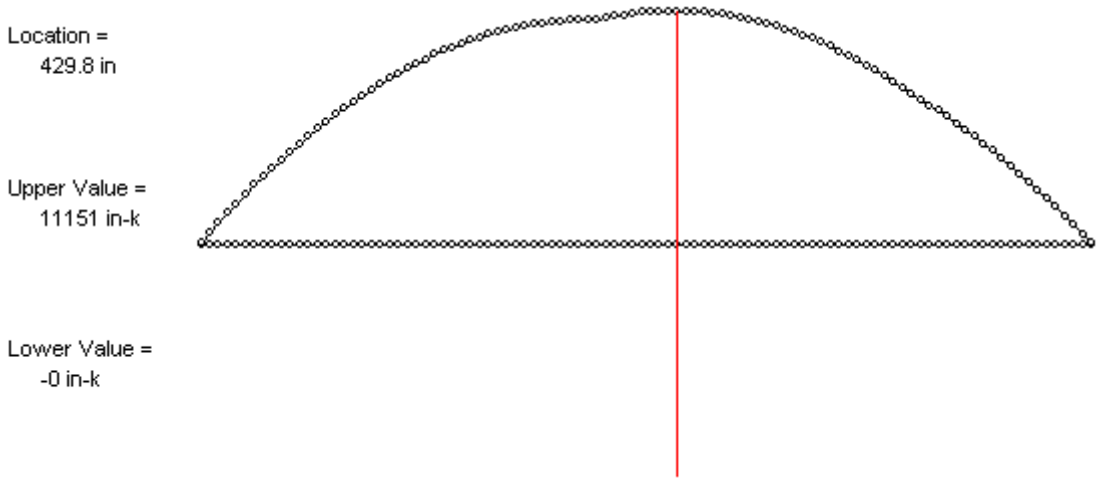

Fig 3.70 Moment envelope that shows the maximum negative moment is Span #2.

After the 1-D maximum responses were obtained, the next step was to determine the maximum response for the individual bridge girders using the computer analysis. In order to do so, the transversal position of the truck's wheels that caused the maximum response in a specific girder, was determined in advance. Figures 3.71 through 3.76 show some of the critical transversal locations that were obtained for the different loading cases.

Once the critical transversal locations were obtained, the loads were applied and the bridge was analyzed and the maximum response was obtained. This maximum response was then divided by the appropriate results obtained from the 1-D analysis, resulting in the calculation of the finite element load distribution factors. Table 3.6 presents a summary of the results obtained through the finite-element analysis of the bridge girder without the sidewalk. Table 3.7 contains the results obtained from the bridge girder with the sidewalk.

Table 3.6 Maximum Responses of the Girders without the Sidewalk

	SPAN #1			
	Exterior Girder Moment (kip-in)		**Interior Girder Moment (kip-in)**	
	Positive	Negative	Positive	Negative
Single loading	1,657.06	290.12	1,598.02	341.50
Two Lanes Loades	1,809.26	329.34	2,463.65	489.12
Three Lanes Loaded	1,785.91	320.04	2,205.41	502.9653
	SPAN #2			
	Exterior Girder Moment (kip-in)		**Interior Girder Moment (kip-in)**	
	Positive	Negative	Positive	Negative
Single loading	5,280.95	12.48	4,189.24	17.18
Two Lanes Loades	6,757.38	14.38	7,239.626	37.50
Three Lanes Loaded	6,594.80	13.84	7,765.80	38.57

Table 3.7 Maximum Responses of the Girders with the Sidewalk

	SPAN #1			
	Exterior Girder Moment (kip-in)		**Interior Girder Moment (kip-in)**	
	Positive	Negative	Positive	Negative
Single loading	1070.18	56.364	1,248.92	269.40
Two Lanes Loades	1188.78	162.68	1,587.37	261.943
	SPAN #2			
	Exterior Girder Moment (kip-in)		**Interior Girder Moment (kip-in)**	
	Positive	Negative	Positive	Negative
Single loading	3,802.58	11.86	3,618.18	11.066
Two Lanes Loades	4,751.24	12.91	5005.25	13.59

According to the results presented in these two tables, we can observe that the maximum moments experienced by the girders have been reduced by the presence of the sidewalk. This might sound logical for the interior girders, since the exterior girder becomes stiffer due to the presence of the curb, and thus attracts more moment. However, we can appreciate how the moments on the exterior girders have been reduced as well, contrary of what one would normally expect. This is due to the fact that the curb is so wide that the effects of the wheel loads cannot affect the exterior girder in the same manner as it did without the sidewalk.

Finally, it can be concluded that the presence of the sidewalk as a structural element has a direct influence on the magnitude of the distributions factors values, thus affecting the design of the structural members, and the economy of the project. Nevertheless, if the

sidewalk were be taken into consideration, special requirements should be implemented so this element can behave as a composite structure with the concrete deck.

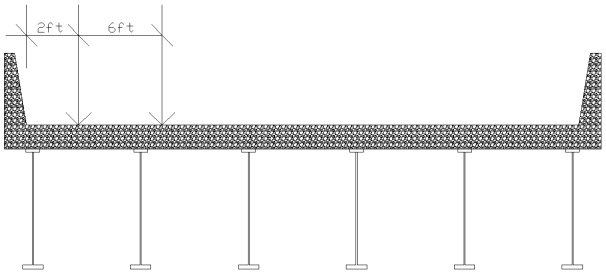

Fig 3.71 Critical transversal position for an exterior girder with one loaded lane.

.

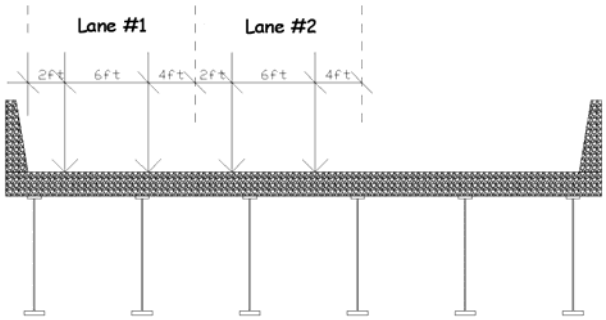

Fig 3.72 Critical transversal position for an exterior girder with two loaded lane.

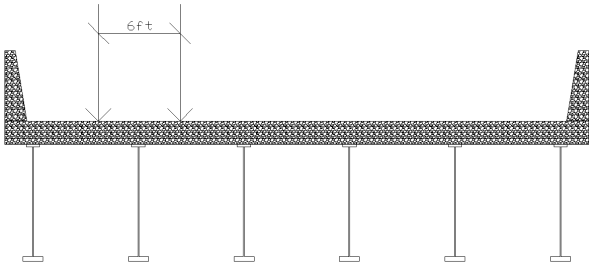

Fig 3.73 Critical transversal position for an interior girder with one loaded lane.

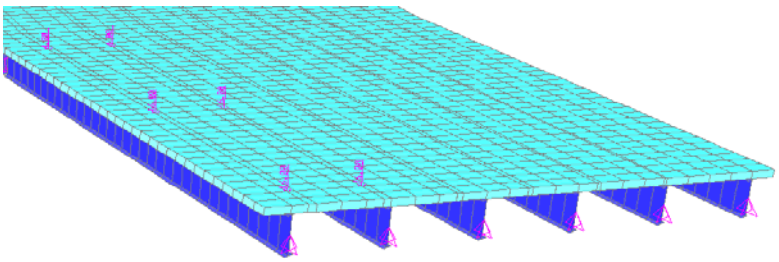

Fig 3.74 Single loading case for exterior girder.

-

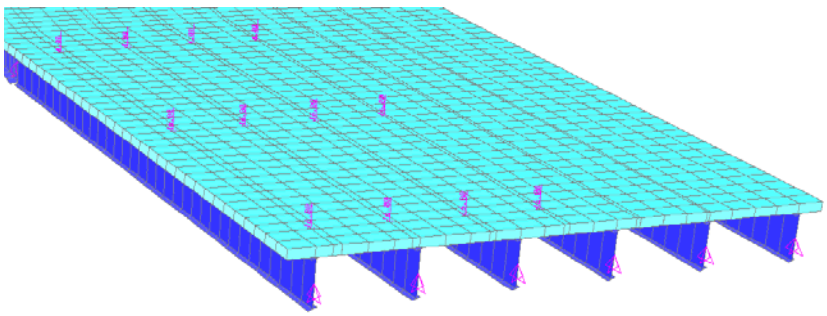

Fig 3.75 Two-loaded lanes case for exterior girder.

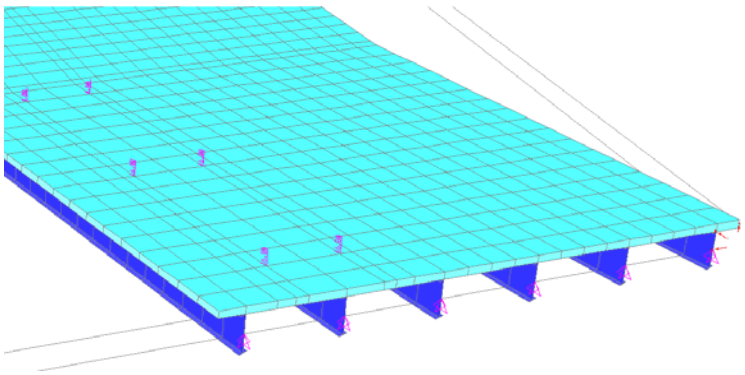

Fig 3.76 Single loading case for interior girder.

3.7.4 Comparison between FEA results and code's distribution factors

The results obtained in Section 3.7.1 through the AASHTO Standard Specifications equations, and those obtained in Section 3.7.2 according to the AASHTO LRFD Specification's equations, are compared with the results obtained through the finite-element analysis. This is done to determine whether or not the code based equations are relatively accurate or if they tend to yield extremely conservative results. Tables 3.8 through 3.10 present these comparisons.

Table 3.8 Moment Distribution Factors for the Single Loading Case without the Curb

Without Sidewalk (One Design lane)							
Girder Type	**Location**	**Moment**	**FEA Model**	**AASHTO LRFD**	**% Error respect to FEA**	**AASHTO 1996**	**% Error respect to FEA**
Interior	Span #1	Positive	0.512	0.555	8.40%	0.793	54.88%
Exterior	Span #1	Positive	0.531	0.543	2.26%	0.793	49.34%
Interior	Span #2	Positive	0.44	0.48	9.09%	0.793	80.23%
Exterior	Span #2	Positive	0.58	0.543	-6.38%	0.793	36.72%

Table 3.9 Moment Distribution Factors for the Two or more Design Lanes Case without the Curb

Without Sidewalk (Two or more Design lane)							
Girder Type	**Location**	**Moment**	**FEA Model**	**AASHTO LRFD**	**% Error respect to FEA**	**AASHTO 1996**	**% Error respect to FEA**
Interior	Span #1	Positive	0.658	0.724	10.03%	0.661	0.46%
Exterior	Span #1	Positive	0.483	0.611	26.50%	0.661	36.85%
Interior	Span #2	Positive	0.632	0.664	5.06%	0.661	4.59%
Exterior	Span #2	Positive	0.58	0.56	-3.45%	0.661	13.97%

Table 3.10 Moment Distribution Factors for the Single Loading Case with the Curb

With Sidewalk (One Design lane)							
Girder Type	**Location**	**Moment**	**FEA Model**	**AASHTO LRFD**	**% Error respect to FEA**	**AASHTO 1996**	**% Error respect to FEA**
Interior	Span #1	Positive	0.4	0.555	38.75%	0.793	98.25%
Exterior	Span #1	Positive	0.343	0.151	-55.98%	0.793	131.20%
Interior	Span #2	Positive	0.39	0.48	23.08%	0.793	103.33%
Exterior	Span #2	Positive	0.41	0.1512	-63.12%	0.793	93.41%

Table 3.11 Moment Distribution Factors for the Two or more Design Lanes Case with the Curb

With Sidewalk (Two or more Design lane)							
Girder Type	**Location**	**Moment**	**FEA Model**	**AASHTO LRFD**	**% Error respect to FEA**	**AASHTO 1996**	**% Error respect to FEA**
Interior	Span #1	Positive	0.423	0.724	71.16%	0.661	56.26%
Exterior	Span #1	Positive	0.317	0.2467	-22.18%	0.661	108.52%
Interior	Span #2	Positive	0.538	0.664	23.42%	0.661	22.86%
Exterior	Span #2	Positive	0.426	0.226	-46.95%	0.661	55.16%

As can be observed from Tables 3.8 and 3.9, the AASHTO LRFD Speciation's distribution factors predicted, with acceptable results, the behavior of the 8th North Bridge. The live load distribution factors were very close to those obtained from the finite element model, at least within 10% of the FEM calculations. In most cases the code over predicted the behavior of the super structures.

This over prediction leads to a more conservative design, since the structural elements will be selected to withstand larger forces than what they will receive in their service live. Another aspect that could be observed is the fact that the code equations had a better performance in the span #2 region than in span #1. It could be said from this fact that when the span being analyzed tends to be very short, less accurate results would be obtained, especially for two or more design lanes.

It can also be noted from these Table 3.8 and 3.9 that there is a big difference between the AASHTO Standard Specifications (1996) estimations and the FEM calculations. This large difference is expectable since these equations only considerer the spacing of the girders as a parameter, and they don't take into account the effect of the length of the span or the rigidity of the elements supporting the deck.

The negative moments were not taken into account for this comparison since they were extremely small compared to the positive moments. This is due to the small continuous behavior that this structure presented. In general, these negative moments were extremely over predicted by both specifications.

As it was shown in Table 3.7, the curb element has a tremendous effect on the maximum responses of the interior and exterior girders. Not only it decreases the moments on the interior girders, but it also diminish the effect on the exterior girder not allowing the wheel load to be placed closed to it. This structural component, and its effect, is believed to not be taken into consideration when the AASHTO LRFD Specifications developed its equation, as can be appreciated by the results from Table 3.10 and 3.11.

The code extremely over predicted the response of the interior girders by an average of 40%, while it under predicted the response of the exterior girders by more than 45%, in one of the worst cases. However, this under prediction is not very alarming, since the bridge girders would always be designed for the biggest moment, which in this case would be that from the interior girders. This fact will lead to an overdesign of the exterior girder in most cases.

Nevertheless, more studied regarding this condition are recommended to be performed in order to obtain a more clear vision of true behavior of this structure. it is recommended that the possible presence of a curb element on a bridge girder should be included into the element analysis and should be taken into account for the creation of new distribution factor equations, since it has been proven that it decreases the maximum responses on every girder on the bridge being analyzed.

CHAPTER 4

A COMPARISON OF LIVE LOAD DISTRIBUTION FACTORS FOR THE WALNUT GROVE ROAD BRIDGE

This Chapter presents a detailed description of an analysis that was carried out on the Walnut Grove Road Bridge. This analysis consisted of the development of a finite-element model (FEM) that could accurately represent the behavior of the studied bridge while being submitted to trucks load, during a live-load test performed by BDI during October of 2008. The comparison between the FEM and the live load test results, as well as the determination of the FE live load distribution factor, were the principal objectives of this study.

Chapter 4 is divided into five sections, where each section describes a single aspect of the investigation. Section 4.1 presents a very detailed description of the Walnut Grove Bridge. Section 4.2 describes all important aspects related to the live load test performed by BDI. Section 4.3 presents an extensive discussion of the results obtained from the live load test by BDI. Section 4.4 explains the process by which the finite-element model was created, the types of element that were used, and how actual boundary conditions were incorporated. It also explains how the live-load test was incorporated into the FE model. Section 4.5 provides a very detailed comparison of the results from the FEM with the data obtained from the live-load test. Section 4.6 presents the equations from the AASHTOO LRFD Specifications used to estimate the live-load distribution factors of the studied bridge, and the process used to obtain the finite-element distribution factor from

the FEM. Finally, Section 4.7 presents a comparison between the AASHTO LRFD calculated values and the FEM results.

4.1 Bridge Description

The Walnut Grove Road Bridge is located along I-5 in Joaquin County, California, as shown in Figure 4.1. This bridge is approximately 60 miles to the northeast of San Francisco, very close to the town of Thornton. The undercrossing is composed of two identical bridges with the same structural components and the exact geometric shape, but supporting opposing traffic directions. The northbound bridge leads to Sacramento and the southbound bridge leads eventually southern California. Both bridges pass over the Walnut Grove Road, which is where it takes its name from. As shown in the picture below, this structure has a skew angle due to the geometric conditions of the highway. This angle is approximately 29 degrees.

Fig 4.1 Aerial view of the Walnut Grove Road Bridge.

Both structures have a roadway width of 38 feet and 6 inches, which includes two 12 foot wide traffic lanes, a 5 feet 3 inch shoulder on the left side and a 9 feet 3 inch shoulder on the right side. The overall width of the bridge is 42 feet and 6 inches, including the barriers. This structure was designed as a single-span bridge, supported at the ends with two abutments, which will be described in more detail later on. The total length of the bridge was approximately 148 feet from the beginning of the bridge to the end of the bridge, and 145 feet and 11 inches from center to center of the abutments, for modeling purposes.

The bridge superstructure is composed of a four-cell, cast in place, pre-stressed concrete box girder, with a specified concrete strength of 4500 psi. The upper flange had a thickness of 8 inches, while the lower flange was 6 inches thick. The webs were thicker,

Fig 4.2 View of the two bridges from the Walnut Grove Road overcrossing

reaching a thickness of 12 inches and a total height of 6 feet. These webs were spaced every 9 feet, as is shown in Figure 4.3. The precast concrete was reinforced using #4, #5 and #6 rebar with a yield strength of 60 ksi.

Since there were four cells in this concrete box girder, there were 5 webs evenly spaced across the width of the bridge. This can be noticed in Figure 4.4, where the webs are represented as if they were girders supporting the upper and lower concrete deck. It can also be noticed that these "girders" were connected by some concrete diaphragms at the mid-span. These diaphragms had the same thickness and height of the webs. It is important to note that if a line was drawn through the mid-span of the bridge, it would pass through the midpoint of every diaphragm. This is very important for the location of the diaphragms since they are placed perpendicular to every girder and do not follow the skew orientation of the bridge. The bridge also had concrete barriers at each edge of the bridge. These barriers have been identified as Type 25. Figure 4.5 shows the barriers.

Another important factor that must be emphasized is that the center of gravity (C.G.) of the pre-stressing steel strands, varied along the length of the bridge. For instance, at the supports of the bridge the distance from the bottom of the structure to the c.g. of the strands was two feet and 6 inches, while at the mid-span it was 8 inches. This distribution was intended to resist the early forces imposed by the self-weight of the structure. This harped arrangement in illustrated in Figure 4.6.

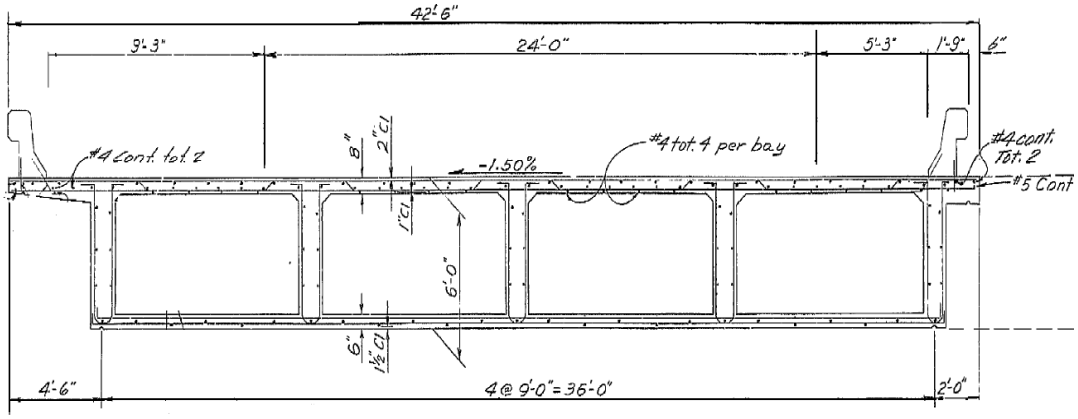

Fig 4.3 Typical section left bridge.

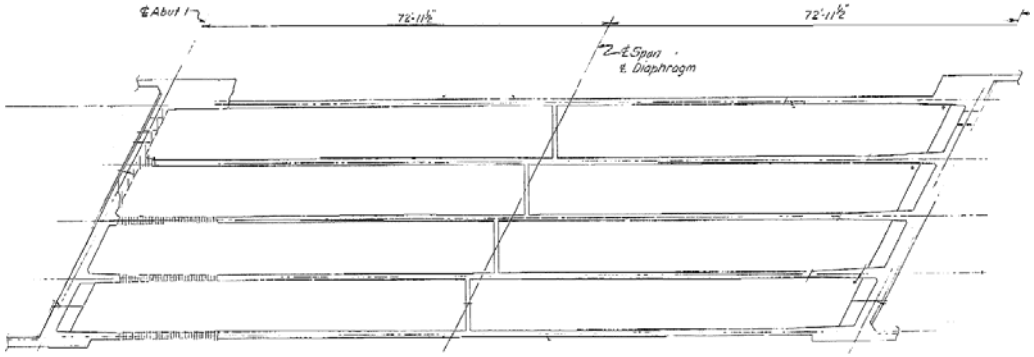

Fig 4.4 Girder layout.

Fig 4.5 View of the barriers on the bridge.

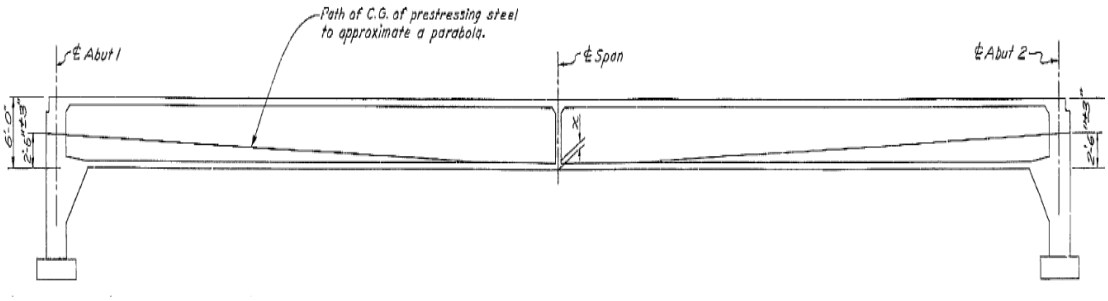

Fig 4.6 Longitudinal section showing the prestressing strands arrangement.

The Walnut Grove Road Bridge was supported at the ends by a structural abutment, which at the same time had attached to it two wing walls at eah side. The abutment was constructed with reinforced concrete with a 28-day compressive strength of 4,500 psi and with #4,#5 and #6 rebars. The abutment had a thickness of 2 feet and 6 inches and a height of about 10 feet. This structure was supported by a 7 inches thick and 5 feet wide concrete pile cap reinforced with #6 bars spaced every foot. This pile cap was at the same time supported by 11 concrete piles of about 8 inches in diameter. Something very important that must be emphasized is the inclination that the abutment presents right at the bottom of the bridge. As can be seen in Figure 4.7, this inclination starts from a distance of 2 feet from the bottom of the bridge, increasing vertically 3 feet every two feet. It is very important to take this fact into consideration in the modeling process, since it provides more bearing surface at the bottom of the bridge and might affect the boundary conditions on the computer model.

The wingwall was attached to the abutment right after the stressing process was completed. It was also constructed using reinforced concrete with a 28-day compressive strength of 4500 psi. It extended at the top 19 feet from the center of the abutment and covered the whole surface of the abutment. It had a thickness of 1 foot all over its

surface. The wing walls are connected one to another with a shear key placed at the bottom of the abutment. As is shown in Figure 4.8, the wing wall not only covered the whole surface of the abutment, but it also extended approximately 6 feet into the left and right side of the bridge, which tends to give more support to this upper part of the bridge.

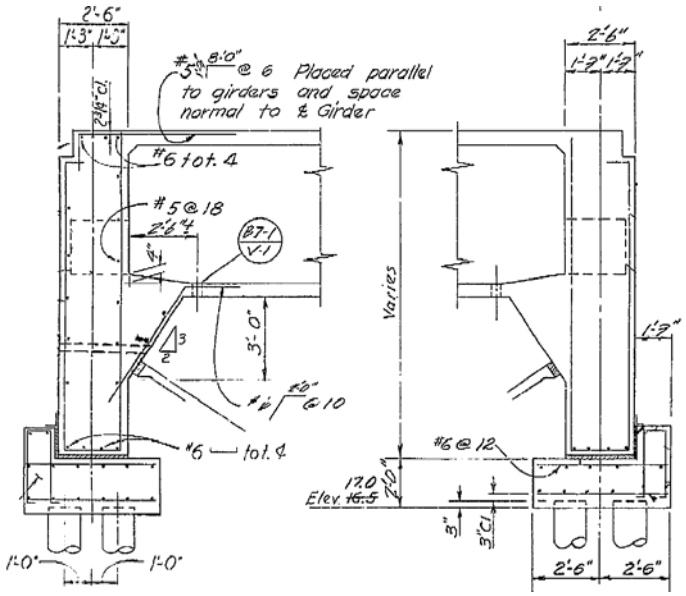

Fig 4.7 Abutments details.

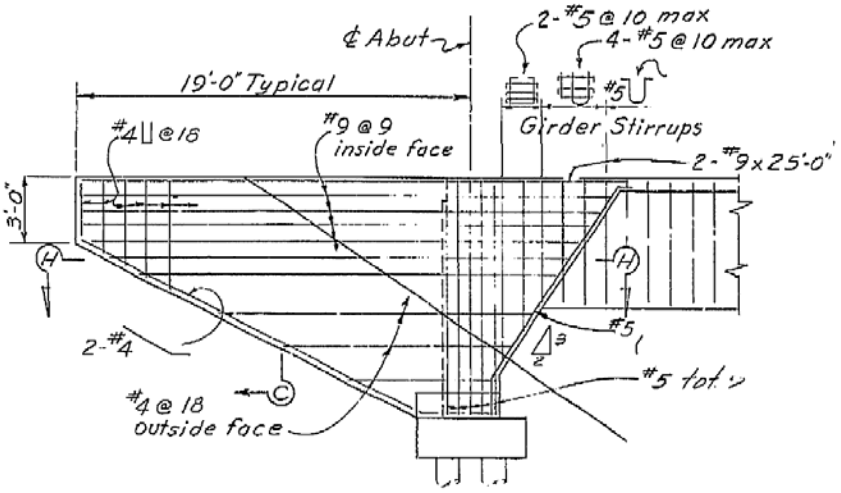

Fig 4.8 Wingwall elevation.

4.2 Live Load Test

During the month of October in 2008, Bridge Diagnostic Inc (BDI) was hired by researches at Utah State University to perform a live load test on the Walnut Grove Road Bridge with the purpose of obtaining field measurements of the structural response of the bridge and to use those measurements to calibrate a finite-element model, from which load ratings of the bridge could accurately be obtained. Another goal of this test was to compare the results with those obtained in a similar test performed by the University of Colorado in 1990, and observe if there were any changes in the behavior of the bridge.

The load test was performed on the south bridge structure, along southbound I-5. It consisted of driving a moving truck load along the length of the bridge along six different paths, previously determined, so the behavior of the structure, due to the imposed live load of the truck, could be measured. In order to record the respond of the bridge, approximately 56 strain gages, attached to the concrete in different locations, were used.

Fig 4.9 Part of the BDI structural testing system (STS).

Strain measurements were recorded at each location using the BDI Structural Testing System (STS). Figure 4.9 shows part of the STS configuration used in this live-load test. These strain gages were assigned a code number and allowed for easier to identification and record of the data associated with it. An example of a strain gage with its code number is shown in Figure 4.10. These sensors had an effective gage length of 3 inches, and a sensitivity of 0.5 micro-strains. They were mounted on the reinforced concrete by using a technique called "tab attachment method." According to the BDI report, this procedure consists in cleaning the mounting area and then installing the sensors using a fast-setting cyanoacrylate adhesive. This adhesive would hold the sensor in place until small steel "tabs" were used to fix the sensor into the reinforced concrete. BDI estimated that around 5 to 10 minutes are required to install each sensor.

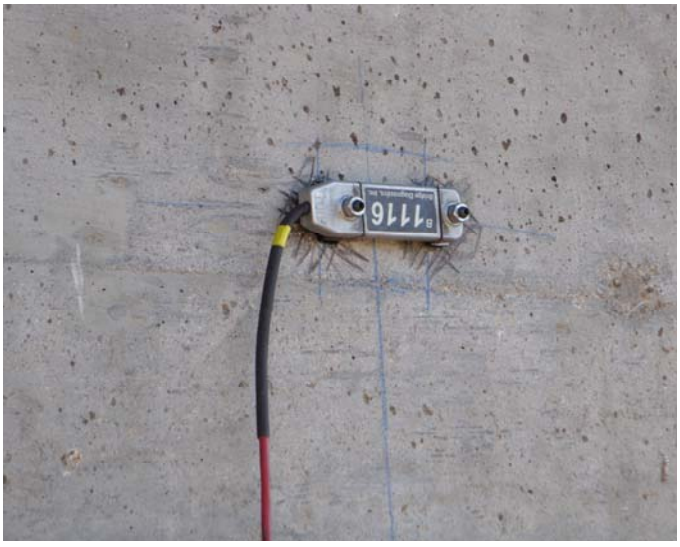

Fig 4.10 Typical strain gage used in the test with its code name (B1119).

The locations chosen for the strain gages were the same locations that were used in the 1990 test. According to the BDI report of this test, the chalk lines and gage locations were still noticeable underneath the bridge, which made the placement of the sensors very easy. These locations are shown in Figure 4.11. According to the sensors layout, the respond of the bridge was recorded near the abutments, at the mid-span and in between these two locations. Section AA was located at a distance of 9.7 feet from the left end following the skew angle of the bridge. Section BB was located at 38.5 feet from the left end of the bridge. Section CC was located at the same distance as Section BB, but it had an orientation perpendicular to the girders. Section DD was placed right at the mid-span of the bridge and Section EE was located at 51.7 feet from the right end of the bridge. These locations would give a better idea of the boundary conditions of the bridge and of the effect of the diaphragms on the lateral load distribution at mid-span.

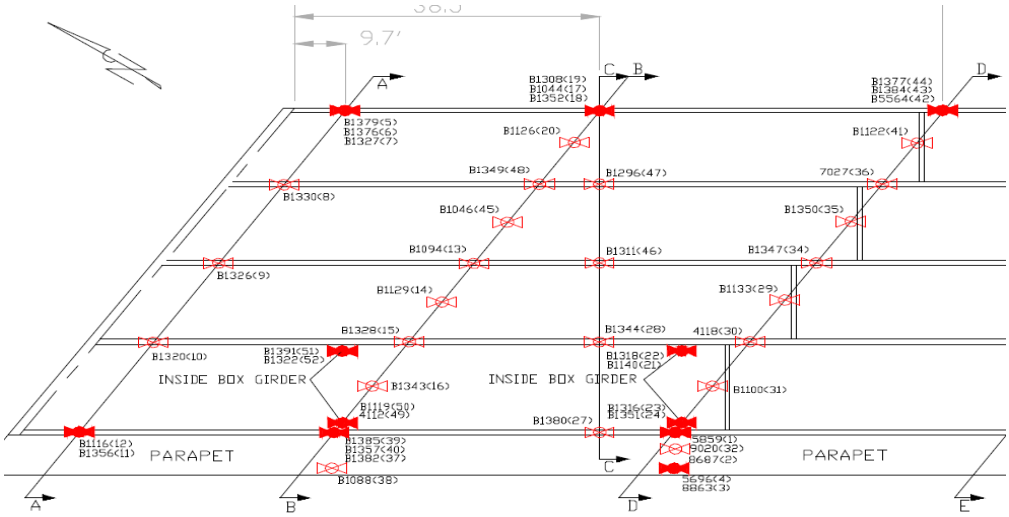

Fig 4.11 Instrumentation plans with gage IDs. (Courtesy of BDI).

Fig 4.12 Sensors ID and locations for Section DD. (Courtesy of BDI).

Figure 4.12 shows the configuration of the strain gages in a typical cross section. As shown in this figure, most of the sensors were placed directly underneath every web of the four-cell concrete box girder. Another group was placed in between the webs and only a few were located directly on the webs. This test configuration was designed to provide a better idea of the behavior of the bridge. Before starting the live load test, a reference point or "zero location" was established so the locations of the trucks could be properly recorded as they drove across the bridge. In this test, the point of reference was chosen to be the north-west corner of the bridge, in the inside part of the barrier, along the expansion joint. This was a very clear spot, since it appeared on the blueprints and would be easy to locate in a finite-element model. This "zero location" can be seen in Figure 4.13.

After the reference point was located, the lateral loading paths were chosen. As mentioned before, there were six different paths along which the truck was driven. These load paths were chosen to replicate the original paths that were used for the 1990 test. However, after carefully comparing the two tests, it appeared that the paths used in the current test were about 7.5 inches west from the paths used in 1990. Nevertheless, this minimal difference was insignificant since the data from the two tests was very similar, as will be explained in Section 4.3.

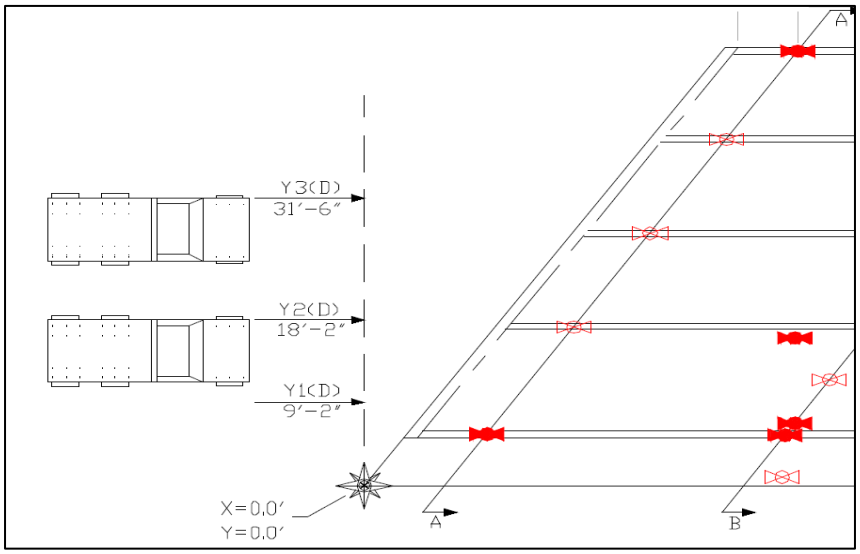

Fig 4.13 Truck paths Y1, Y2 and Y3. (Courtesy of BDI).

As can be seen in Figure 4.13, Y1 was located at 9 feet and 2 inches from the reference point, Y2 at 18 feet and 2 inches and Y3 at 31 feet and 6 inches. At the same time Y4, Y5 and Y6 were at 7.5 feet, 16.5 feet and 29.83 feet, respectively, from the reference point.

Two types of test were performed for the live-load test, a semi-static load test and a high-speed load test. The semi-static test was conducted at an average speed of 5 mph. It was intended to simulate the application of static loads on the bridge. The strain readings and truck positions were stored at a sample rating of 33.33 Hz, while the truck was moving along the bridge at this speed. For this test, the truck was driven along Y1, Y2, Y3,Y4,Y5 and Y6 paths. On every single path, the truck was driven using the driver-side wheel. The high-speed load test was conducted at an average speed of 45 mph along load paths Y5, and Y6, using the driver-side wheel. The purpose of this test was to determine

how much an impact load affects the behavior of the entire structure. For this type test, the strains were recorded at a sample rate of 100 hz.

The process by which the truck position was recorded is one the greatest enhancements of the STS system. This process consists of the usage of a device called "Auto-clicker," which aids in the determination of the truck's location along the bridge. As the truck is moving across a specified loading path, the auto-clicker sends a radio signal to the STS, which receives it and puts a mark in the data. The auto-clicker sends this signal every time the wheel on the truck completes one wheel revolution. With this process, the strain readings can be compared in terms of truck position instead of time. It is very important to measure the length of a wheel revolution before the beginning of the test. For this test, one wheel revolution was equal to 10 feet and 10 inches. The test started at 10 – ½ rev from the reference point. Figure 4.14 shows how the auto-clicker is mounted into the truck.

Fig 4.14 Auto-clicker mounted on the test truck.

The test truck used in this test was a three-axle dump truck. Its dimensions and axle weights were similar (within 3%) of the truck used in 1990. The front axle had a width of 6 feet and 9 inches with a measured weight of 13,760 pounds. The two rear axles had a width of 6 feet with a measured weight of 17,230 pounds on each axle. The total gross vehicle weight was computed as 48,220 pounds. The spacing between the front axle and the first rear axle was measured as 16 feet, while the spacing between the two rear axles was measured at 4 feet and 9 inches. Figure 4.15 shows the footprint of the dump truck. Figure 4.16 shows a picture from the test truck taken during the test.

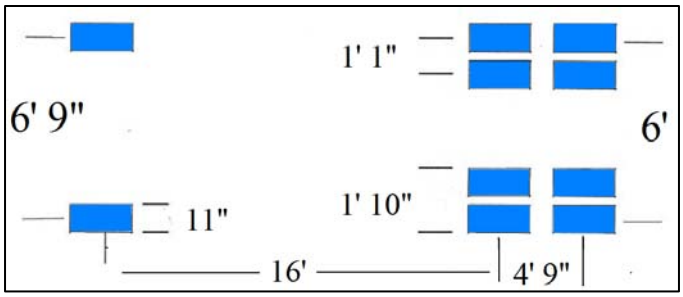

Fig 4.15 Test truck footprint.

Fig 4.16 Picture of the dump truck used in the test.

4.3 Live Load Test Results

After the live-load test was performed, the data was graphically reviewed by the BDI personal in order to determine its quality and to have an idea of the behavior of the structure subjected to the imposed live load. After reviewing the data, the BDI crew discovered some important aspects about the data taken from the live-load test and the behavior of the structure. On the other hand, a second review on the data was made in this research with the intention of confirming the conclusions stated in the BDI report. As stated in the BDI report, these aspects were: *Reproducibility and linearity, low strain response, additional stiffness at mid-span, end-restraint at the abutments, lateral load distribution and similarity with the 1990 test.*

4.3.1 Reproducibility and linearity

As it was mentioned before, the load truck was driven twice along each load path and the strain measurements were recorded every time. By plotting the response history of one strain gage in the same path, it could be observed if there were any variations. This comparison can be seen in Figure 4.17. The figure shown below was constructed by plotting the response history of one strain gage, from sections BB, CC and DD, using the same loading path, Y1. The data was obtained from BDI after performing the live-load test. As can be seen, the tests with identical truck paths produced extremely closed results (within 2%), which can therefore be concluded that the data had some degree of reproducibility and thus, was of excellent quality. More figures showing this aspect can be seen in the Appendix.

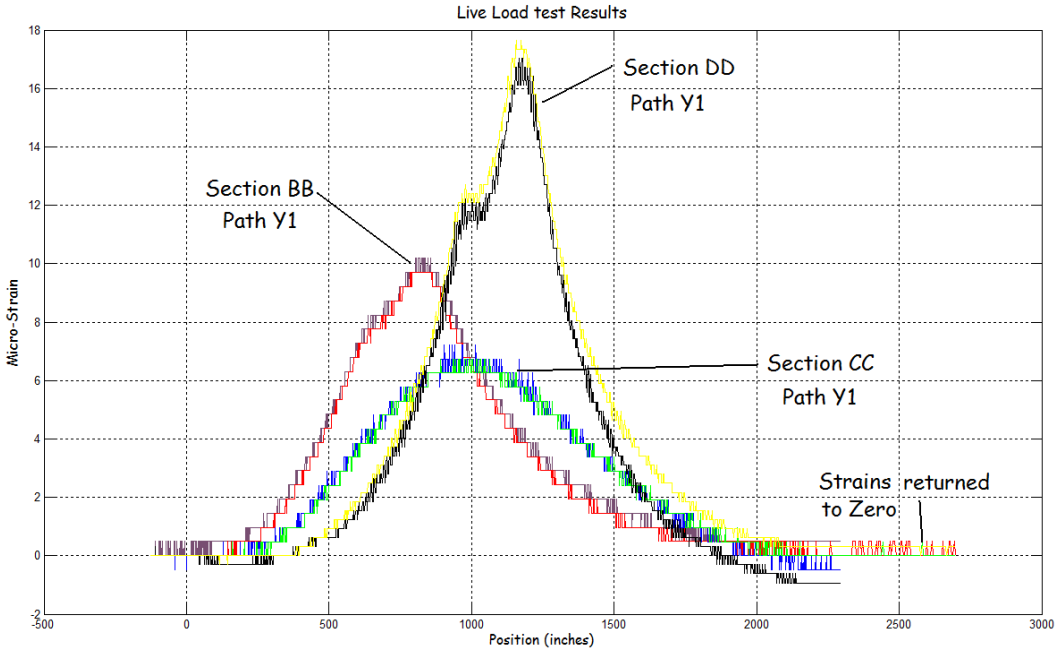

Fig 4.17 Reproducibility and linear behavior of the data.

Another fact that can be appreciated from Figure 4.17 is that all the data returns to zero when the test is finished, which indicates that the structure showed a linear-elastic behavior, as previously reported by BDI.

4.3.2 Low strain responds

According to the BDI reports, the strains recorded during the test were very low since the maximum values were located below 20 micro-strains. BDI believes that this is caused because the structure was very stiff and the test truck did not weigh enough to produce a bigger response. If we take a close look to every figure, we will notice that indeed the strains recorded from the live load test were extremely low.

4.3.3 Additional stiffness from mid-span diaphragms

In order to investigate the effect that the diaphragms had on the lateral load distribution, the response history of three strain gages placed along Section DD were plotted against the response history of three strain gages from Section BB. The strain gages from Section DD were B1347, 7027 and 4118. The strain gages from Section BB were B1094, B1349 and B1328. These sensors can be located in Figure 4.10 and 4.11. The response history was obtained from the data recorded by BDI during the live-load test. Figure 4.18 shows the results of these plots. From Figure 4.18, we can observe that the magnitudes at the quarter-span are too far apart from each other, while the magnitudes at the mid-span are closer. This is because at mid-span there is a better lateral load distribution due to presence of the diaphragms. The diaphragms increased the lateral stiffness of the box girder by acting as a transverse beam.

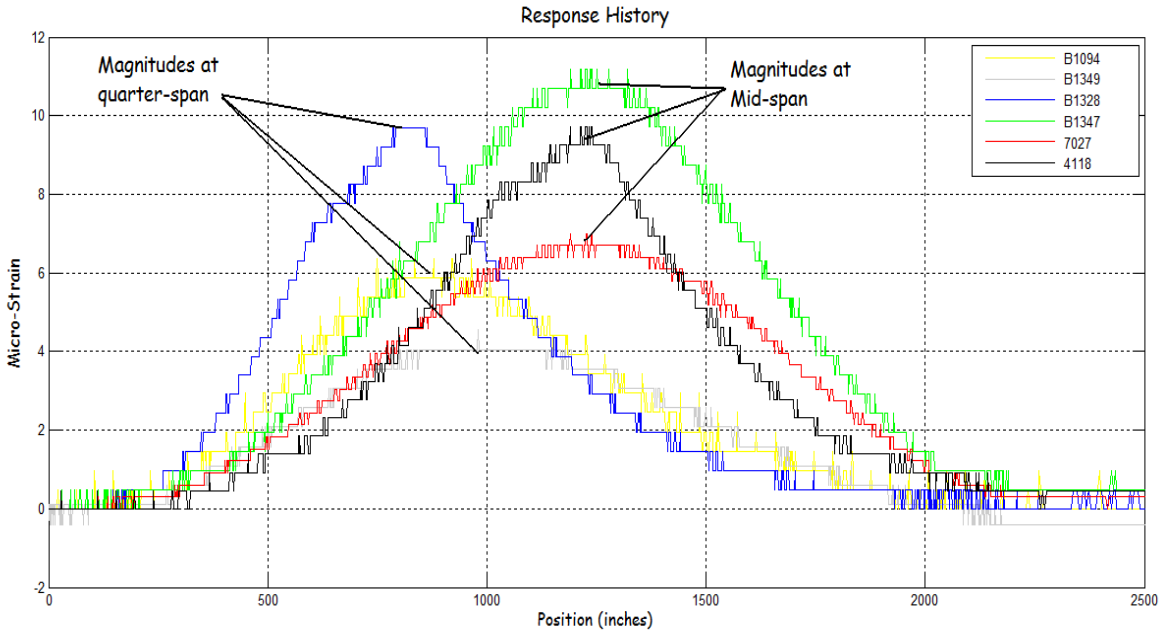

Fig 4.18 Lateral load distribution at quarter and mid-span.

4.3.4 End-restraint at the abutments

In order to determine the end-restraint at the abutments, the response history of two different sensors close to the abutment were plotted for Y1, Y2 and Y3. Strain gages B1326 and B1330 were chosen since they are located in Section AA, which is very close to the abutments. As can be observed from Figures 4.19 and 4.20, both sensors present the same behavior as the trucks drives away from the abutment. It is noticeable that there is some kind of restraint, which is proved by the negative strains registered when truck was located far away from the left end. This condition is shown in both Figure 4.19 and 4.20. This demonstrates the presence of a nearly fixed-end condition at the abutments.

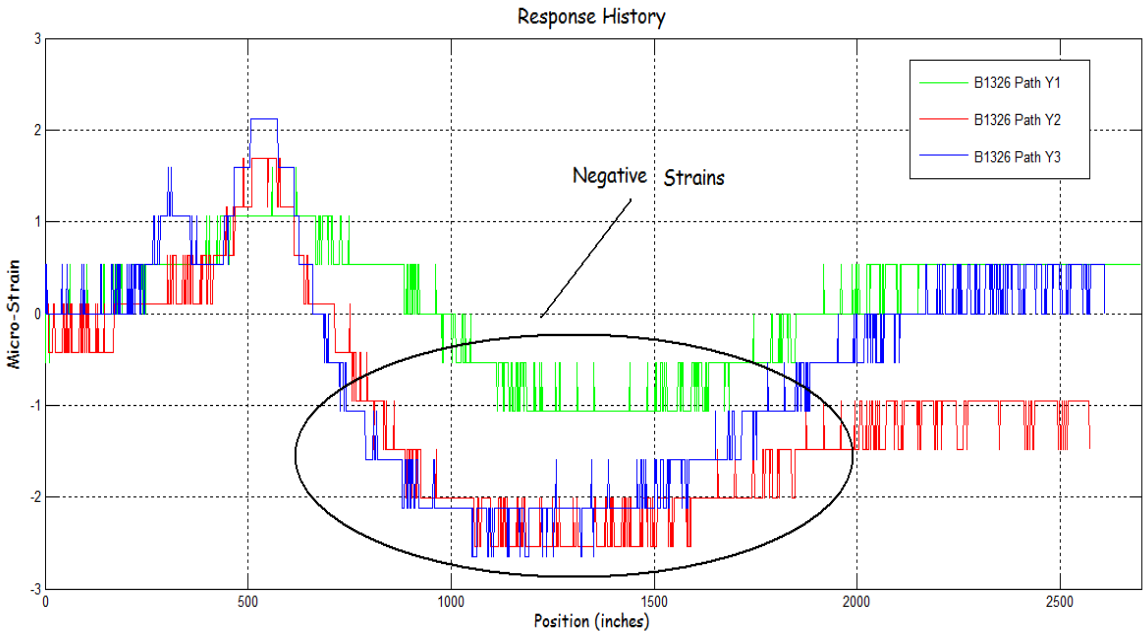

Fig 4.19 End restraint condition at the abutment (B1326).

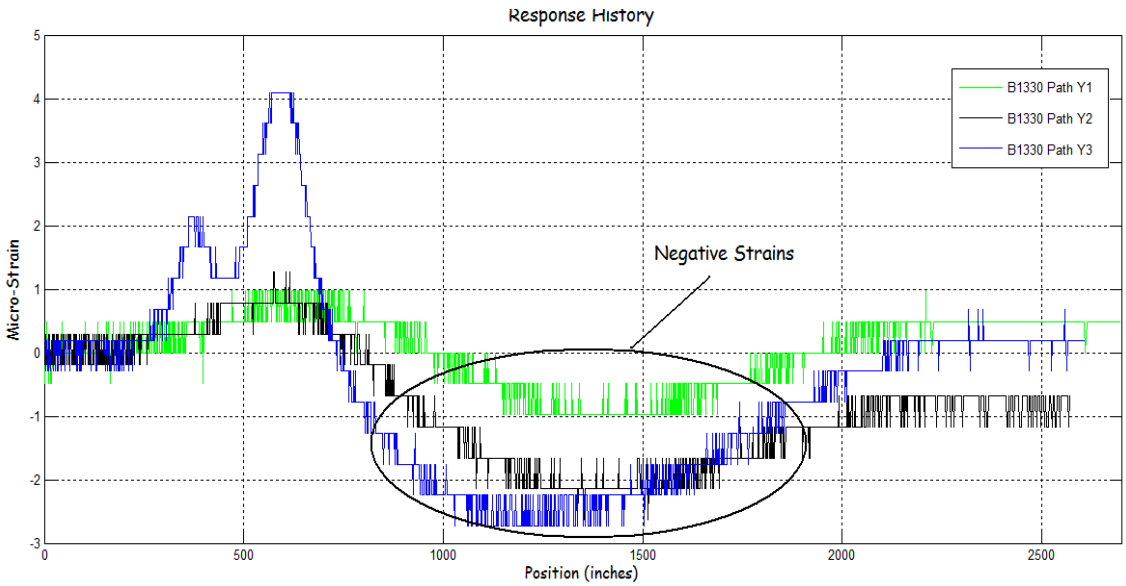

Fig 4.20 End restraint condition at the abutment (B1330).

4.3.5 Lateral load distribution

In order to determine the lateral load distribution of the structure, the strains of the gages that were placed directly underneath every web at each section were observed for the loading paths Y1, Y2 and Y3. A specific truck position for each condition was chosen to be evaluated. These values were plotted underneath the corresponding gage for simpler comparison. Figures 4.21, 4.22, and 4.23 show the result of these plots. Despite the fact that the maximum responses did not occur at the same time at all gages due to the skew orientation of the bridge, we can still appreciate some lateral load distribution across the width of the structure at any sections, especially at the mid-span. The most important factor is that the gage that is placed at the furthest location from the load applied, received a very significant amount of the load, which demonstrate the capacity of the structure to distribute any load very well across its width.

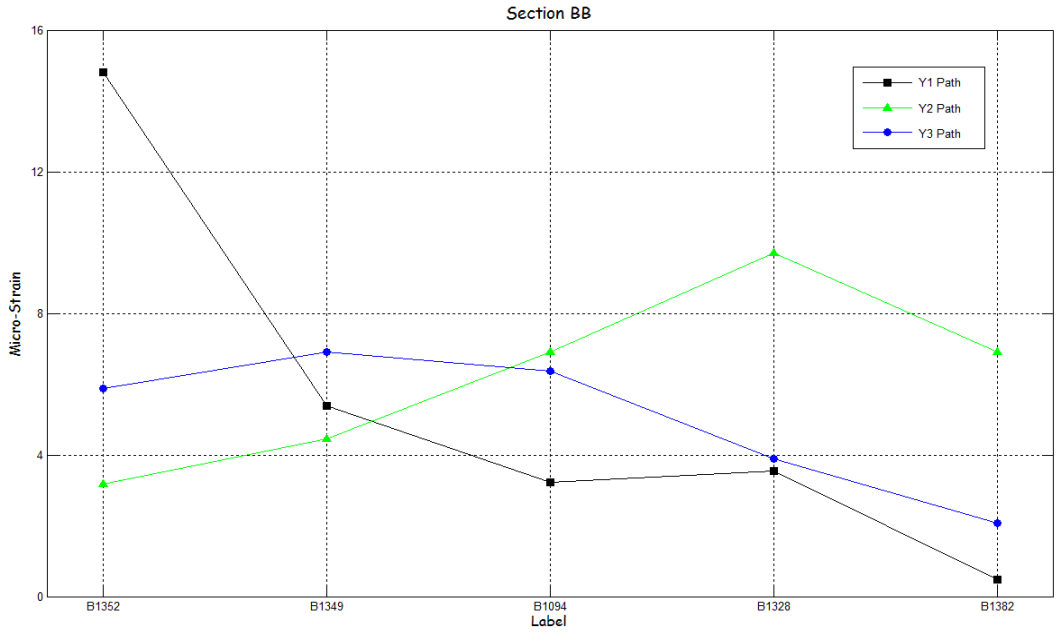

Fig 4.21 Lateral distribution at Section B-B.

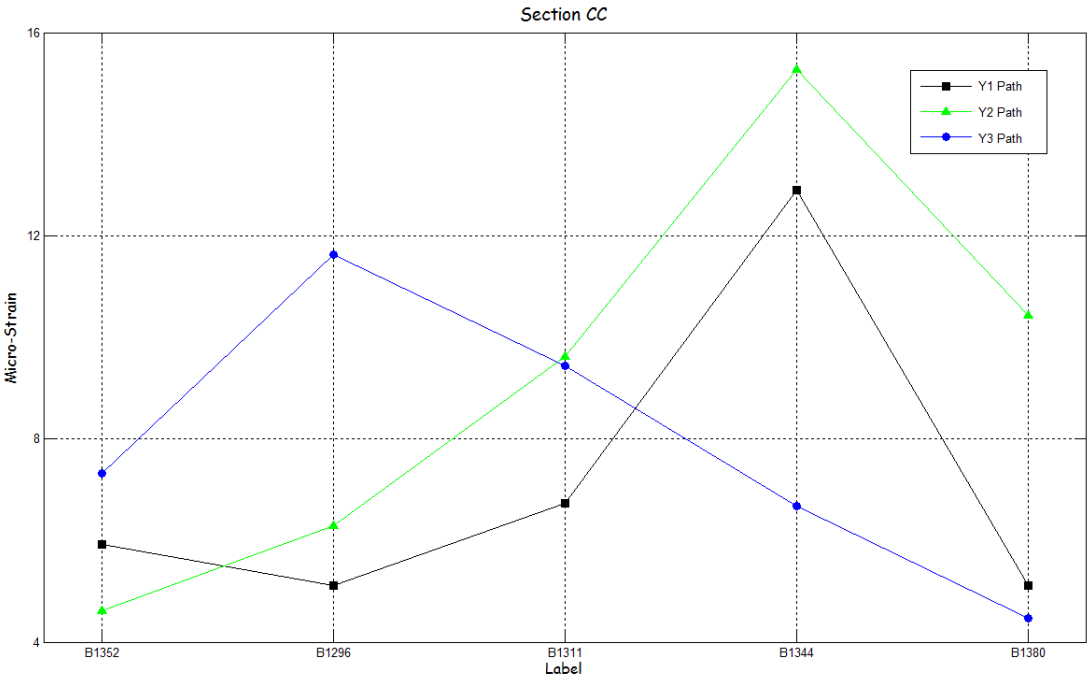

Fig 4.22 Lateral distribution at Section C-C.

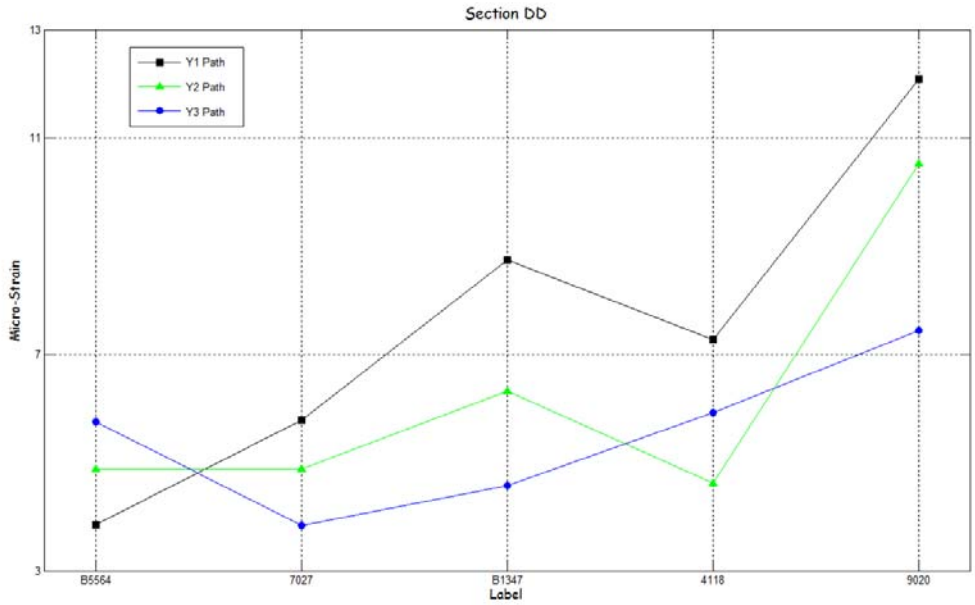

Fig 4.23 Lateral distribution at Section D-D.

4.3.6 Similarity with the 1990 test

As mentioned before, all the loading conditions from the 1990 test were nearly duplicated in this new test in order to determine any change in the structure. The comparison was made by plotting the new data with the old data at the exact same locations. In this case we will plot the response history from the strain gages B1347, B1311, B1347, B1320, and B1326 corresponding to the new test and we will compare those with the strain gages TRAN745, TRAN761, TRAN752, TRAN015, and TRAN779, which correspond to the old test, at the same position. These plots were made for paths Y1, Y2, and Y3. As we can observe in Figures 4.24, 4.25, 4.26, and 4.27, the data recorded in the new test presented magnitudes very similar to those obtained in the 1990 test (within 8%). This means that the bridge has not suffered any significant change in its structure and behaves almost the same as 18 years ago. Figure 4.27 show the comparison

between the strain gages that were located close to the supports. As can be observed, the fixity of the supports has not experienced any major change with time.

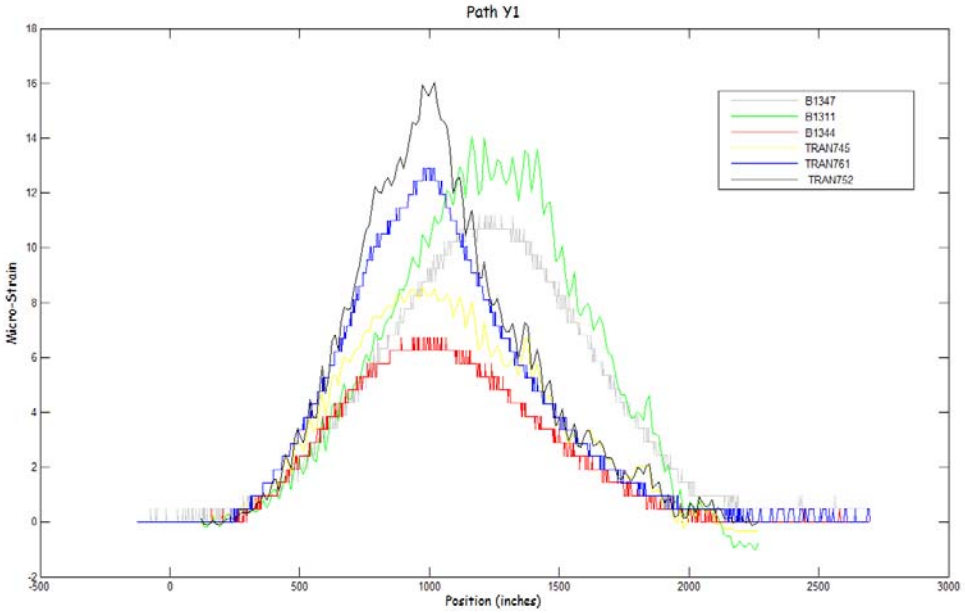

Fig 4.24 Comparison of the old test with the new test for Path Y1.

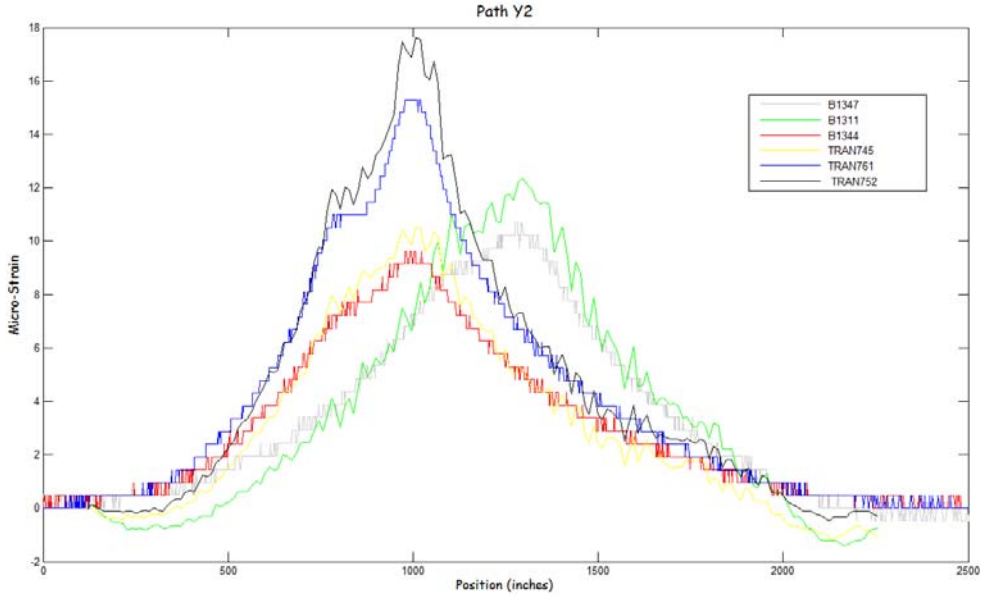

Fig 4.25 Comparison of the old test with the new test for Path Y2.

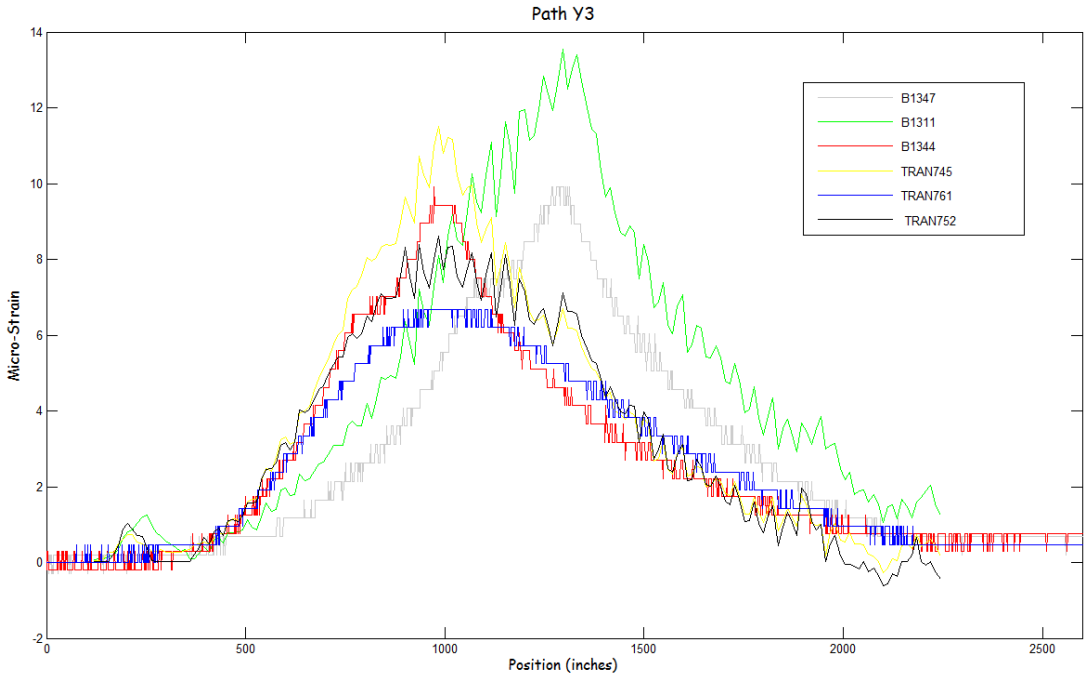

Fig 4.26 Comparison of the old test with the new test for Path Y3.

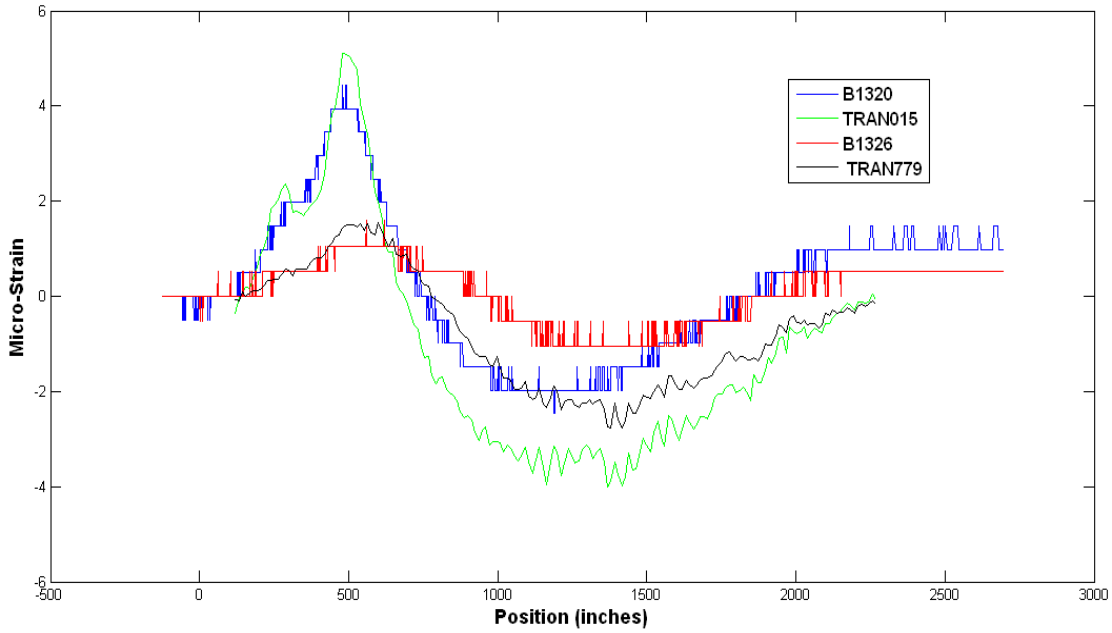

Fig 4.27 Comparison of the old test with the new test for Path Y1.

4.4 Finite-Element Model

The finite-element model for the Walnut Grove Bridge was created using the computer program SAP2000. For the model process, the structure was broken up into four different elements, the upper deck, the webs, the bottom flanges and the diaphragm, where every individual element was modeled according to its geometric and structural properties. These elements were modeled using thick-shell elements. The reason why shell elements were chosen is because they capture the out of plane deformation and rotation (bending behavior) of a plate and combine it with the in-plane deformations of a plane element. Between thin and thick elements, thick elements were chosen because the mesh used in the modeling generated elements with a ratio of the thickness to the length bigger than the recommended value of 0.1 for thin elements. Also, the sap manual states that a thick element is more accurate even when shear deformations are insignificant. However, this accuracy is very sensitive to large aspect ratio and distorted elements. That is why this model was developed using elements with aspect ratio no larger than 3 and very little distortion in almost all cases. A total of 10,400 nodes and 10,700 area elements were used in this model.

4.4.1 Elements representation

As stated before, the deck was modeled using a mesh composed of thick-shell elements. These elements had a thickness of 8 inches and were initially modeled with a concrete strength of 4500 psi, as described in Section 4.1. However, during the analysis process the strength properties were varied in order to calibrate the model. This process

will be explained in more detail later on. Around 4,260 nodes and 4,130 shell elements were used to model the upper concrete deck.

The mesh used to represent the concrete deck was laterally divided in such a way that nodes were placed in the same locations as the webs. Also, nodes were placed at the same position of the loading paths previously described in Section 4.2. With this lateral distribution a close replication of the loading conditions from the live load test could ensured. Longitudinally, the mesh was divided, mostly, into 22.5 inches and 11.03 inch elements. This distribution was created with the primary purpose of closely representing the locations of the truck's wheels as the truck was driven across the bridge and to capture the behavior of specific points on the structure for further comparisons. As a result, the biggest aspect ratio obtained was about 2.8, which is smaller than the recommended value of 4.

The inside corner of most of these elements from the mesh was 90 degrees, as we can appreciate in Figure 4.28. However, in order to represent the skew form of the bridge, distorted 4-node elements and triangular elements were used at the boundaries of the structure, which can also be seen in Figure 4.28. These elements were limited to the minimal amount possible, since their performance is not as accurate as an orthogonal 4-node element.

The bottom flanges were also modeled using thick-shell elements .These elements had a thickness of 6 inches and an initial strength of 4500 psi, which was later changed in value with the purpose of modeling calibration, as will be explained later on. Around 3,800 nodes and 3,700 shell elements were used to model the bottom flange. The bottom flange had a smaller width (37 feet) than the concrete deck (42.5 feet), as previously

described in Section 4.1. Figure 4.29 shows how the width of the concrete deck, represented by the dark lines, exceeds the transversal dimension of the bottom flange. The bottom flange mesh had very similar characteristics compared to the deck mesh. The skew form was also modeled using the same types of distorted and triangular elements, and the majority of the shell elements used in the mesh had a 90 degree angle at the corners.

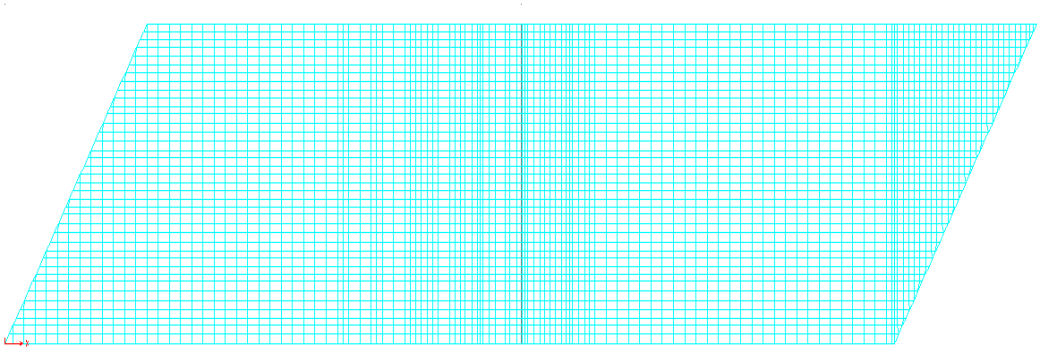

Fig 4.28 Concrete deck finite element representation.

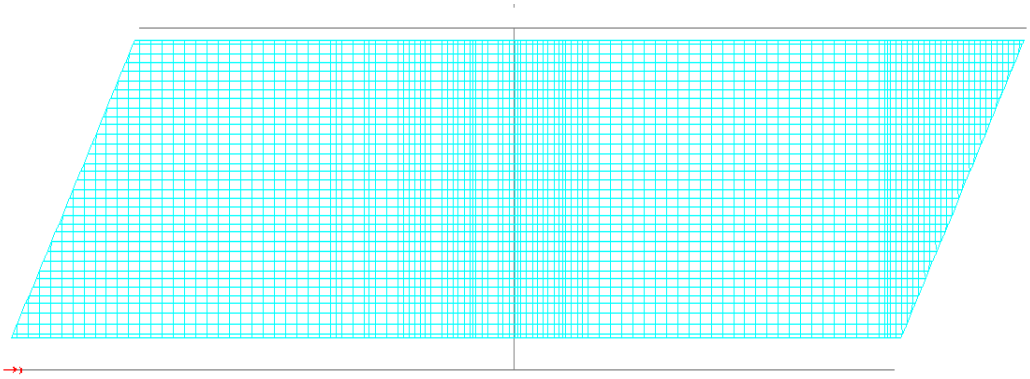

Fig 4.29 Bottom flange finite element representation.

The criteria used to generate the mesh for the bottom flange was the same used for the concrete deck. Longitudinally, the bottom flange mesh had the same distribution as the upper deck mesh, characteristic that was necessary for the connection of these two elements through the web. Laterally, the mesh was divided also the same way as the concrete deck. This was necessary to accomplish the connection of the transversal diaphragms to the concrete deck and bottom flange.

The concrete webs and transversal diaphragms were also modeled using thick-shell elements. They both had a thickness of 12 inches and an initial concrete strength of 4500 psi. This value was later varied in order to calibrate the model, process that will be discussed in Section 4.5. Close to 2,340 nodes and 2870 shell elements were used to model these two structural components.

The concrete web was vertically divided into five elements of equal length, 13 inches, and longitudinally divided using the same criteria as the deck mesh and bottom flange mesh. The transversal diaphragms were also vertically divided into five elements and longitudinally divided into eight elements. The maximum aspect ratio found for the web and the diaphragm was 2.54 and 1.2, respectively. All the shell elements used in the web and diaphragm mesh had inside corners of 90 degree. No triangular or distorted elements were used in any of meshes. Figure 4.30 shows a representation of these two elements. As can be observed, the diaphragms were placed perpendicular to the webs.

As a final process, all these elements were connected together as a result of the web mesh sharing common nodes with the upper and bottom flange meshes. The upper deck and the bottom flange were separated by a distance of 65 inches, as is shown in Figure 4.31. These two meshes were connected through the web elements.

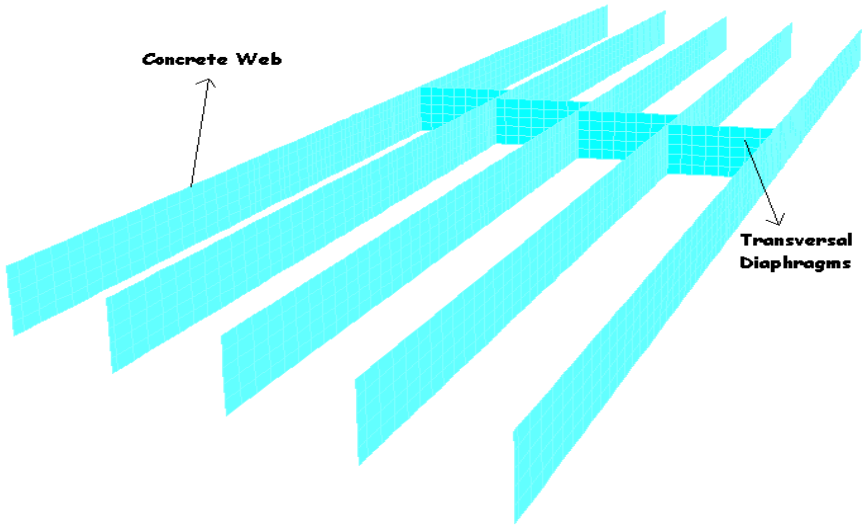

Fig 4.30 Web and diaphragm finite element representation.

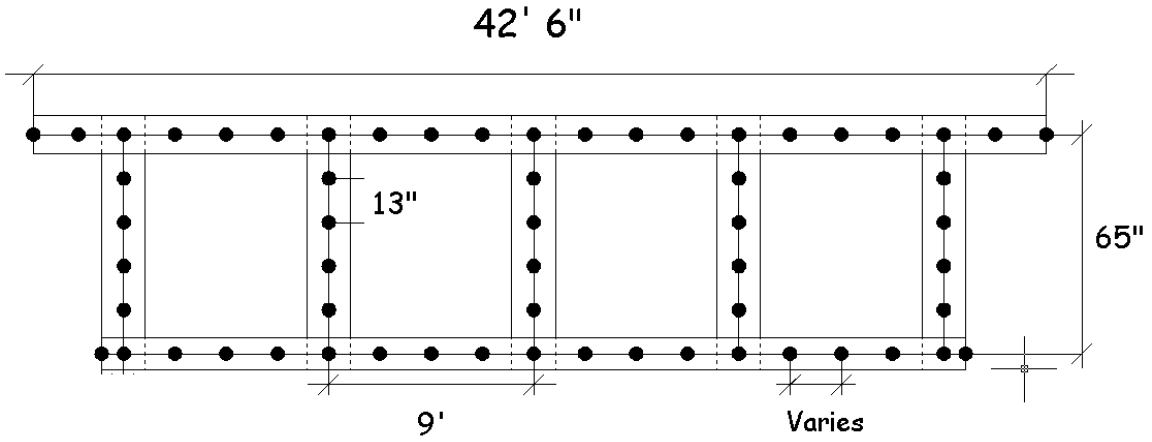

Fig 4.31 Cross section of the finite element model.

4.4.2 Boundary conditions

As explained in Section 4.3, the structure presented some kind of end restriction, which translates into a nearly-fixed condition. This nearly-fixed condition allows almost no rotation at the ends. According to the characteristic of our model, one way of representing these restrictions is by using some sort of mechanism that would prevent any node from the boundary to move horizontally. A horizontal movement of the nodes translates into axial displacement, if all the nodes move into the same direction, and as rotation, if the top and bottom nodes move in opposite direction. This characteristic is seen in Figure 4.32.

A fixed condition would not allow any type of axial movement or rotation at the boundary of the structure. This condition can easily be modeled by simply placing some hinges at the nodes, which would not allow any type of horizontal movement. By doing so, any rotation and translation are totally restricted. This representation can be seen in Figure 4.33. However, as mentioned before, the structure did not behave as if it were fixed at the ends, apparently because the supports were not rigid enough to totally prevent any horizontal movement. Instead, the supports allowed some displacement at the end nodes. This condition can be represented by using springs elements at every node at the ends, as shown in Figure 4.33. The springs are assigned with a constant of rigidity “K”, which will be related with the rigidity of the supports at every node.

Another important characteristic of the structure’s boundary conditions is the extended vertical support inflicted on the structure due to the geometric shape of the abutments. For instance, as we can observe in Figure 4.7, the abutment extends a little bit further at the bottom flange than at the upper deck, which is translated in more vertical

support in that area of the structure. On the other hand, Figure 4.8 shows that the geometric shape of the wing walls also applied some degree of support at the exterior parts of the upper deck. These vertical supports, applied to the structure by the abutment and the wing walls, were modeled using vertical springs at every node located within the geometric range of these structural elements.

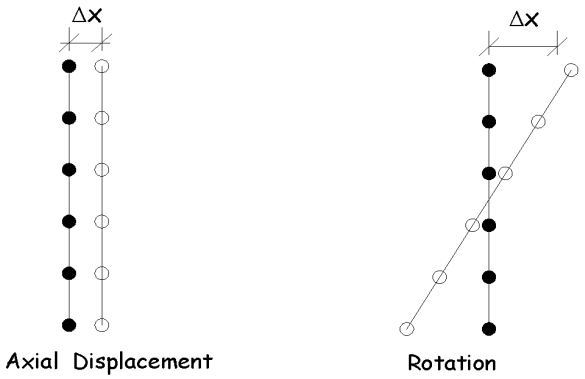

Fig 4.32 Possible movement of the nodes.

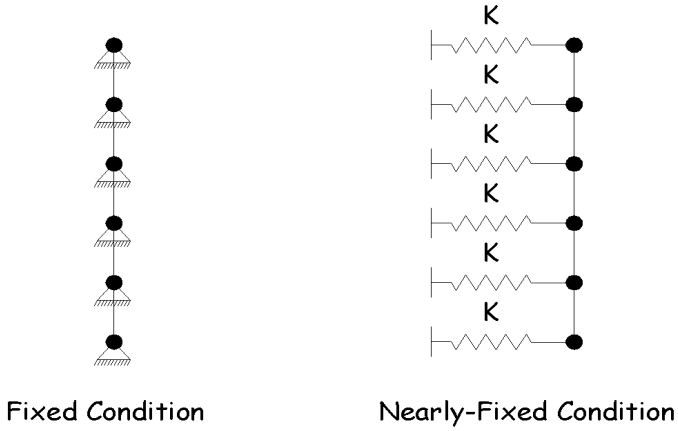

Fig 4.33 FEM representation of a fixed and nearly-fixed condition.

In order to determine the vertical and horizontal rigidity of the springs used in the model, the abutment and the wing walls were modeled using a finite-element approach in SAP2000. Solid elements were selected to represent the support structures. A solid element is an 8-node element with 3 degrees of freedom at each node. An example of this particular element is presented in Figure 4.34.

This type of element is a direct extension of the rectangular plane elements and also carries the defect of the "parasitic shear." This condition is improved by using the "incompatible mode" option that helps represent the bending deformation. The solid elements were chosen due to the complicated geometry of the abutment and wing walls. Only the material properties have to be entered in order to create solid elements in SAP2000, which in this case a value of 4,500 psi for the concrete strength was used. Around 1,590 nodes and 1,030 solid elements were used in the model. Figures 4.35 and 4.36 show a 3D view of the model for the abutment and wing walls.

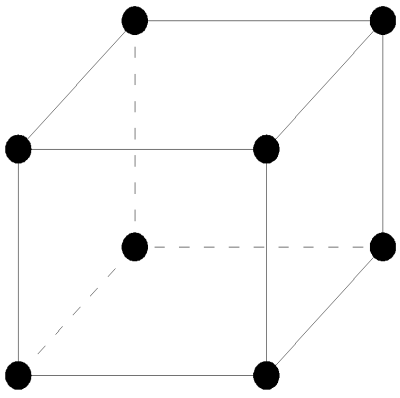

Fig 4.34 Solid element representation.

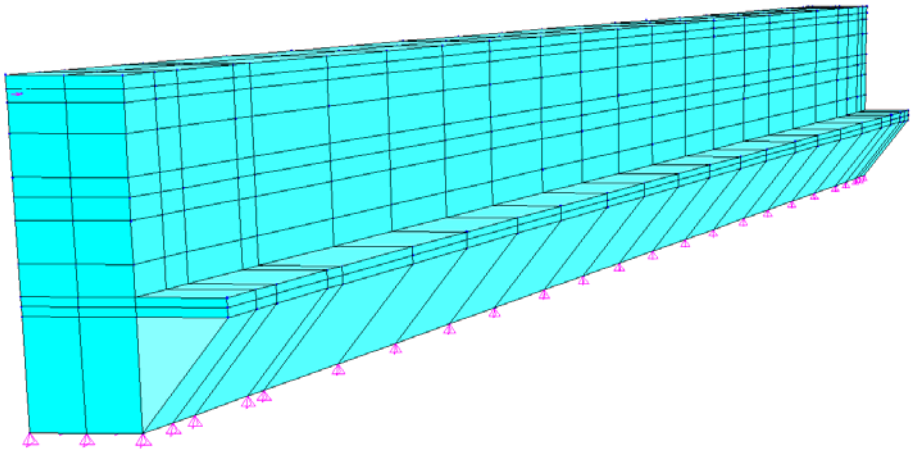

Fig 4.35 Abutment finite element model.

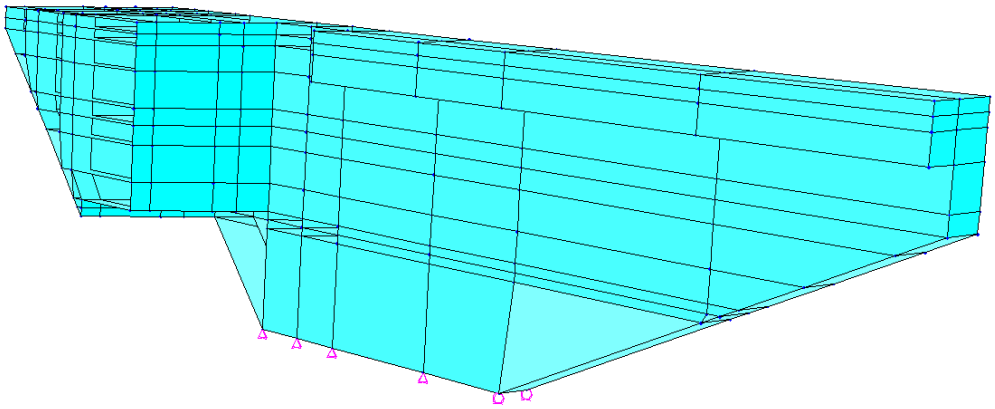

Fig 4.36 Wing wall finite element model.

After the model was assemble, the vertical and horizontal rigidity of the support at specific nodes were obtained by simply placing a vertical or horizontal dummy load at every node, one at a time, a measuring the vertical or horizontal deflection caused by that load. Figure 4.37 shows an example of the application of vertical and horizontal loads into the support.

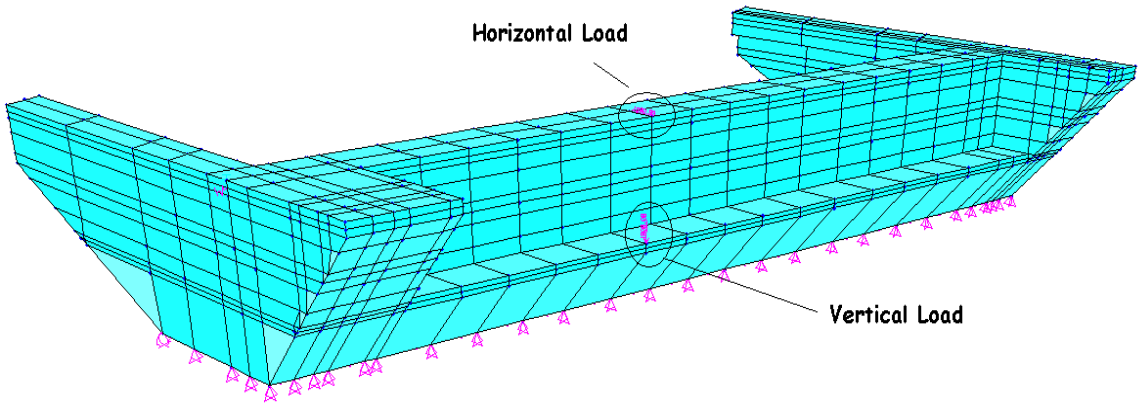

Fig 4.37 FEM of the support with vertical and horizontal loads.

The rigidity at every point was obtained by dividing the load value by the measured displacement. In our model this rigidities were measured in kips/in. Extremely high rigidities, above 100,000 kips/in, were represented by a hinge support. The rigidity of the left wing wall reached an average value of 11,000 kip/in at every node, while the right one obtained 7,700 kip/in. This difference was expected since the left wing wall was more rigid than the right one. The rigidities obtained in the extended part at the bottom of the abutment ranged from 32,000 kips/in to 19,000 kips/in. The horizontal rigidities of the abutments reached an average value per node of 7,600 kips/in at the top and 44,600 kips/in at the bottom.

These values were introduced into the finite element model of the bridge. Figures 4.38 and 4.39 show how the horizontal and vertical springs were placed in the finite-element model. In Figure 4.38, it can be observed the contour of the wing walls, represented by the spring elements. In Figure 4.39, we can appreciate the limits of the support extension at the bottom flange.

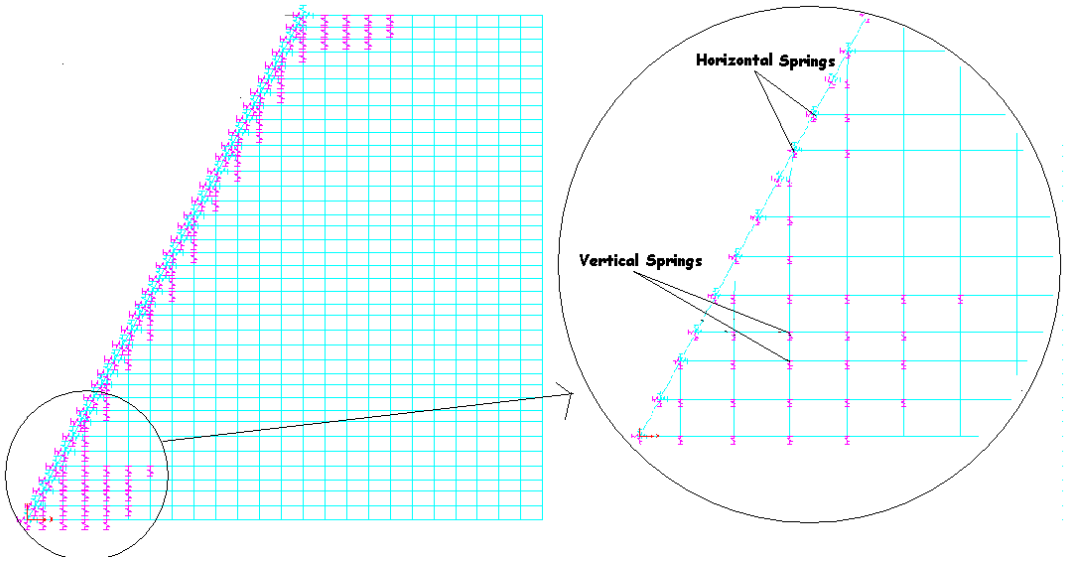

Fig 4.38 Horizontal and vertical springs at the upper Deck.

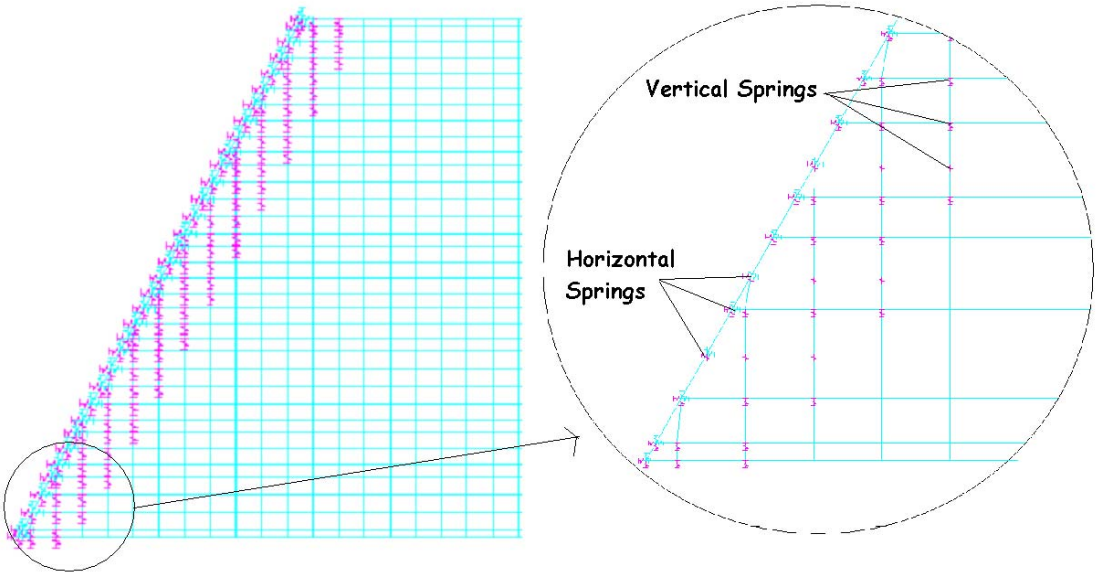

Fig 4.39 Horizontal and vertical springs at bottom flange.

4.4.3 Truck load and loading path description

The loads from the truck test were applied to the Walnut Grove Bridge finite element model as concentrate loads. As explained before in Section 4.2, the loading truck had three different axles, however, for modeling simplicity, the two rear axles were fused into just one axle, located in the middle of the original axles. With this assumption, our simulated truck had two different axles separated by a distance of 220.5 inches, which explains the division of the deck mesh into segments of 22.05 and 11.03 inches. The width of the two axles varied due to the configuration of truck wheels. The front axle had a width of 81 inches while the rear axle had a width of 59 inches. The width represents the center to center distance at every axle. These two dimensions were adapted into the finite-element model as is shown in Figure 4.40. This figure shows the footprints of the simulated truck along loading path Y3.

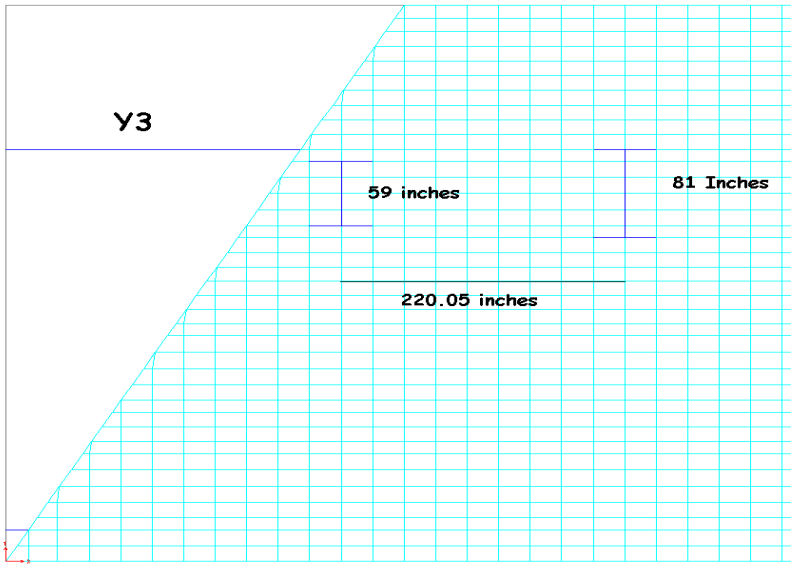

Fig 4.40 Loading truck dimensions in the FEM.

For this analysis, only three loading paths were examined, Y1, Y2 and Y3. The mesh was laterally divided to account for these three locations, as is shown in Figure 4.41. According to the live-load test described in Section 4.2, the truck was driven along the loading path using the driver-side wheels. This condition was also simulated in the finite-element model by placing nodes to the right side of every loading path, according to the axle's width.

The loading truck was positioned at different longitudinal locations along the length of the bridge, at intervals of 22.05 and 11.03 inches. For every single location, the finite-element model was analyzed and the results were recorded for further comparison with the live-load test. Approximately 53 truck positions were evaluated for every loading path, which means that the finite-element model was run and analyzed approximately 150 times. Figures 4.42, 4.43 and 4.44 show a figure of the application of the truck loads along paths Y1, Y2 and Y3 respectively, at a truck location of 477.45 inches from the reference point.

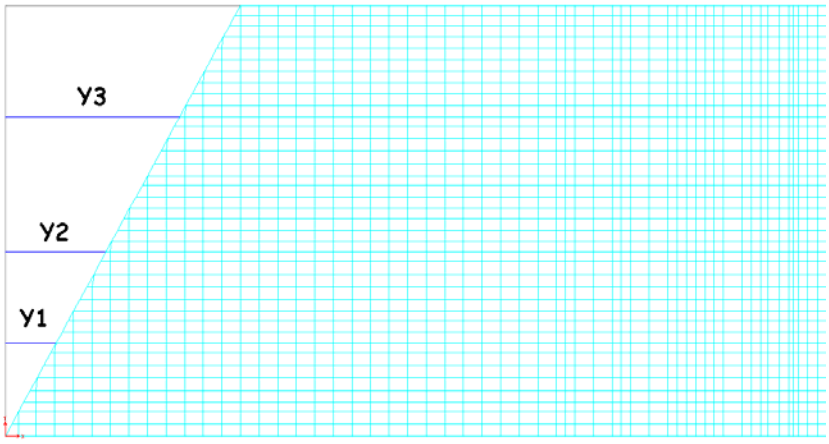

Fig 4.41 Loading path in the finite element model.

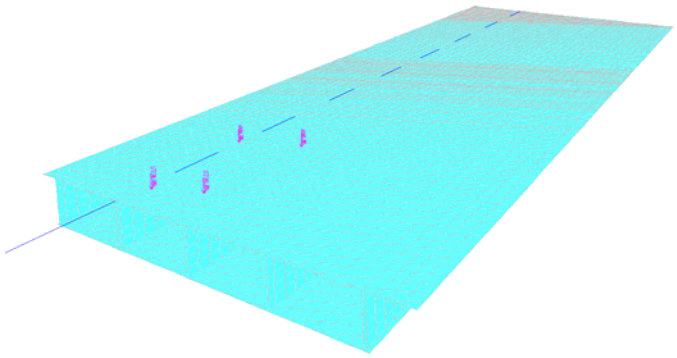

Fig 4.42 Truck loads along path Y3.

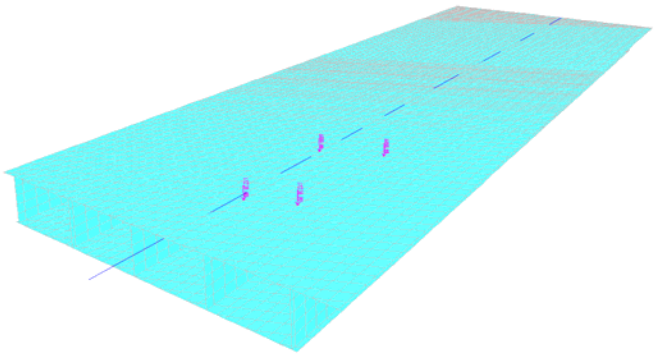

Fig 4.43 Truck loads along path Y2.

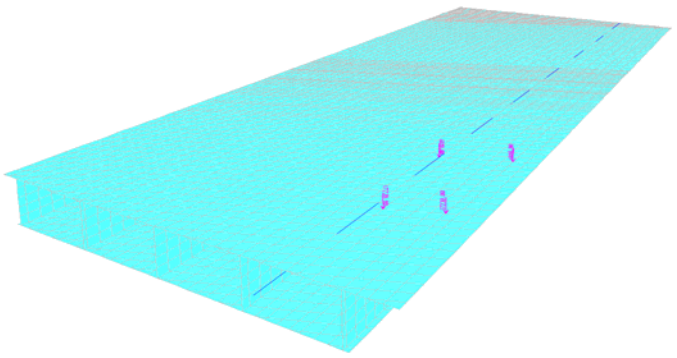

Fig 4.44 Truck loads along path Y1.

4.5 Comparison of FEM and Live-Load Results

In order to compare the finite-element model results with the live load test data, four specific locations were chosen at the bottom flange. These four locations are represented with the strain gages B1347, 7027, B1311, and B1344.The first two strain gages belong to Section DD of the instrumentation plans, while the last two belong to Section CC. Figure 4.45 shows the location of these points of interest in the finite-element model. These four points were chosen because of their easy location and because they were placed directly underneath the concrete webs.

Every time the finite-element model was run for the 53 locations of the truck loads, the average stress in the longitudinal direction was recorded for each location. These stresses were subsequently used to calculate an associate strain at those locations. This was simply done by dividing the recorded stresses by the corresponding modulus of elasticity. Around 600 strains values were calculated using this in this approach.

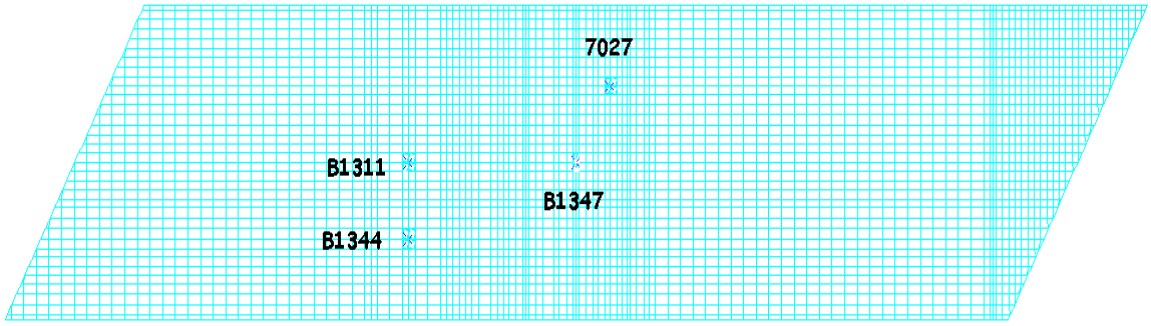

Fig 4.45 Location of four sensors at the bottom flange FEM.

The calculated strains were plotted against the truck's position and a direct comparison was performed between these results and the live-load test data. Several differences were notice in the first models, which led to several modifications to the original finite-element model. The modifications were based on the variation of the material properties until a close match was obtained between the FEM and live load test results. As a result, the bottom flange, web, diaphragm and upper deck ended with different concrete compressive strengths from the original value of 4,500 psi.

It was believed that the structure properties would vary longitudinally, since the pres-stressing strand distribution was not homogeneous across the length of the structure and because there were some visible cracks at the supports, which translates to a decrease in stiffness in those areas. The bottom flange mesh was broken up into four different types of sections. Each section resulted in very different material properties. This can be appreciated in Figure 4.46, where the new areas are labeled as bottom1, bottom2, bottom3, and bottom4. At the same time, the upper deck was also divided into different sections. Only two types of section were perceived in the upper deck mesh. According to Figure 4.47, these sections are designated as deck 1 and deck 2. Apparently, the concrete strength at the deck did not vary that much compared to the bottom flange.

The material properties from each new section were manually varied until reasonable results were obtained. Also this variation process affected the web and transversal diaphragms. As a result, the concrete web was modeled with compression strength of 2,000 psi, while in the diaphragms a value of 4,000 psi was used. Table 4.1 lists the final material properties used in every section of the finite-element model.

As can be observed from Table 4.1, the strength on the bottom flange is decreasing toward the supports while in the deck is increasing. This difference in strength might be caused by the presence of very dense cracks, by the variation in depth of the reinforcement bars and steel strands at any location, and by the influence of the actual concrete strength. These final values do not represent the actual values of concrete strength at those locations, but they were used to improve the accuracy of the model. However, they do give an idea of the variation in strength of the concrete deck and bottom flange.

Table 4.1 Initial and Final Values of the Concrete Strength in the FEM

	Concrete Strength	
	Initial Value	**Final Value**
Sections		
Bottom 1	4,500 psi	8,000 psi
Bottom 2	4,500 psi	6,000 psi
Bottom 3	4,500 psi	1,000 psi
Bottom 4	4,500 psi	500 psi
Deck 1	4,500 psi	2,000 psi
Deck 2	4,500 psi	3,000 psi
Web	4,500 psi	2,000 psi
Diaphragm	4,500 psi	4,000 psi

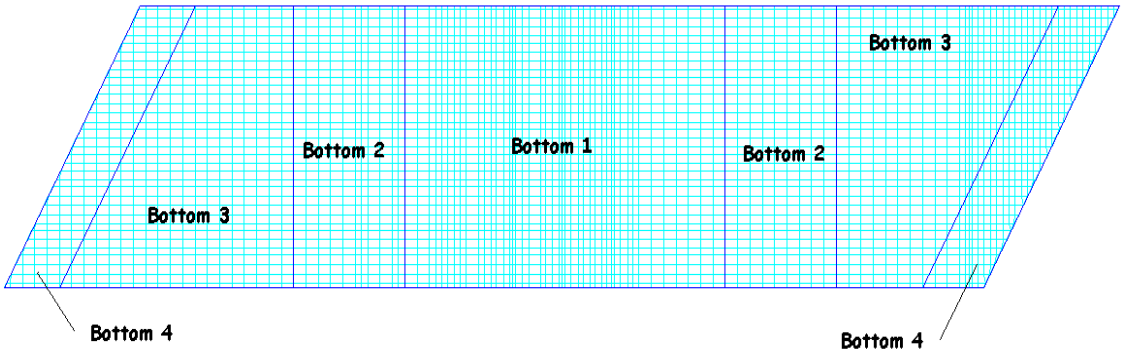

Fig 4.46 Bottom flange sub-division.

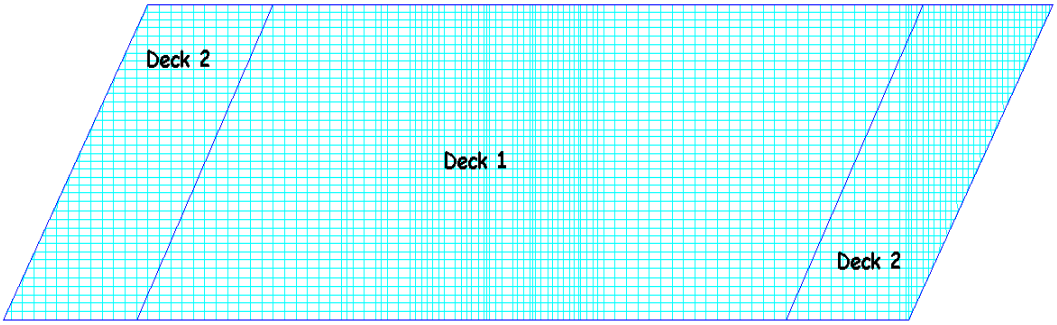

Fig 4.47 Upper deck sub-division.

After the model was calibrated, a direct comparison between the FEM and the recorded live-load test strains was performed for the last time. The next 12 figures compare how the FEM results related to the live-load test results for the three loading path selected and at the four specified locations. Figures 4.48 to 4.51 show a comparison for the loading path Y1, Figures 4.52 to 4.55 represent the comparison for the loading path Y2 and Figures 4.56 to 4.59 exhibit the similarity with the live load test for the loading path Y3.

-Loading Path Y1

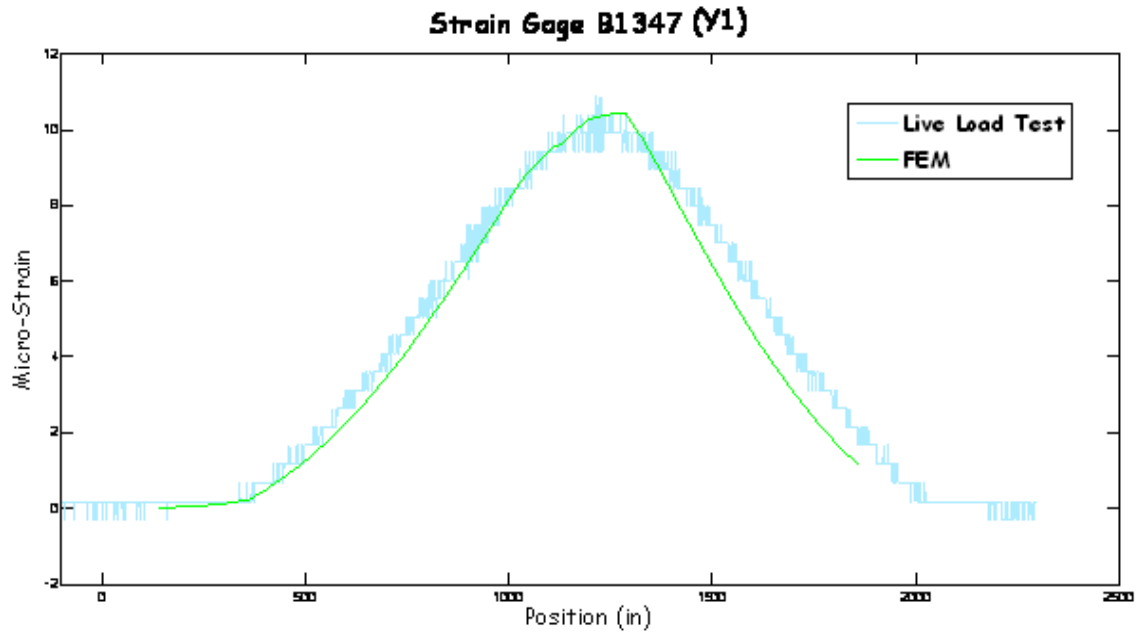

Fig 4.48 Comparison between FEM and load test (B1347).

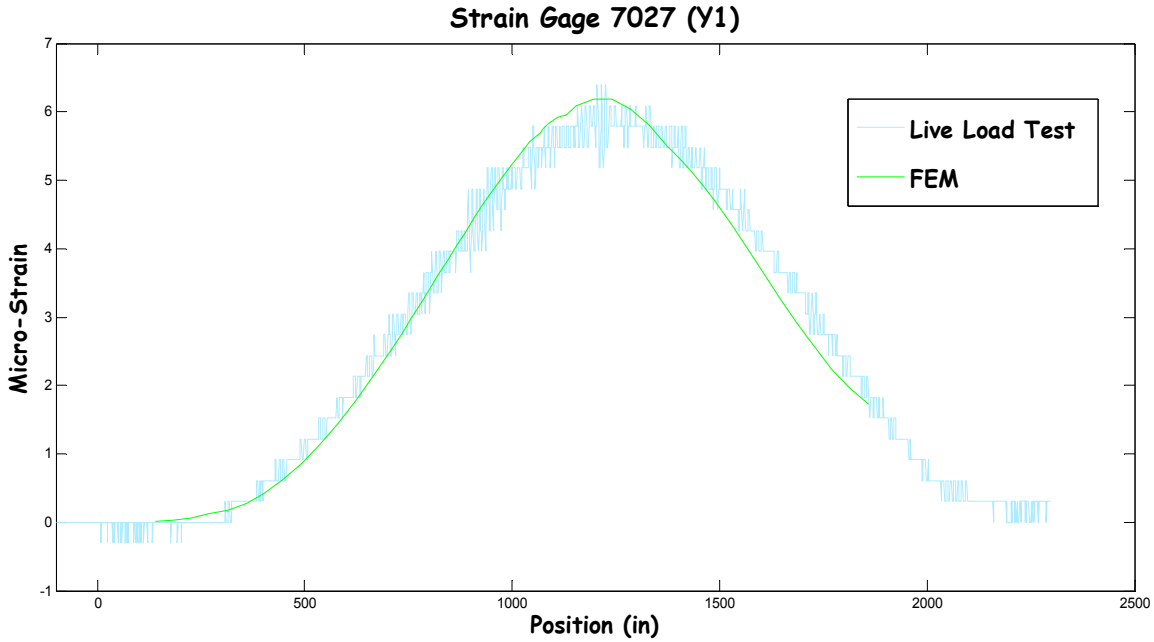

Fig 4.49 Comparison between FEM and load test (7027).

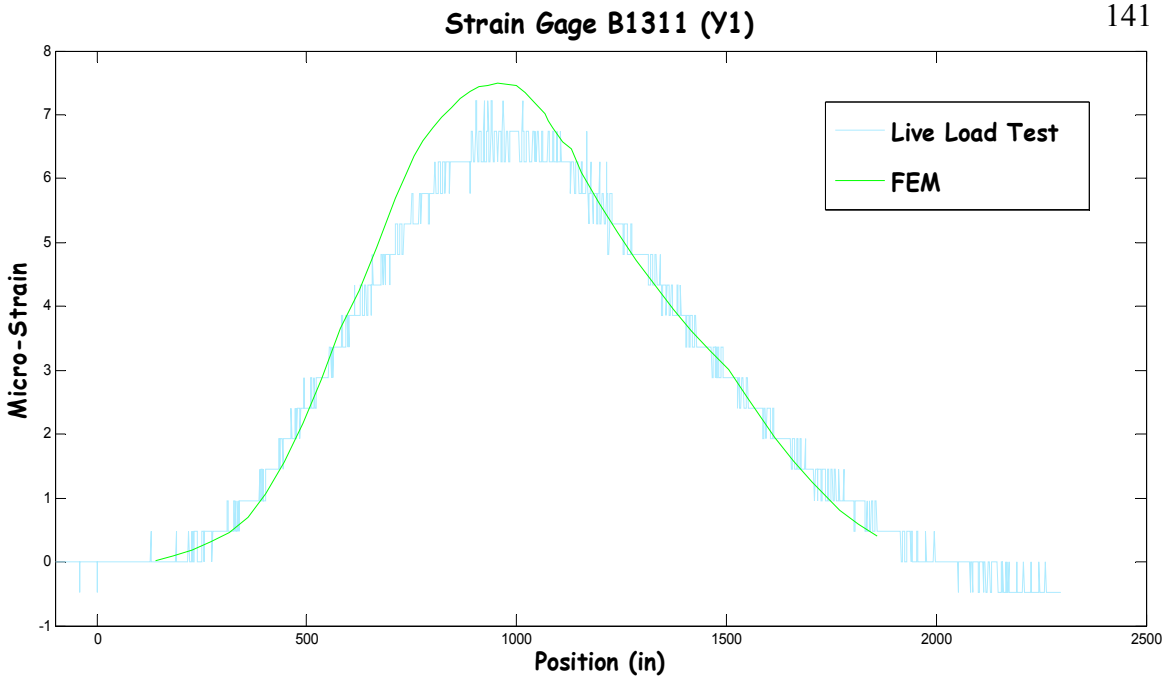

Fig 4.50 Comparison between FEM and load test (B-1311).

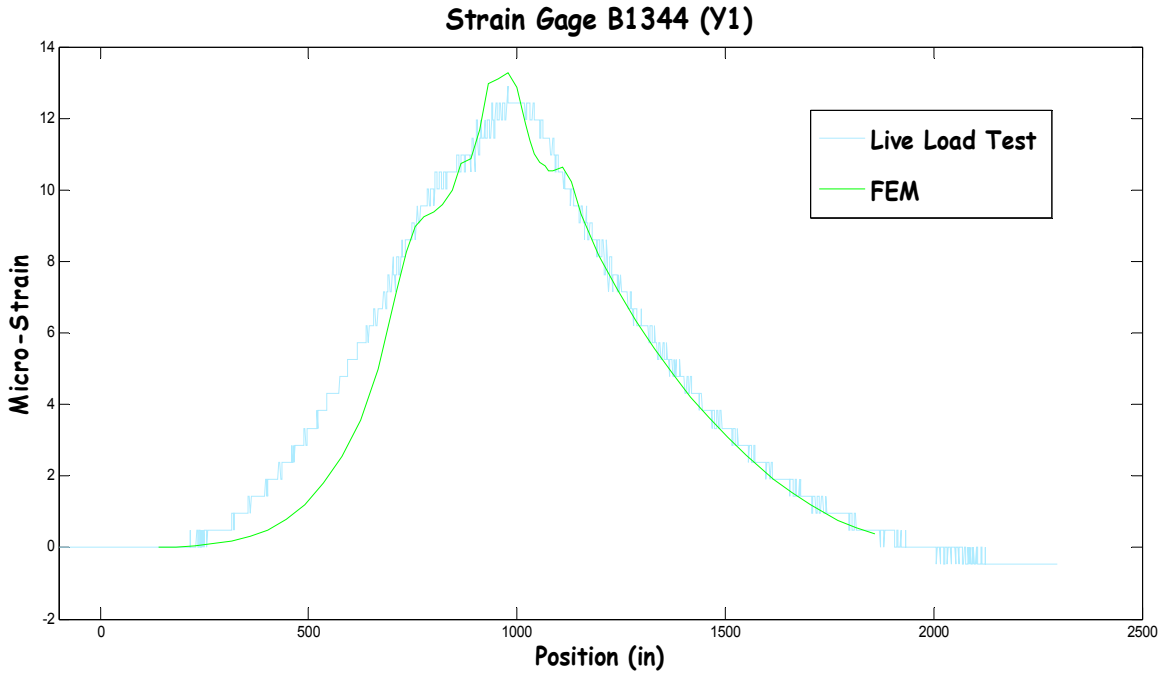

Fig 4.51 Comparison between FEM and load test (B-1311).

-Loading Path Y2

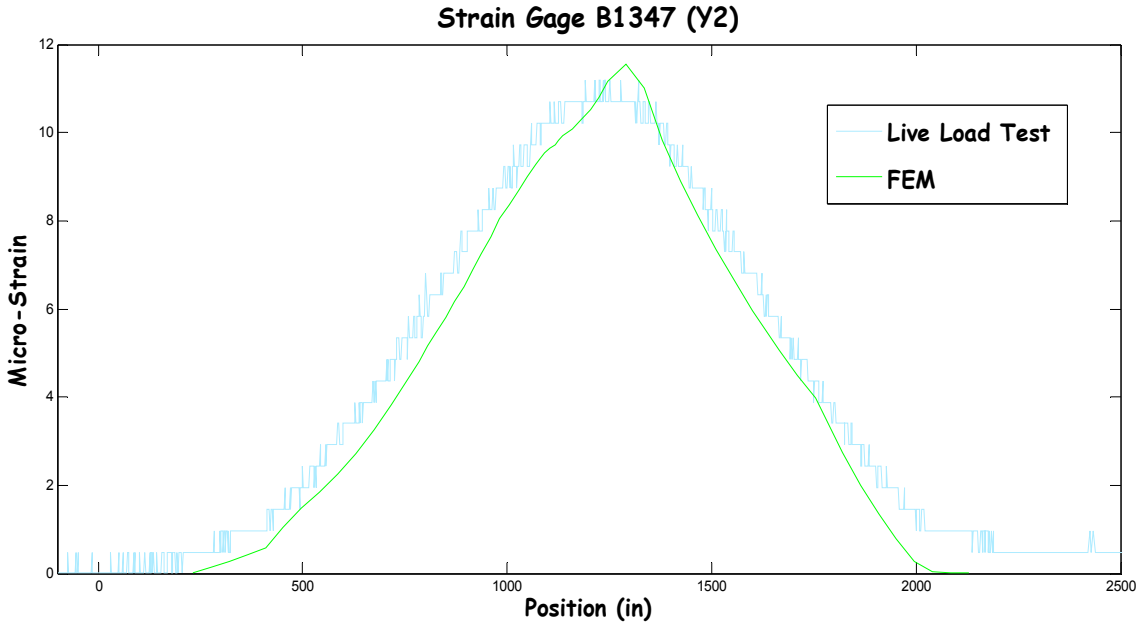

Fig 4.52 Comparison between FEM and load test (B-1347).

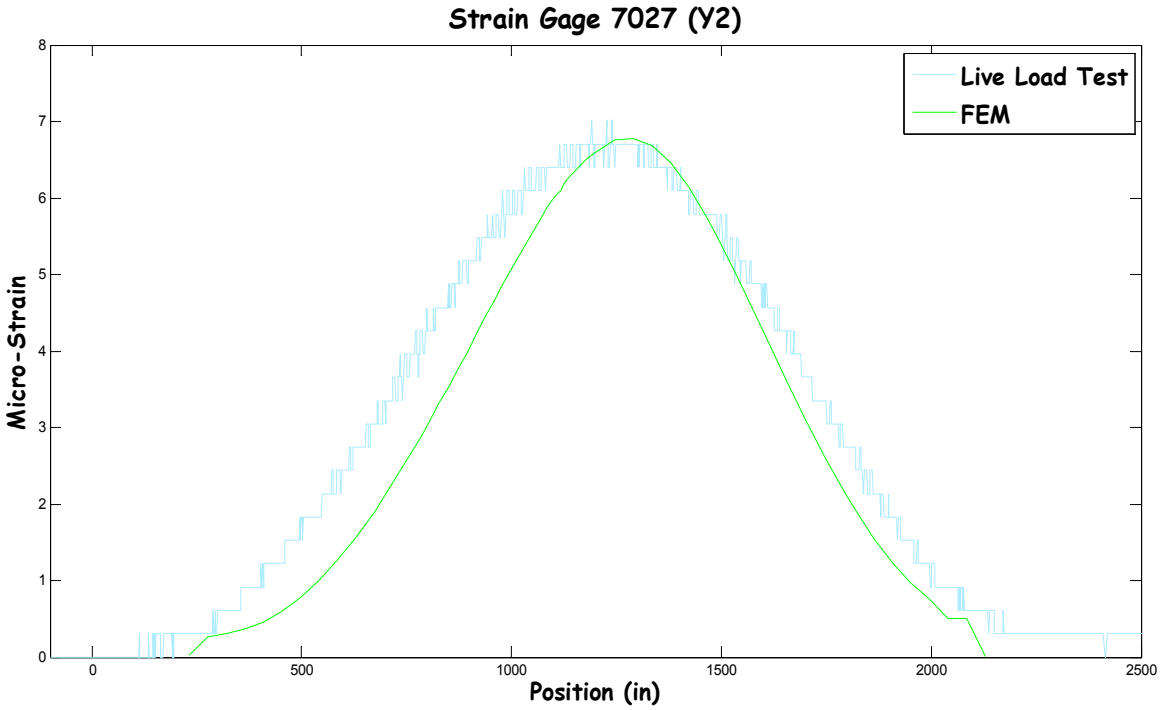

Fig 4.53 Comparison between FEM and load test (7027).

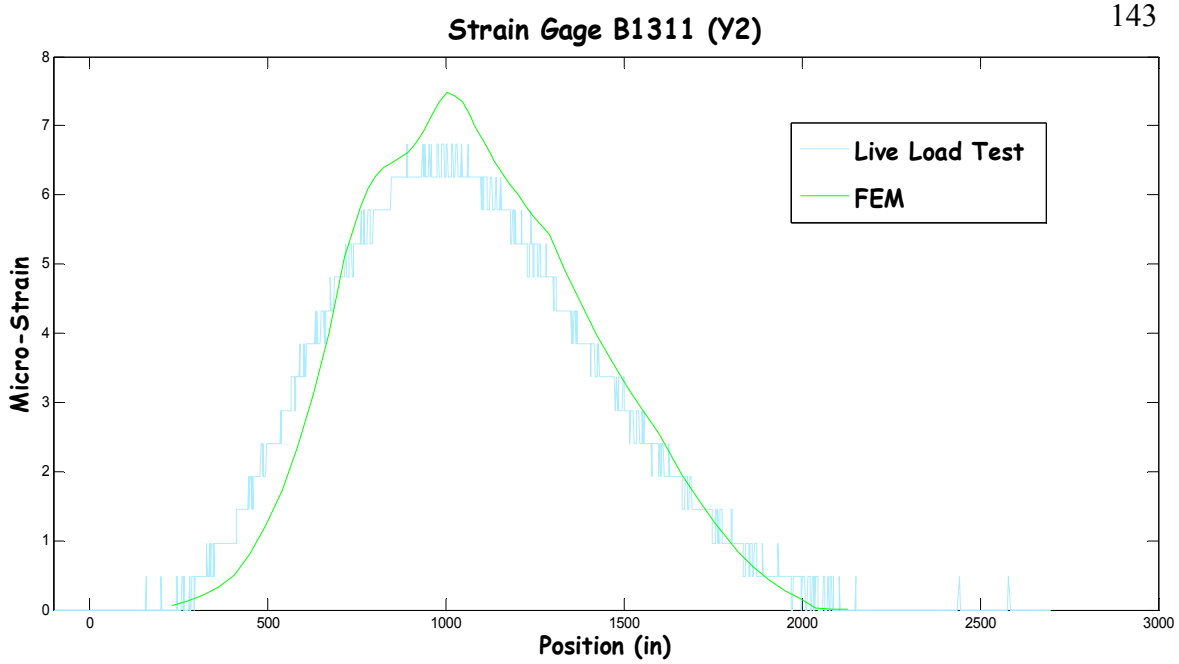

Fig 4.54 Comparison between FEM and load test (B-1311).

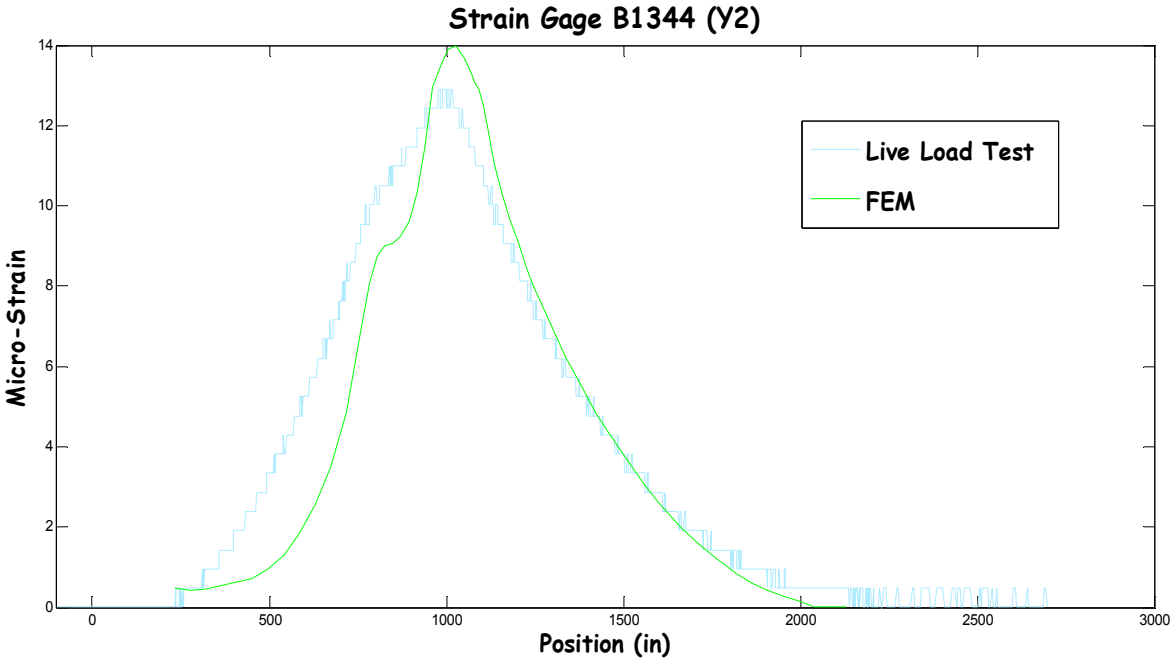

Fig 4.55 Comparison between FEM and load test (B-1344).

-Loading Path Y3

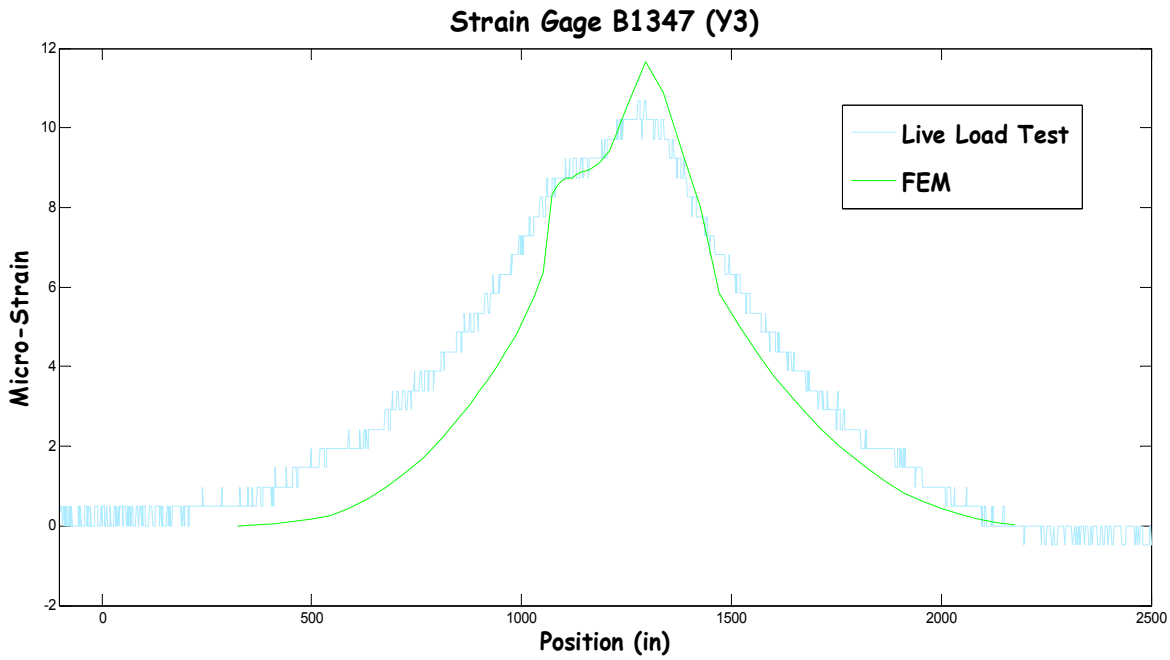

Fig 4.56 Comparison between FEM and load test (B-1347).

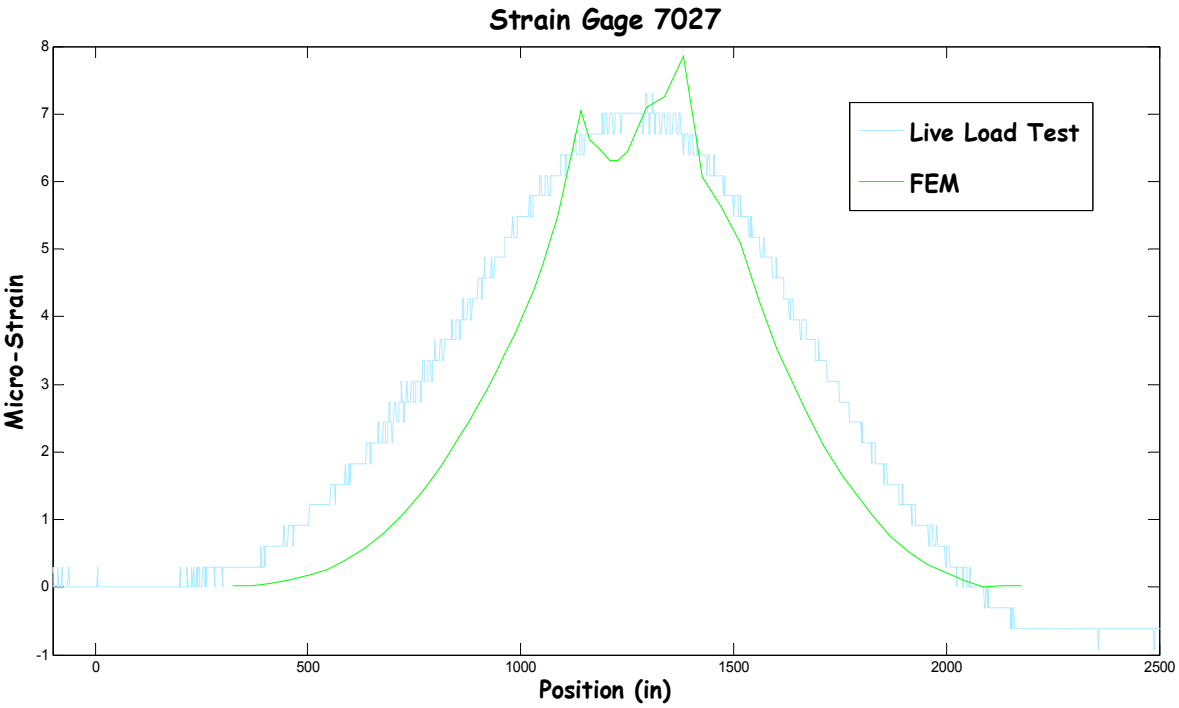

Fig 4.57 Comparison between FEM and load test (7027).

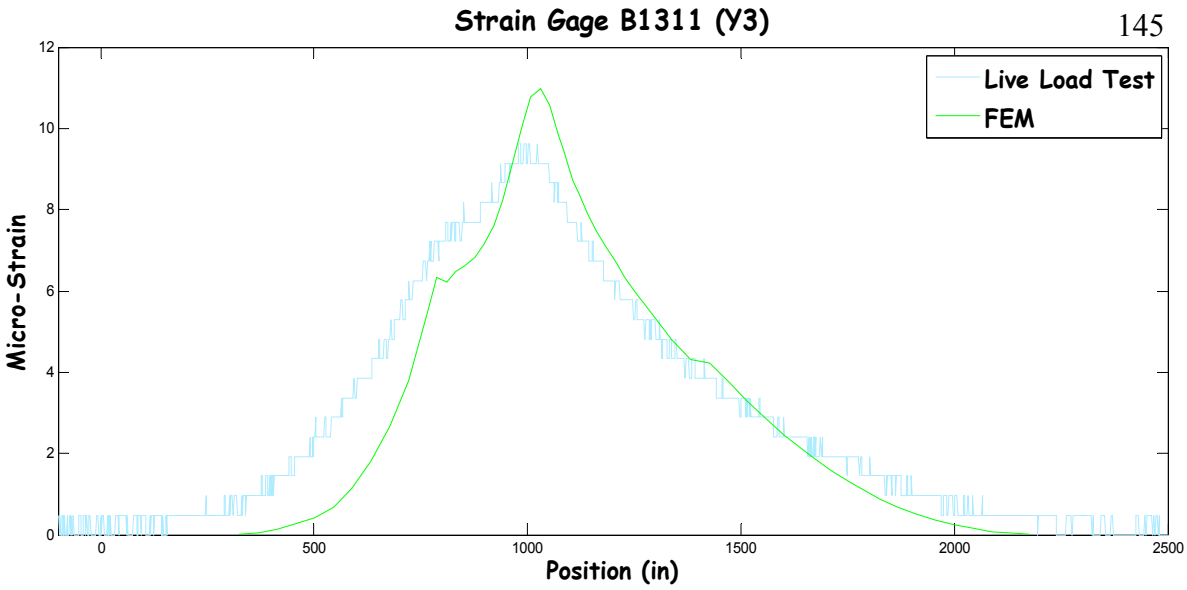

Fig 4.58 Comparison between FEM and load test (B1311).

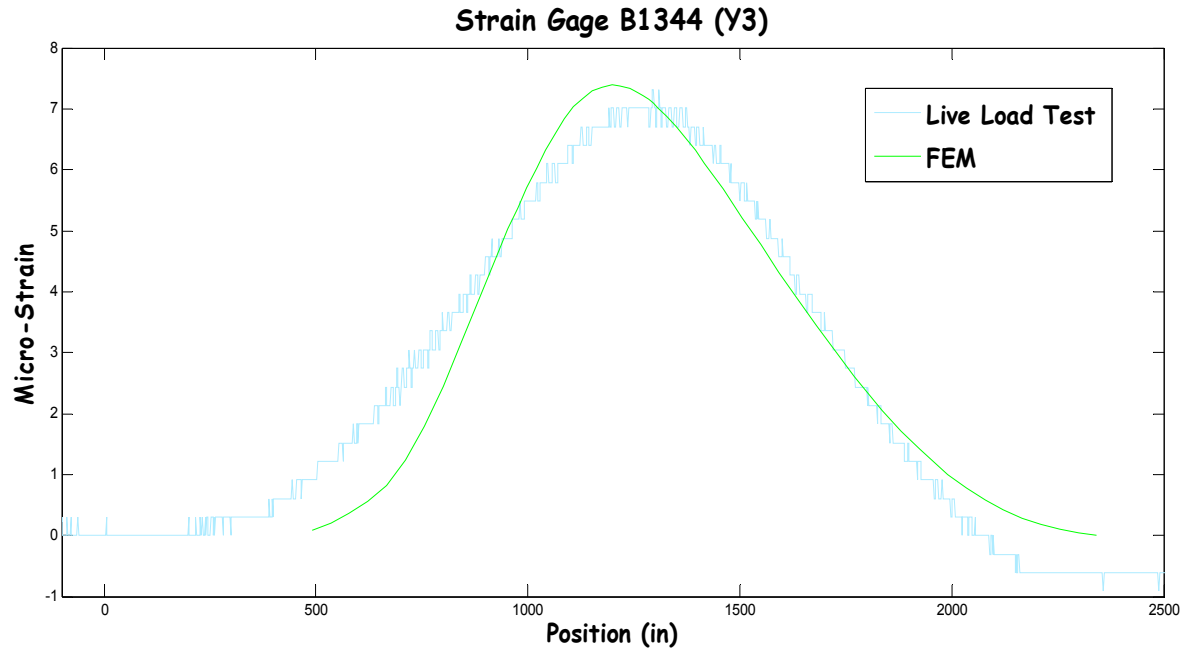

Fig 4.59 Comparison between FEM and load test (B1344).

As we could observe in the figures above, the difference between the finite element model and the live load test results was minimal. Path Y1 was the one with the closest results among all the loading paths analyzed. This characteristic is expected since the data from the loading path Y1 was the one used for the calibration process of the model. However, the other two loading paths presented very close results to the live load test. In every case, the maximum strains were either matched or overestimated by the finite element model.

As it was done Chapter 3, the FEM results were also compared with the live-load test by plotting both data against each other. The accuracy of the model was measured by creating a linear best fit line from the plotted data and obtaining a corresponding correlation. Figure 4.60 shows this comparison. As can be observed from this figure, the strain values obtained from the FEM had a good correlation with those obtained from the live-load test. The correlation factor was computed as 0.9895. This value gives an excellent idea of the accuracy of the finite-element model. The slope of the linear best fit line was calculated as 1.009. This value states that the live-load test results are within 0.9% of the strains obtained from the FEM, which also demonstrate the capacity of the finite-element model to replicate the structural behavior of the Walnut Grove Bridge.

In addition to this analysis, the transversal distribution of the FEM moment over the width of the bridge was plotted and compared with the moment distribution obtained from the live-load test (Section DD). Figures 4.61 through 4.63 show this comparison performed for load paths Y1, Y2, and Y3, respectively. The calculated moments in all cases either matched or exceed the measured values obtained from the live-load test. The maximum calculated moment exceeded the maximum measured moment at least in 3%.

According to the results obtained from the longitudinal and transversal comparison between the FEM and the live-load test results, it can be concluded that this computer model has the capacity to reproduce the actual behavior of this superstructure, and thus, is capable of replicating the load distribution factors for this bridge.

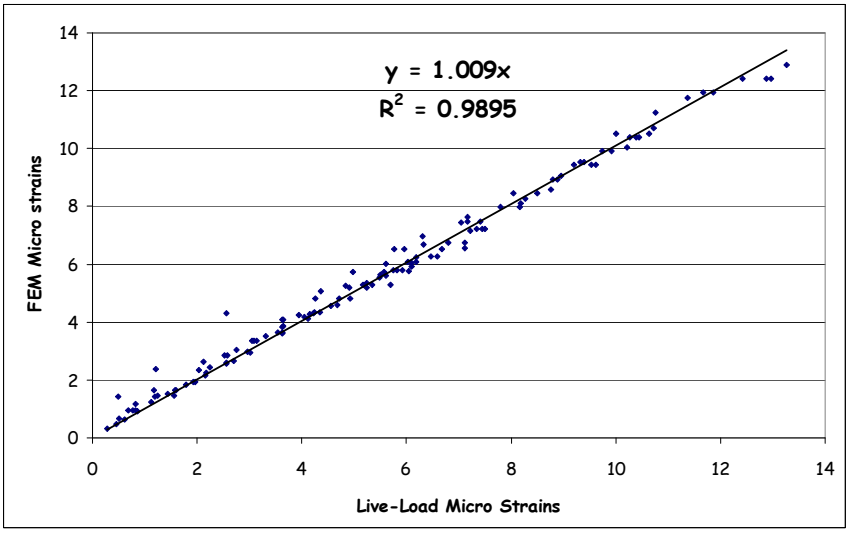

Fig 4.60 Strain values from the FEM and live-load test (Y1,Y2, and Y3).

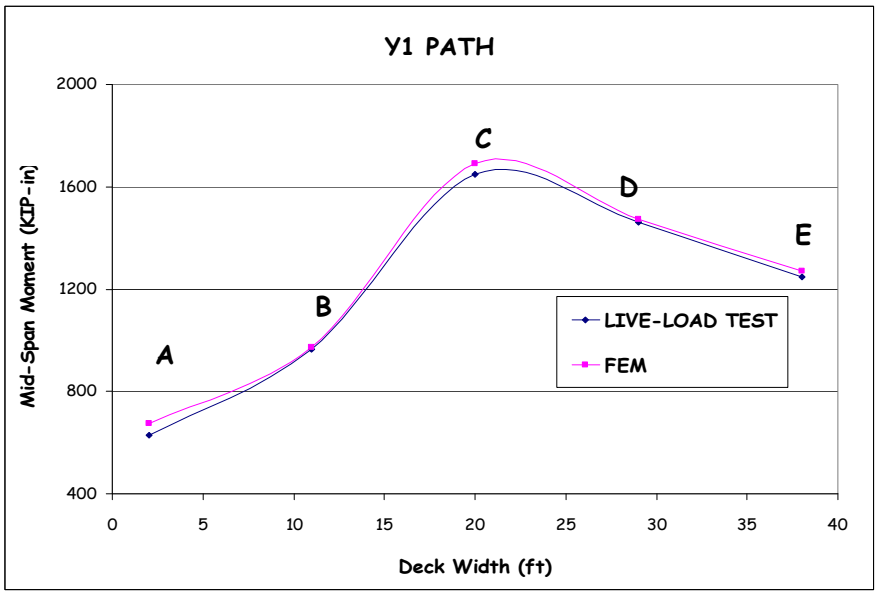

Fig 4.61 Transverse comparison between FEM and live-load test (Y1 Load Path).

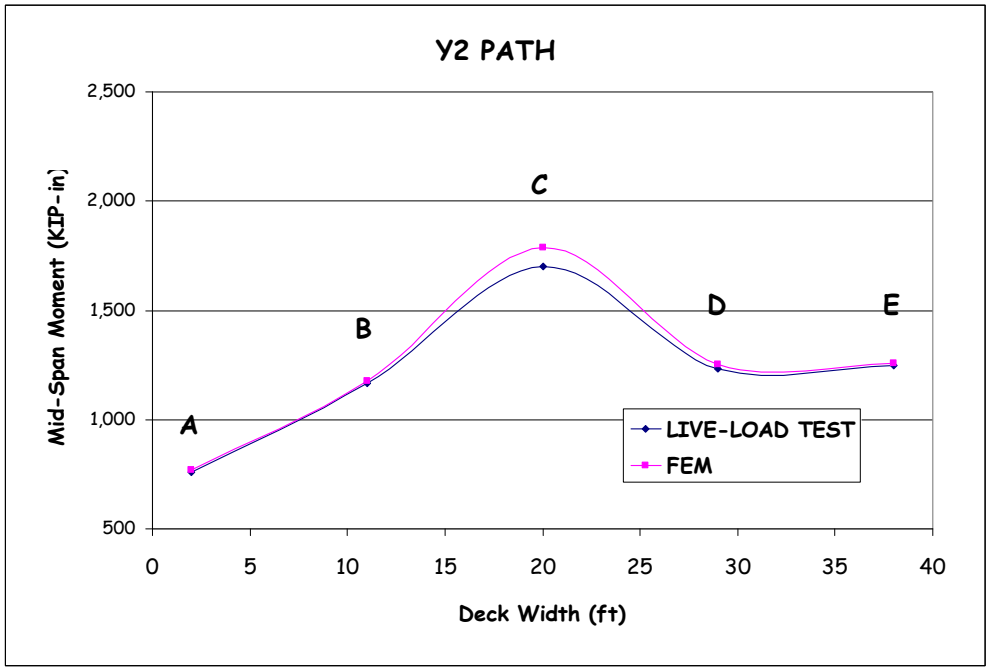

Fig 4.62 Transverse comparison between FEM and live-load test (Y2 Load Path).

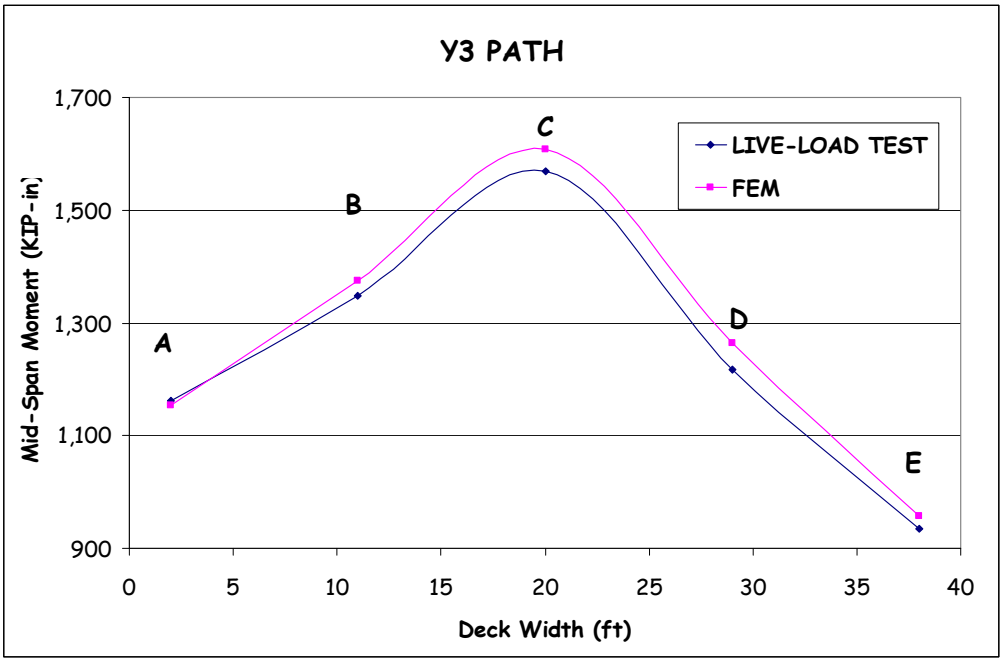

Fig 4.63 Transverse comparison between FEM and live-load test (Y3 Load Path).

4.6 Live-Load Distribution Factor

The live-load distribution factors will be calculated using the AASHTO LRFD Standard Specifications of 2006. The equations contained in these specifications will be used to obtain a theoretical value of the live load distribution factors. These values will later be compared with those obtained from the finite-element analysis. The equation that will be used for this analysis will be explained in Section 4.6.1. The procedure for the estimation of the live-load distribution factors using a FE approach will be discussed in Section 4.6.2.

4.6.1 AASHTO LRFD Specifications (2006)

A brief description of this specification was presented in Chapter 3. According to Table 4.6.2.2.1-1 from this specification, a cast-in-place concrete multicell box girder bridge is classified as a type "d" structure. The load distribution factors equations for this type of structure were derived using an I section of the box, composed by the web, the overhang for the exterior web, and half of the flanges between adjacent webs. According to Table 4.6.2.2.2b-1 from the same specifications, the moment distribution factor for an interior I section of an non-skewed bridge is calculated using Equations 4.1 and 4.2, which are shown below:

-For one design lane loaded:

$$DFM_I^{ns} = \left(1.75 + \frac{S}{3.6}\right)\left(\frac{1}{L}\right)^{0.35}\left(\frac{1}{N_c}\right)^{0.45} \qquad (4.1)$$

-For two or more design lanes loaded:

$$DFM_I^{ns} = \left(\frac{13}{N_c}\right)^{0.3}\left(\frac{S}{5.8}\right)\left(\frac{1}{L}\right)^{0.25} \quad (4.2)$$

Where:

DFM_I^{ns} = Interior Girder Distribution Factor for Moment of non-skewed bridges

S = Girder Spacing (ft)

L = Span Length (ft)

N_c = Number of cells in an concrete box girder

These equations are only valid if the requirements presented in Table 4.2 are met. Moreover, as in the equations presented in Chapter 3, these equations inherently include a multiple presence factor, which was presented in Table 3.4 from Chapter 3.

Table 4.2 Requirements for Equation 4.1 and 4.2

Spacing	7 <= S <= 13
Length	60 <= L <= 240
NO. of Beams	Nc>= 3

The distribution factor for an exterior girder can be calculated using Equation 4.3, presented below:

$$DFM_E^{ns} = \frac{W_e}{14} \quad (4.3)$$

where:

DFM_E^{ns} = Exterior Girder Distribution Factor for Moment of non-skewed Bridges

W_e = half the web spacing, plus the total overhang (ft); $W_e \leq S$

The AASHTO LRFD Specifications also provides a modification factor to account for the effect of skew in the calculation of the distribution factors. This modification factor is represented by Equation 4.4, which is shown below.

$$DFM_I^{skew} = (sk) \times DFM_I^{ns} \quad (4.4)$$

where:

DFM_I^{skew} = Interior girder distribution factor for moment of skewed bridges

sk = skew correction factor for moment

$$sk = 1.05 - 0.25(\tan\theta) \leq 1.0 \quad (4.5)$$

θ = skew angle where $0^0 \leq \theta \leq 60^0$

If $\theta > 60^0$ use $\theta = 60^0$

4.6.2 Finite Element Analysis (FEA) distribution factors

The process that will be used to determine the FE distribution factors will be the same that the one previously described in Section 3.6 from Chapter 3. As it was explained before, each girder was combined into groups, which in this case included the effective width for both, upper and bottom flanges, for interior girders and the overhang plus the half width of the spacing between webs, for exterior girders. These "groups" were located at the mid-span of the bridge, since these locations produced the maximum moment on the entire structure. For the negative moment, these groups were located near the supports, where the maximum negative moment was recorded.

The truck was moved longitudinally, and once the critical longitudinal location was obtained, it was moved transversally across the loaded lanes, following the same process explained in Chapter 3. Up to three design loaded lanes were taken into consideration for the analysis. The maximum moments were obtained for every case. Since there were two types of exterior girders, at each side of the bridge, with different flange width, the maximum recorded moment between the two was selected for the load distribution factor calculations, and the equation associated with this girder was used for comparison purpose.

Once the maximum moments were selected, the FE distributions factors were obtained using Equation 3.10 from Chapter 3. For this case, the maximum moment of a single beam was obtained by placing a single design truck at a critical location and modeling the girder as a 1-D beam.

Accoding to the AASHTO LRFD Specifications (2006), the load distribution factor equations were developed without taking into consideration any possible intermediate diaphragm in the superstructure. Since this structure presents interior diaphragms at the mid-span, the live load distribution factors for this bridge may differ from the code estimations. In order to verify this behavior, two models were investigated, one including the intermediate diaphragms (actual condition), and the second one without it. These results will be presented in Section 4.7.2.

4.7 Comparison of Distribution Factors

This section will present a comparison between the calculated distribution factors for a cast-in-place concrete multicell box girder bridge, using the AASHTO LRFD Specifications (2006), and the finite-element analysis. Section 4.7.1 will present the calculations of these distribution factors using the AASHTO LRFD Specifications (2006) equations. Section 4.7.2 will show the live-load distribution factors obtained through the FEA of the different loading cases. Finally, Section 4.7.3 will present a comparison between the results obtained in Sections 4.7.1 and 4.7.2.

4.7.1 AASHTO LRFD Specifications (2006) distribution factors

The live-load distribution factors was calculated for both, interior and exterior girders. Table 4.3 presents a brief description of the bridge properties.

Table 4.3 Bridge Girder Properties

S=	9 feet	**We 1=**	9 feet
L=	145 feet 11 in	**We 2=**	6 feet 6in
Nc=	4	**Skew Angle =**	28^0 40' 50"

*For one design lane:

$$DFM_I^{ns} = \left(1.75 + \frac{9}{3.6}\right)\left(\frac{1}{145.916}\right)^{0.35}\left(\frac{1}{4}\right)^{0.45} = 0.398$$

$$sk = 1.05 - 0.25(\tan 28.68) = \underline{0.91324}$$

$DFM_I^{skew} = 0.91324 \times DFM_I^{ns} =$ **<u>0.3636</u>**, for interior girders

*For two or more design lane:

$$DFM_I^{ns} = \left(\frac{13}{4}\right)^{0.3}\left(\frac{9}{5.8}\right)\left(\frac{1}{145.9166}\right)^{0.25} = \underline{0.636}$$

$DFM_I^{skew} = 0.91324 \times DFM_I^{ns} = \underline{\mathbf{0.5807}}$, for interior girders

For the exterior girders, the same load distribution factor is used for the one and two design lanes cases:

$DFM_E^{ns} = \frac{9}{14} = \underline{\mathbf{0.643}}$, for inside ext. girders

$DFM_E^{ns} = \frac{6.5}{14} = \underline{\mathbf{0.4643}}$, for outside ext. girders

$DFM_E^{skew} = 0.91324 \times DFM_E^{ns} = \underline{\mathbf{0.587}}$, for inside ext. girders

$DFM_E^{skew} = 0.91324 \times DFM_E^{ns} = \underline{\mathbf{0.424}}$, for outside ext. girders

4.7.2 Calculation of FEA distribution factors

As it was explained before, the calculations of the finite-element distribution factors require the analysis of a single beam submitted to a single design truck at a specific location. This location would yield the maximum moment that the single beam would experience due to this loading condition. Since this superstructure presents a nearly-fixed condition at the ends, negative moments may be obtained by the application of live loads into the model. Therefore, the single beam was analyzed simulating the end conditions of the bridge, and the maximum positive and negative moments, experienced by the 1-D beam, were obtained in this process. According to this analysis, the maximum positive moment was recorded as 14,535.26 kips-in, while the maximum negative moment was recorded as 13,300.308 kips-in.

Another analysis was performed for the simply-supported case of the bridge. It was found that Caltrans had designed this superstructure as if it were simply-supported, without considering the fixed-end conditions. With this analysis, the accuracy of the design of this structure will be investigated. The single beam was also analyzed for this conditions and the maximum moment was recorded as 28,197 kips-in.

After the maximum response of the single beam was obtained, the next step was to determine the maximum moments experienced by every group of girders, using the finite-element model analysis. All the interior girders were analyzed for positive and negative moments, and the maximum values were selected for the load distribution factors calculations. A similar approach was used for both exterior girders. At the same time, the maximum moments obtained through the analysis of the structure without including the diaphragms, were also recorded. These values were used to calculate the load distribution factors of this condition. Tables 4.4 through 4.7 present all the maximum moment obtained through the finite-element analysis.

Table 4.4 Maximum Response Influenced by Diaphragms (Fixed Case)

	MODEL WITH DIAPHRAGM			
	Exterior Girder Moment (kip-in)		**Interior Girder Moment (kip-in)**	
	Positive	Negative	Positive	Negative
Single Loading	3,060.51	3,534.07	3,612.42	3,551.86
Two Lanes Loaded	5,701.73	5,153.00	7,081.08	6,530.28
Three Lanes Loaded	7,449.89	5,954.95	9,527.84	8,278.88

Table 4.5 Maximum Response Obtained without the Diaphragms (Fixed Case)

	MODEL W/O DIAPHRAGM			
	Exterior Girder Moment (kip-in)		Interior Girder Moment (kip-in)	
	Positive	Negative	Positive	Negative
Single Loading	3,935.51	3,564.36	4,397.89	3,743.04
Two Lanes Loaded	6,193.18	5,171.34	8,060.44	6,567.01
Three Lanes Loaded	7,516.51	5,963.38	9,886.57	8,320.70

Table 4.6 Maximum Response Influenced by Diaphragms (Simply-Supported Case)

	MODEL WITH DIAPHRAGM	
	Exterior Girder Moment (kip-in)	Interior Girder Moment (kip-in)
	Positive	Positive
Single Loading	5,124.10	6,507.23
Two Lanes Loaded	9,664.78	12,192.52
Three Lanes Loaded	13,330.01	17,264.32

Table 4.7 Maximum Response Obtained without Diaphragms (Simply-Supported Case)

	MODEL W/o DIAPHRAGM	
	Exterior Girder Moment (kip-in)	Interior Girder Moment (kip-in)
	Positive	Positive
Single Loading	6,068.51	7,759.66
Two Lanes Loaded	10,289.41	13,071.19
Three Lanes Loaded	13,426.98	17,767.76

As can be appreciated in these four tables, there is a perceptible difference between the moments obtained by modeling the actual conditions of the bridge and the moments obtained by modeling the bridge without the diaphragms. This difference is expectable since these structural elements are so rigid that they improve the lateral moment

distribution across the width of the structure, reducing the concentration of moment on any critical location.

The effect of the structural diaphragms was only observed for the moments obtained at the mid-span of the structure, location where the structural diaphragms were placed. For instance, the negative moments did not experience any significant change from one model to the other. On the other hand, the positive moments did experience some changes, especially for the single loading and two lane loaded cases.

The presence of the diaphragms in the structure did not have a major effect in the three lane loading case, which produced the maximum moments among the three. While in one model, the wheel loads, located away from the studied girder, did not have that much influence on the girder, on the other model they did thanks to the lateral distribution property of the diaphragms. This condition produced a "trade off" between the influence of the closest wheel loads to the girder and the effect of furthest one. This resulted in the studied girder experiencing the same amount of moment for both cases, with and without the diaphragms.

As a result of these observations, it can be concluded that the diaphragm do affect the maximum moment's magnitude on the structure, but only for bridges with one or two loaded lanes. The possible presence of a third loaded lane would make the effect of the diaphragm not to be taken into the analysis, provided that this case yields the maximum moment among the other cases. This is because the structure will always be designed for the biggest moment obtained from the three loading cases.

4.7.3 Comparison between FEA results and code's distribution factors

The results obtained in Section 4.7.1, through the equations of the AASHTO Standard Specifications are directly compared with the load distributions factors obtained from the finite-element analysis. This comparison would determine the accuracy of the code based equations. Tables 4.8 through 4.11 present this comparison.

Table 4.8 Moment Distribution Factors with the Diaphragms (Fixed Case)

With Diaphragms					
Girder Type	**Case**	**Moment**	**FEM**	**AASHTO LRFD**	**% Error respect to FEM**
Interior	One lane	Positive	0.298	0.364	21.92%
Interior	Two or more lanes	Positive	0.557	0.58	4.10%
Interior	One lane	Negative	0.320	0.364	13.46%
Interior	Two or more lanes	Negative	0.529	0.58	9.62%
Exterior	One lane	Positive	0.253	0.587	132.32%
Exterior	Two or more lanes	Positive	0.436	0.587	34.74%
Exterior	One lane	Negative	0.321	0.587	82.70%
Exterior	Two or more lanes	Negative	0.383	0.424	10.57%

Table 4.9 Moment Distribution Factors without the Diaphragms (Fixed Case)

W/o Diaphragms					
Girder Type	**Case**	**Moment**	**FEM**	**AASHTO LRFD**	**% Error respect to FEM**
Interior	One lane	Positive	0.363	0.364	0.14%
Interior	Two or more lanes	Positive	0.578	0.58	0.32%
Interior	One lane	Negative	0.338	0.364	7.67%
Interior	Two or more lanes	Negative	0.532	0.58	9.07%
Exterior	One lane	Positive	0.358	0.587	64.06%
Exterior	Two or more lanes	Positive	0.484	0.587	21.27%
Exterior	One lane	Negative	0.324	0.587	81.15%
Exterior	Two or more lanes	Negative	0.384	0.424	10.41%

Table 4.10 Moment Distribution Factors with Diaphragms (Simply-Supported Case)

With Diaphragms					
Girder Type	**Case**	**Moment**	**FEM**	**AASHTO LRFD**	**% Error respect to FEM**
Interior	One lane	Positive	0.277	0.364	31.30%
Interior	Two or more lanes	Positive	0.520	0.58	11.45%
Exterior	One lane	Positive	0.218	0.587	169.18%
Exterior	Two or more lanes	Positive	0.402	0.587	46.08%

Table 4.11 Moment Distribution Factors without Diaphragms (Simply-Supported Case)

W/o Diaphragms					
Girder Type	**Case**	**Moment**	**FEM**	**AASHTO LRFD**	**% Error respect to FEM**
Interior	One lane	Positive	0.330	0.364	10.10%
Interior	Two or more lanes	Positive	0.536	0.58	8.29%
Exterior	One lane	Positive	0.258	0.587	127.29%
Exterior	Two or more lanes	Positive	0.405	0.587	45.03%

As can be observed from the previous tables, the moment distribution factor from the model without the diaphragm presented closer results to the code estimations (within 10% for interior girders) when compared with the real model of the Walnut Grove Bridge. These results are expectable since it was established before that the code equations were developed for structures without any intermediate diaphragm between spans.

It can also be appreciated that, for both cases, the exterior girder's behavior was not accurately predicted by the code. The only case that presented acceptable results was the two or more loaded lane case for negative moment (fixed case), where the maximum moment was located at the outside exterior girder, which presented the smallest flange of the two exterior girders. Apparently the code does not yield good results when the

exterior girder presents a flange width close to webs' spacing, as it was the case for the inside exterior girder.

On the other hand, the behavior of the interior girders was acceptably predicted by the code's equations, especially in the second model of the fixed case model (within 0.5%). The negative moments estimation was less accurate compared to the positives moment (within 10% for the second model), but still presented very close values.

In the simply-supported case, the code estimated with good accuracy the behavior of the interior girders (within 10% for the second model). As in the fixed case, the exterior girders response wasn't accurately calculated by the code equations, which demonstrate the deficiency of these equations to estimate the maximum response of the exterior members from a multicell concrete box girder bridge. According to the load distributions factors observed in Table 4.10, it can be concluded that the Walnut Grove Road Bridge was overdesigned by almost 12% for the simply-supported analysis. It is appropriate to mention that this overdesign goes beyond the 12% of the actual loads, since the real condition of the bridge, fixed at both ends, will decrease the maximum response of the structure to half the value obtained through the simply-supported analysis.

Overall, the code over predicted the maximum moment in every case, which would be applied to the sections of the bridge for its design. This over prediction is considered to be minimal, since the largest moment obtained for the design belonged to the interior girder, and this was accurately estimated by the code.

CHAPTER 5

SUMMARY AND CONCLUSION

This chapter presents a summary of the research performed on the 8th North Bridge and the Walnut Grove Road Bridge, and the conclusions that were obtained based on the findings that were obtained in Chapters 3 and 4. The summary of the investigation is disclosed in Section 5.1 of this Chapter. Section 5.2 discusses the results obtained from the analysis of the two structures and presents the conclusions that were formulated based on the analysis.

5.1 Summary

A live-load test was performed on the 8th North Bridge with the purpose of measuring the structural behavior of the bridge. Loads were applied by driving a truck along six predetermined load paths. The response of the bridge was measured in 63 different locations of on the structure. The recorded data from this test was used to calibrate a finite-element model. This model was intended to replicate the structural behavior of the 8th North Bridge. The model was developed using solid elements to represent the barrier, shell elements to represent the pre-cast concrete deck and frame elements to represent the steel girders. The steel girders were modeled using the same eccentricity from the concrete deck that existed on the bridge. This was done to increase the accuracy of the model. The composite action of the steel girders and concrete deck was modeled using body constraints to connect these two elements. A second model was included into the analysis, which presented a sidewalk on both side of the bridge. After the FE model was proved to accurately replicate the behavior of the studied bridge, theoretical values for the

live-load distribution factors were obtained for both models. These values were later compared with the AASHTO Standard Specifications (1996) and the AASHTO LRFD Specifications (2006) estimations in order to determine their accuracy in predicting an accurate live load distribution factor.

A second analysis was performed on the Walnut Grove Road Overcrossing. A live-load test was also performed on this structure. This test was done with the purpose of obtaining field measurements of the structural response of the bridge. Another goal of this test was to compare the results with those obtained in a similar test performed by the University of Colorado in 1990, and observe if there were any changes in the behavior of the bridge. According to the test results, the bridge showed a very good lateral load distribution, typical in a concrete box girder bridge. The recorded data was also used to calibrate a three-dimensional finite-element model of the structure. In this model all structural element were modeled using shell elements. The boundary conditions were obtained by modeling the supports using solid elements. The effect that the support would have on the structure was represented by horizontal and vertical springs that were directly applied to the model. After the calibration of the model, the finite-element distribution factors were obtained from this model. A second model was also studied, which didn't include the intermediate diaphragm presented in the actual structure. The FE distribution factors were compared with the AASHTOO LRFD Specifications (2006) equations. The effect of the intermediate diaphragms was also investigated.

5.2 Research Findings and Conclusions

The live-load test performed on the 8th North Bridge served to outline two important characteristics of this bridge, which are outlined as follows:

- Composite behavior between the concrete deck and steel girders. According to the live-load data obtained from the live-load test, the 8th North Bridge behave as a composite structure since there strain measured at the top and bottom of every girder at Section EE did not differ in signs, as would occur if the steel girders would acting non-composite with the concrete deck. Also, the theoretical neutral axis values was calculated and compared with test results neutral axis. These two values were found to be very close.
- Discontinuity of the Structure. At the beginning of this study, this superstructure was believed to be continuous over the supports. However, the data from the live-load test proved the opposite, reveling that there was not a complete continuity of the bridge at this points. Any point close to the support should reflect large negative moment compared to the positive moment. However, as could be observed in the results of the live-load test, this characteristic was not found in any of the data collected from the strain gages near the supports.

Through the finite-element model of the 8th North Bridge it was determined that the combination of frame and shell elements, to represent steel girders and concrete deck, was the most accurate among the other options. This was proven to be true since this model replicated the actual behavior of the structure within 1% of the measured values from the live-load test. It is also proven that the eccentricity has a major effect when modeling two separate components. This characteristic has to be carefully considered

when creating a finite-element model, since the results may vary if this condition is not modeled. The use of body constraint proved to be very efficient when simulating the composite behavior of the bridge. This amazing tool was the key of success for this model.

After the finite-element analysis of the two proposed cases for this bridge was performed, it was found that the presence of the side walks reduced the maximum moments experienced by the girders of the first model. Due to this fact it was concluded that this structural element has a major effect on the magnitudes of the distribution factors values.

After comparing the theoretical values obtained from both models with the code based equations results, it was determined that the AASHTO LRFD Specifications (2006) more accurately predicted the live-load distribution factors in comparison to the AASHTO Standard Specifications (1996). This result was expected since the 8th North Bridge differs in many aspects from not the typical bridge that was used to develop the equations in the AASHTO Standard Specifications (1996).

It was also found that the AASHTO LRFD Specifications (2006) predicted with more accuracy the behavior of the bridge in the first model (within 10%), than in the second model (within 40%). Apparently, the code equations were not designed based on bridges that included sidewalks as part of their structure. Although the code equations over predicted the behavior of the bridge including the sidewalk, these would result in the design of a very expensive structure. This is why it is recommended that this type of structure be taken into account for the creation of new distribution factor equations. In the

meanwhile, a finite-element analysis is strongly recommended if this type of structure is to be designed.

Moreover, the live-load test performed in the Walnut Grove Road Bridge yielded some interest results regarding the structural behavior of this structure. These observations are presented as follow:

- Lateral Load Distribution. It was found that this structure had an excellent performance in the lateral load distribution across its width. This is a very important characteristic of concrete box girder bridges. This quality allows the structure to diminish any moment concentration across the width of the structure.
- Additional Stiffness from mid-span diaphragms. It was shown, through the analysis of the recorded data from the live load test, that there was an improvement in the lateral distribution of the load at mid-span. This is due to the presence of very stiff diaphragms at the mid-span of the structure.
- End Restraint at the Abutments. It was found from the recorded data that there was a nearly-fixed condition at the support of the structure. This condition was determined because strains gages located near the support registered large amount of negative moments compared to the maximum positive moment recorded at this location. This was the most challenging issue in the modeling process of this structure.

In the finite-element model for the Walnut Grove Road Bridge, the use of shell elements to represent every structural component of the structure presented very accurate results. The model replicated the behavior of the structure to within 2% of the measured values. The key for this extraordinary result was the well implementation of the boundary

conditions of the bridge into the model. As it was explained in Chapter 4, the supports were modeled using solid elements. Vertical and horizontal spring elements were assigned into the model according to the rigidity of the support at every particular location. This accurate representation of the boundary conditions is believed to be the main reason of the success of this model.

Once the accuracy of the model was proved, finite-element distribution factors were calculated for the original model and the proposed model without the intermediate diaphragms. It was found that there was an appreciable difference in moment between these two approaches. The diaphragms reduced the maximum positive moment on the structure in about 18% for the single loading case, 13% for two loaded lanes and 4% for three loaded lanes. These results are expectable since the large rigidity of the diaphragms helps improve the lateral distribution of the moments across the width of the structure.

Finally, when the theoretical live-load distribution factors were compared with those calculated using the AASHTO LRFD Specifications (2006), it was found that these equations had a better performance in the proposed model without the intermediate diaphragms (within 10% for the exterior girder). This result is not surprising since the code states that the equations presented in its context were not developed for structures that included any intermediate diaphragms within spans. Overall, the code did not predict the response of the exterior girders with acceptable accuracy. It is recommended to perform more studies concerning the analysis the exterior web of this type of structures. As a conclusion it can be said that the AASHTO LRFD Specifications (2006) are acceptable provided that the maximum design moment is located in the interior girders and that the whole structure will be designed based on this moment.

REFERENCES

American Association of State Highway and Transportation Officials (AASHTO). (1996). *Standard Specifications for Highway Bridges*. 16th Edition, Washington, D.C.

American Association of State Highway and Transportation Officials (AASHTO). (2006). *AASHTO LRFD Bridge Design Specification*. 3rd Edition. Washington, D.C.

Barr, P.J., Yanadori, N., Halling, M.W., and Womack, K.C. (2007). "Live-load analysis of a curved I-girder bridge." *J. Bridge Engrg*., ASCE, 12(4), 477-484.

Chajes, M.J., Mertz D.R., and Comander, B. (1997). "Experimental load rating of a posted bridge." *J. Bridge Engrg.*, ASCE, 2(1), 1-10.

Chen, Y., and Aswad, A. (1996). "Stretching span capability of prestressed concrete bridges under AASHTO LRFD." J. Bridge Engrg., ASCE, Volume 1, Issue 3, pp. 112-120.

Dr. Beam (1996-1998). Ver. 1.2, Dr. Software.

Hughs, E., and Idriss, R. (2006). "Live-load distribution factors for prestressed concrete, spread box-girder bridge." *J. Bridge Engrg*., ASCE,11(5), 573-581.

Mabsout, M.E., Tarhini, K.M., Frederick, G.R. and Kesserwan, A. (1998). "Effect of continuity on wheel load distribution factor in steel girder bridges." *J. Bridge Engrg.,* ASCE,3(3), 103-110.

Newmark, N. M., Siess, C. P., and Peckham, R. R. (1948). "studies of slab and beam highway bridges. Part I: Test of simple-span right I-beam bridges." *Bulletin Series No. 375*, Engrg. Experiment Station, University of Illinois, Urbana, Ill.

Sennah, K., and Kennedy, J.B. (1999). "Load distribution factors for composite multicell box girder bridges." *J. Bridge Engrg*., ASCE, 4(1), 71-78.

SAP2000.(1997). "Integrated finite element analysis and design of structures." V.14. Computers and Structures Inc., Berkeley, Cal.

Westergaard, H.M. (1930). "Computation of Stress in bridge slabs due to wheel loads." *J. Bridge Engrg*., ASCE, 2(1), 1-10.

APPENDIX

A.1 8th Noth Bridge Live-Load Test Data

Figures A.1 through A.6 show some plots of the data recorded in the live-load test of the 8th North Bridge, for the Y6-double loading. We can observe from these figures, especially figures A.1, A.3, A4 and A.6, that there was not any continuity on the structures over the supports.

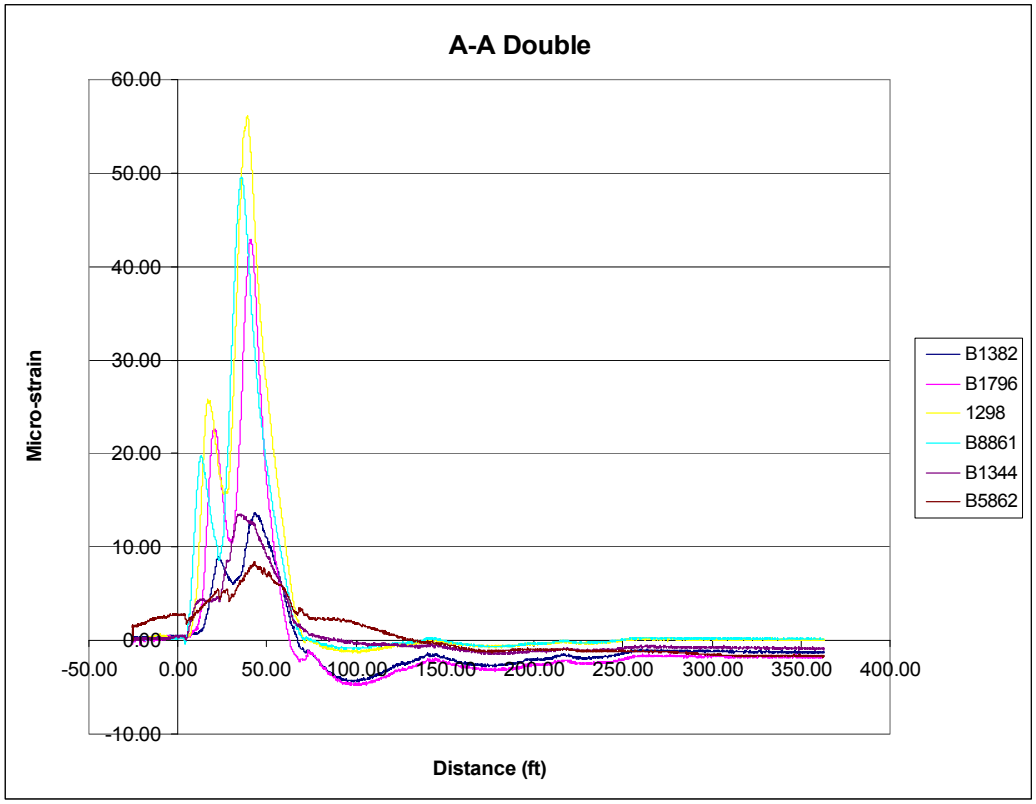

Fig A.1 Live-load test results for Section AA (Y5-Double).

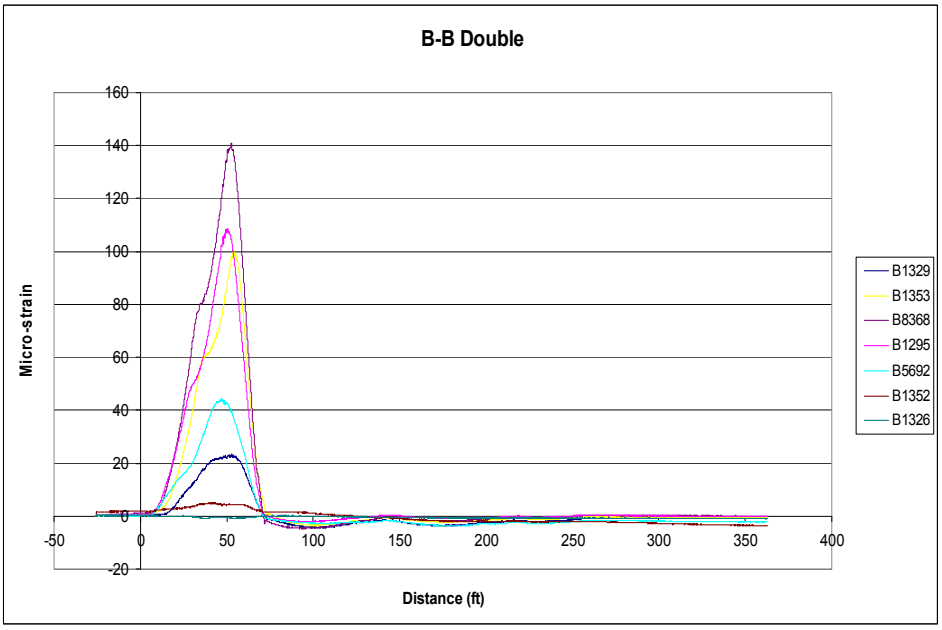

Fig A.2 Live-load test results for Section BB (Y5-Double).

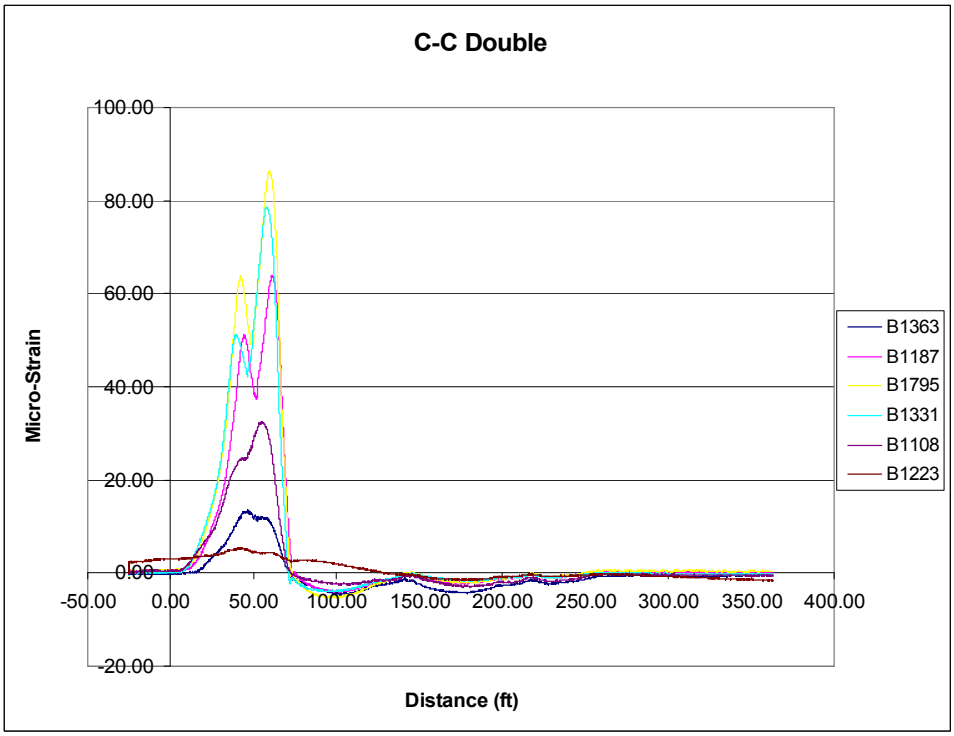

Fig A.3 Live-load test results for Section CC (Y5-Double).

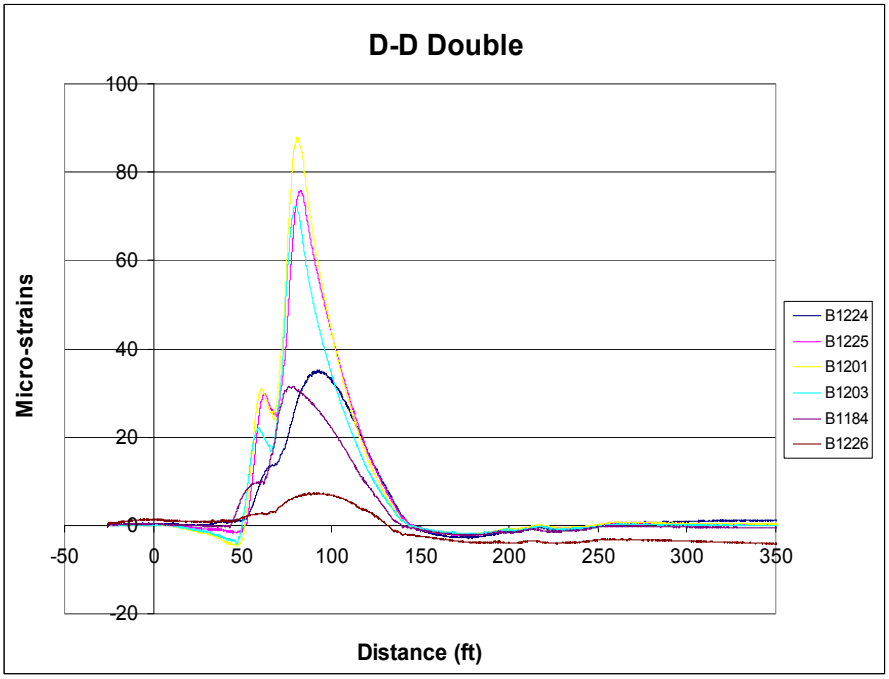

Fig A.4 Live-load test results for Section DD (Y5-Double).

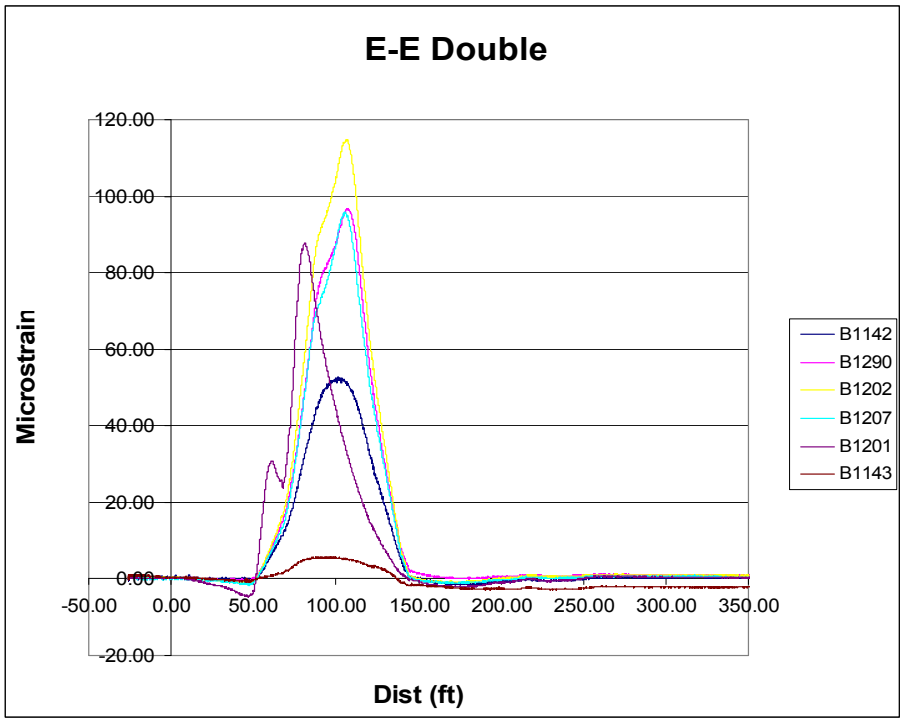

Fig A.5 Live-load test results for Section EE (Y5-Double).

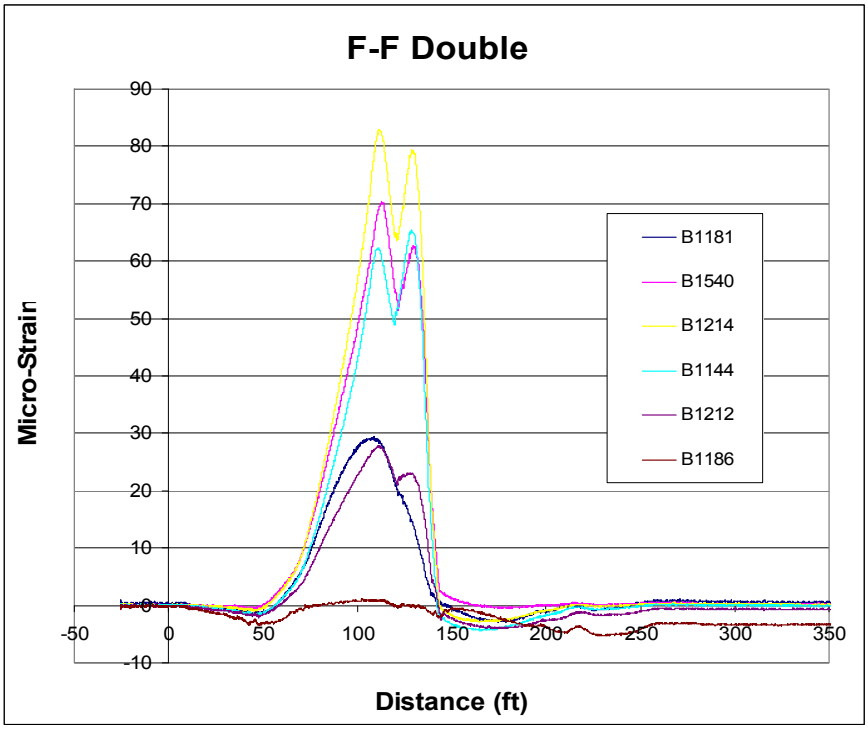

Fig A.6 Live-load test results for Section FF (Y5-Double).

The data recorded in live-load test was used to calculate an associate neutral axis in the exterior and interior girders of the bridge. This was done to prove the composite behavior of the steel girders. Strain gages located at section EE were used for the interior girders while strain gages at section BB were used for exterior girders. As previously described in Chapter 3, the calculated neutral axis was found to be 33.66 inches from the bottom of the girder, while the neutral axis of the girders alone was found to be 14.13 inches. These values were compared with the calculate values from the live-load test. Figure 3.26 and A.7 shows the variation of the neutral axis according to truck position in the live-load test. As can be observed the calculated values are closer to neutral axis of the composite section, represented by the red line. This demonstrates the composite behavior of the interior girders.

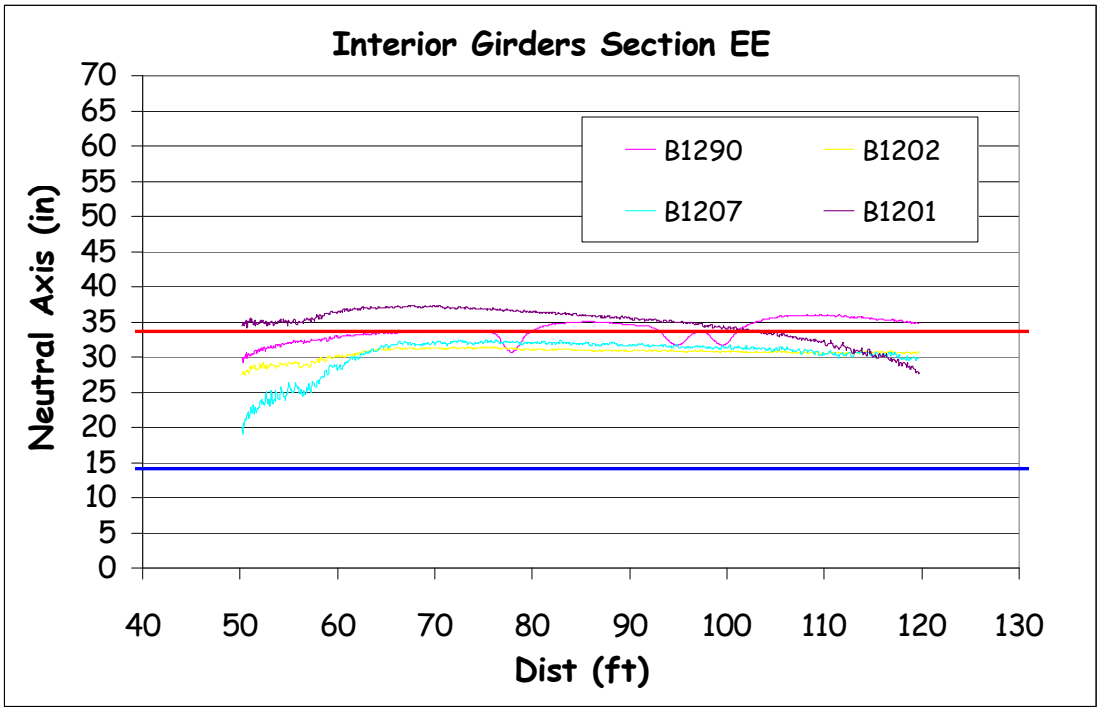

Fig A.7 Location of neutral axis for Section EE (Test Y5-Double).

A similar comparison was done for the exterior girders. The theoretical neutral axis for the exterior girders, considering the presence of the concrete barrier, was found to be 49.70 inches, measured from the bottom of the girder. The neutral axis of the steel girder for section BB was found to be 19.625 inches. The neutral axis was calculated at section BB using the data from loading path Y6 and Y5-double. Figures A.8 and A.9 show the variation of the neutral axis according to the truck position. As can be observed, the calculated values are very close to the theoretical value of 49.70 inches. This demonstrates, not only that the exterior girder acts compositely with the concrete deck, but also that the barriers are acting compositely with the pre-cast concreted deck.

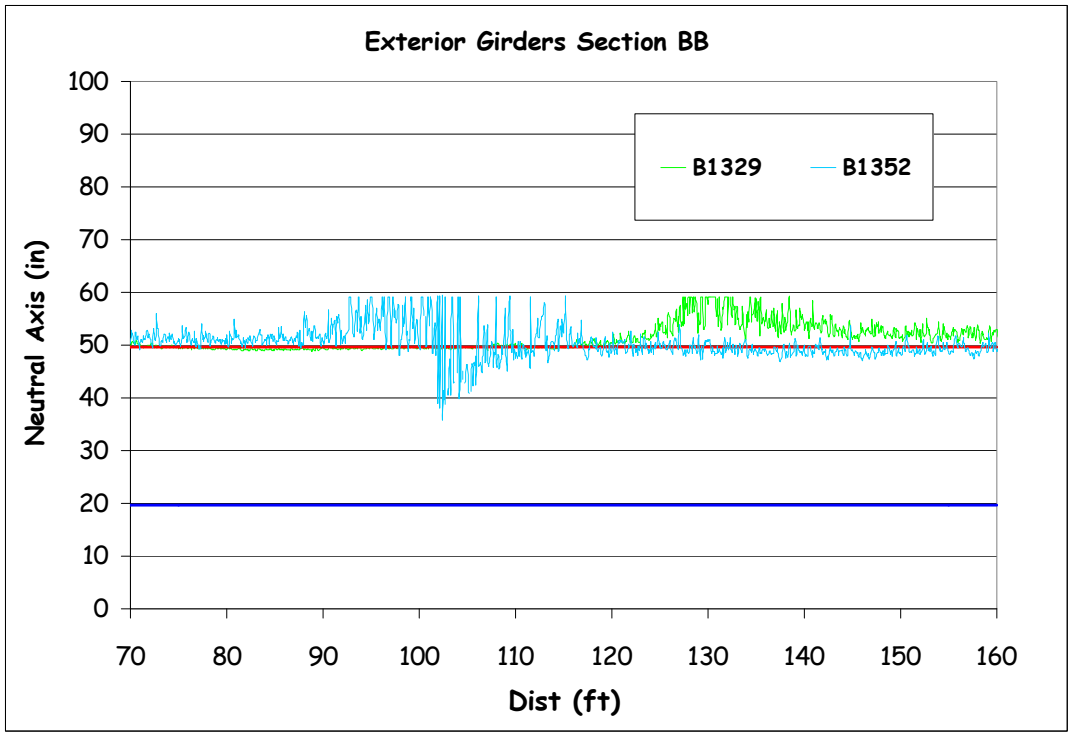

Fig A.8 Location of neutral axis for Section BB (Test Y6).

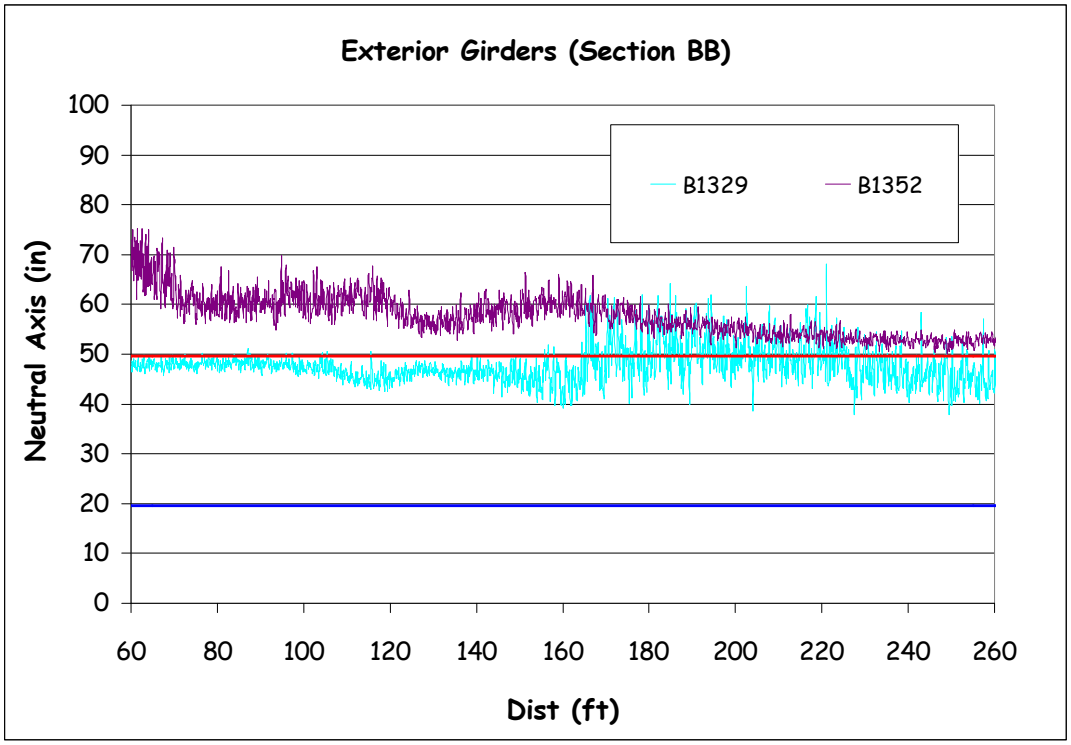

Fig A.9 Location of neutral axis for Section BB (Test Y5-Double).

A.2 Walnut Grove Road Bridge Live-Load Test Data.

The following figures present the results obtained from the live-load test performed on the Walnut Grove Bridge. Figures A.10 through A.12 presents a comparison between the new live-load test performed in 2008 and the old test performed in 1990. These comparisons are presented for section AA from both tests. As we can observed from these figures, the nearly-fixed condition, presented at the end of the structure, hasn't suffered any major change since 1990.

Moreover, Figures A.13 through A.17 present different plots of the data that was recorded on the live-load test at sections BB and EE for load paths Y1, Y2 and Y3.

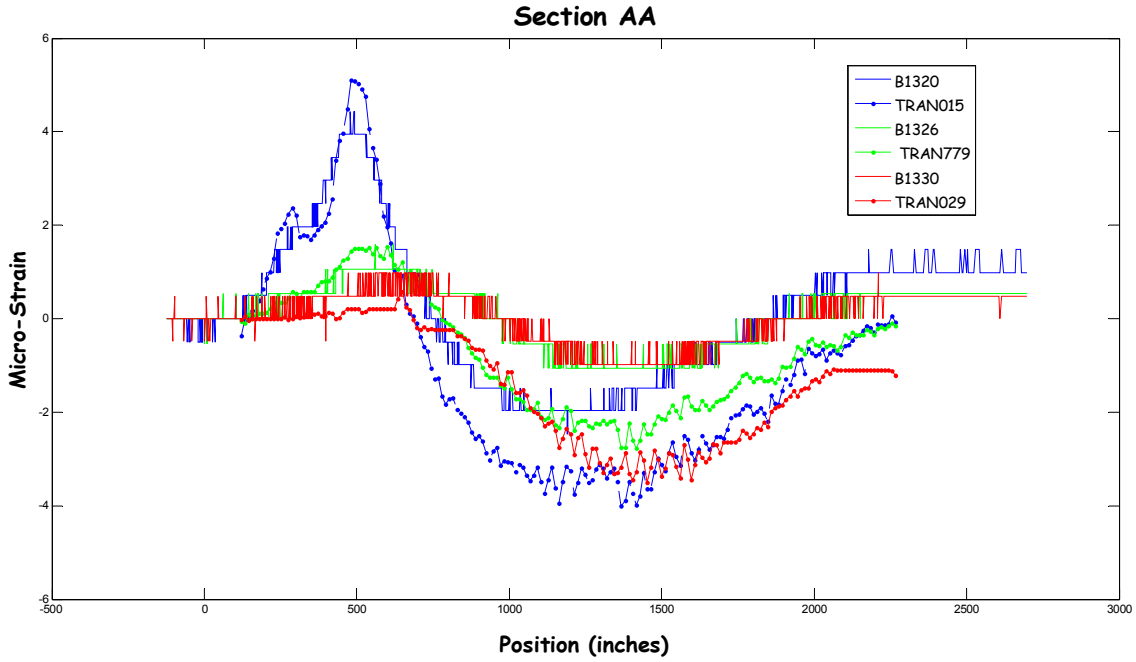

Fig A.10 Comparison of the old test with the new test for Path Y1.

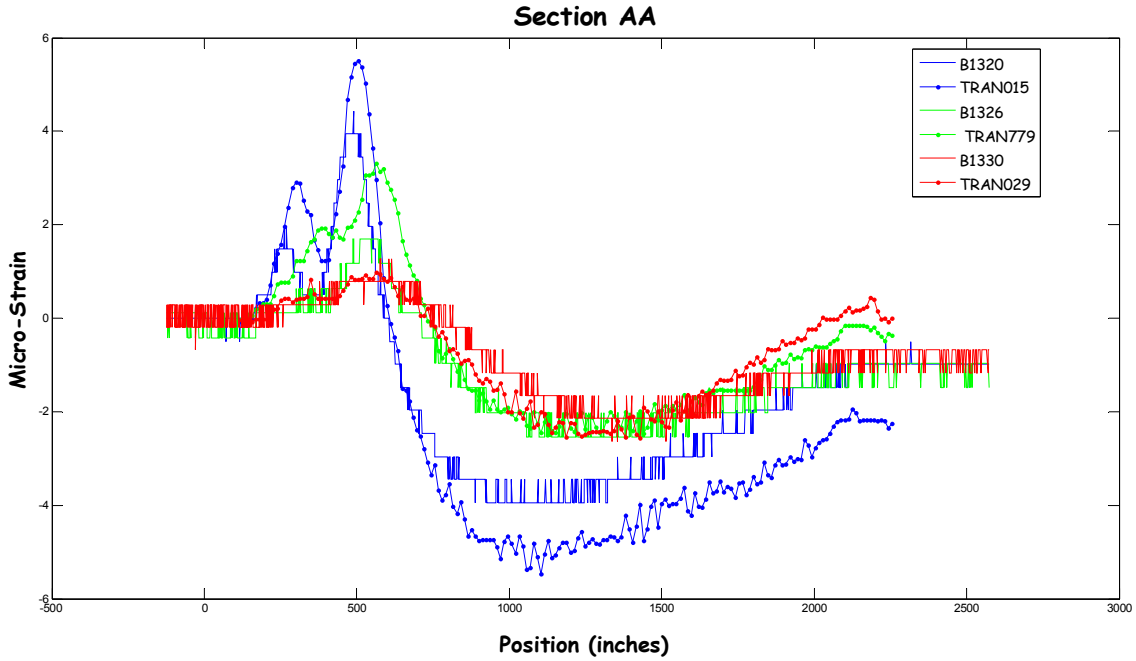

Fig A.11 Comparison of the old test with the new test for Path Y2.

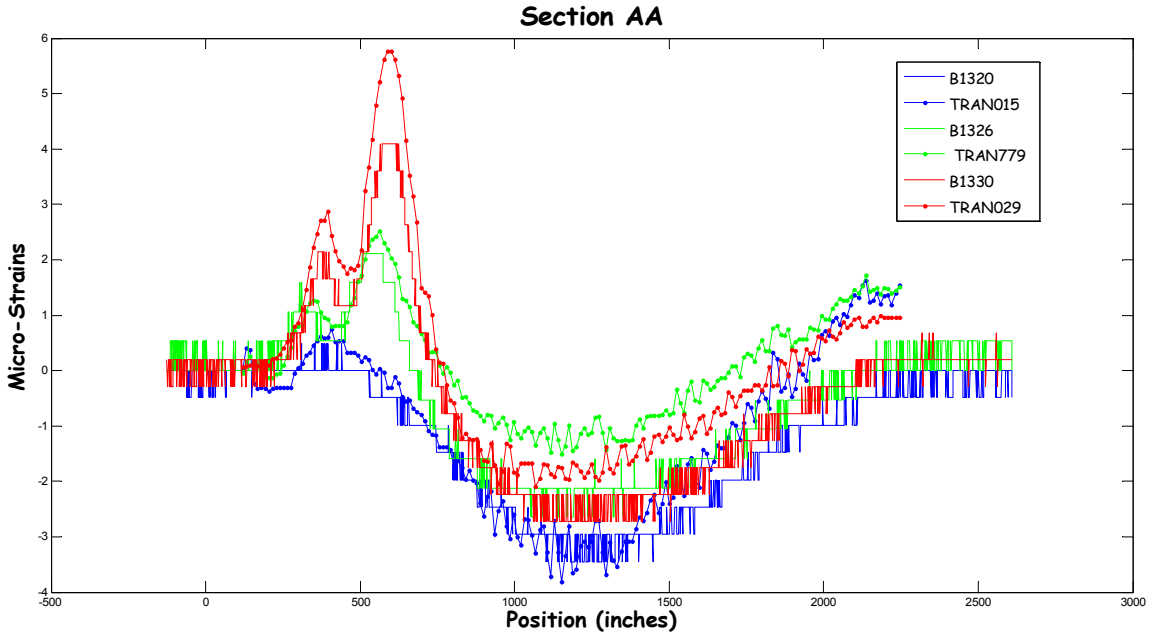

Fig A.12 Comparison of the old test with the new test for Path Y3.

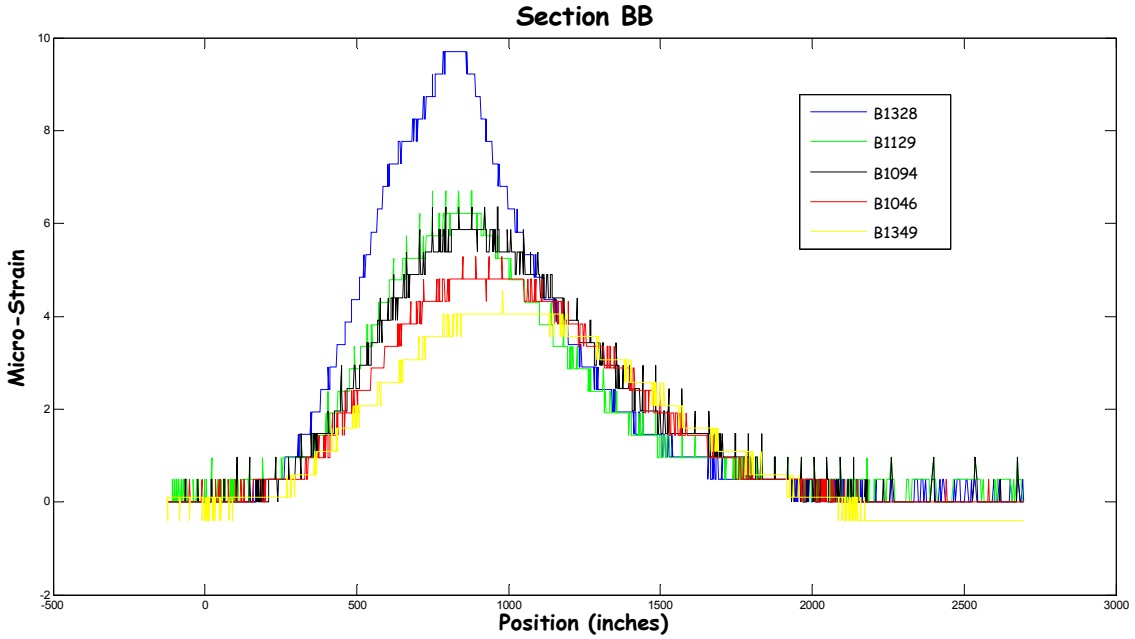

Fig A.13 Measured strain at Section BB for load path Y1.

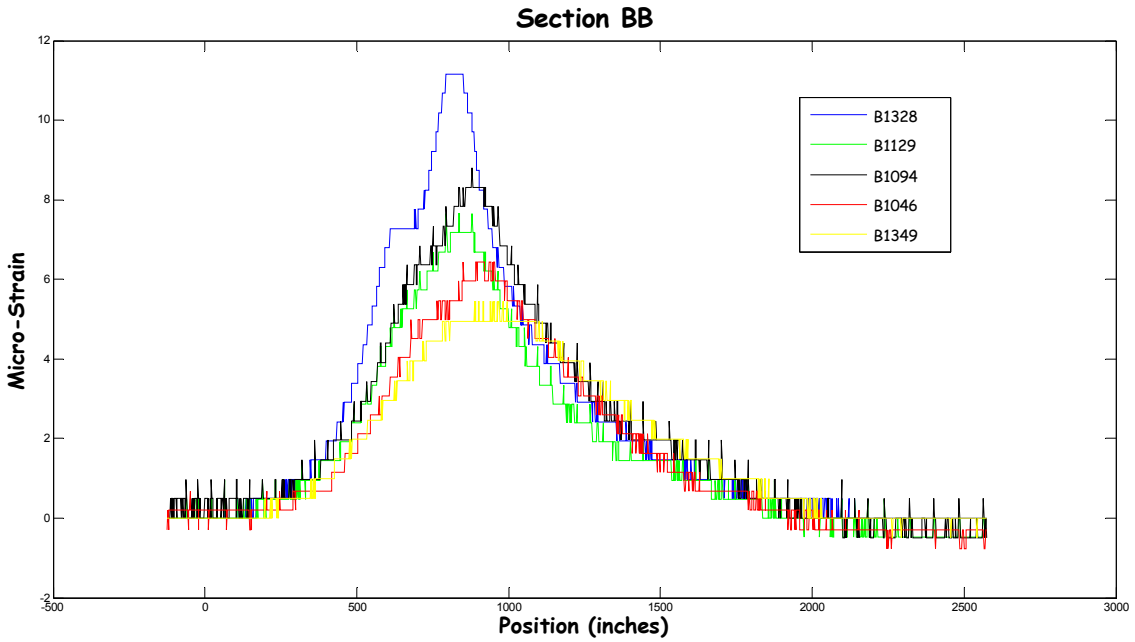

Fig A.14 Measured strain at Section BB for load path Y2.

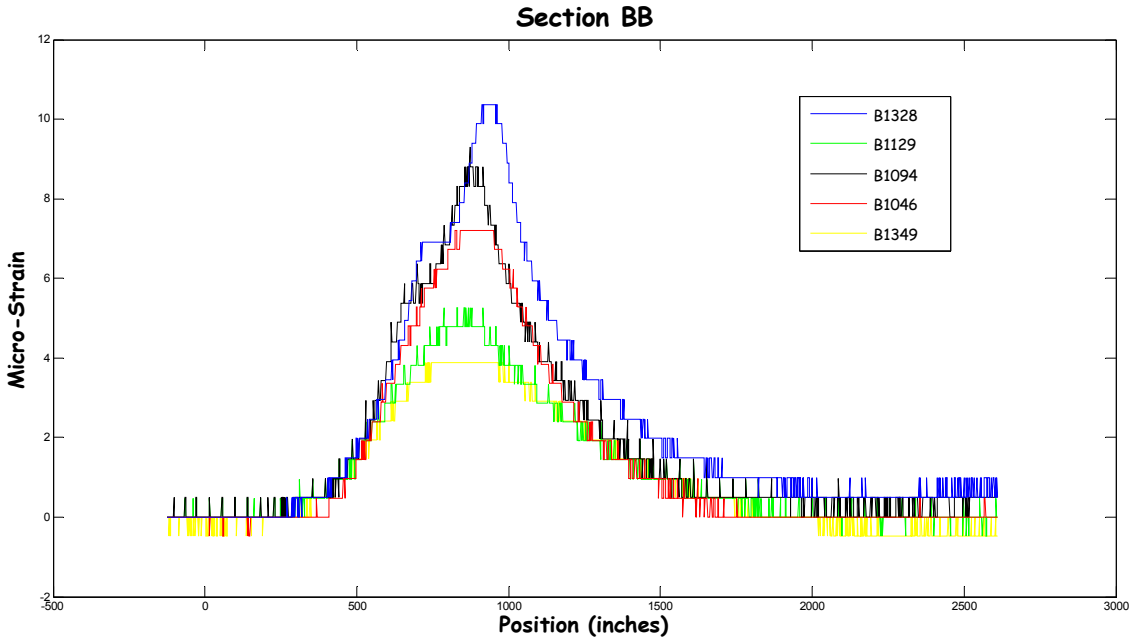

Fig A.15 Measured strain at Section BB for load path Y3.

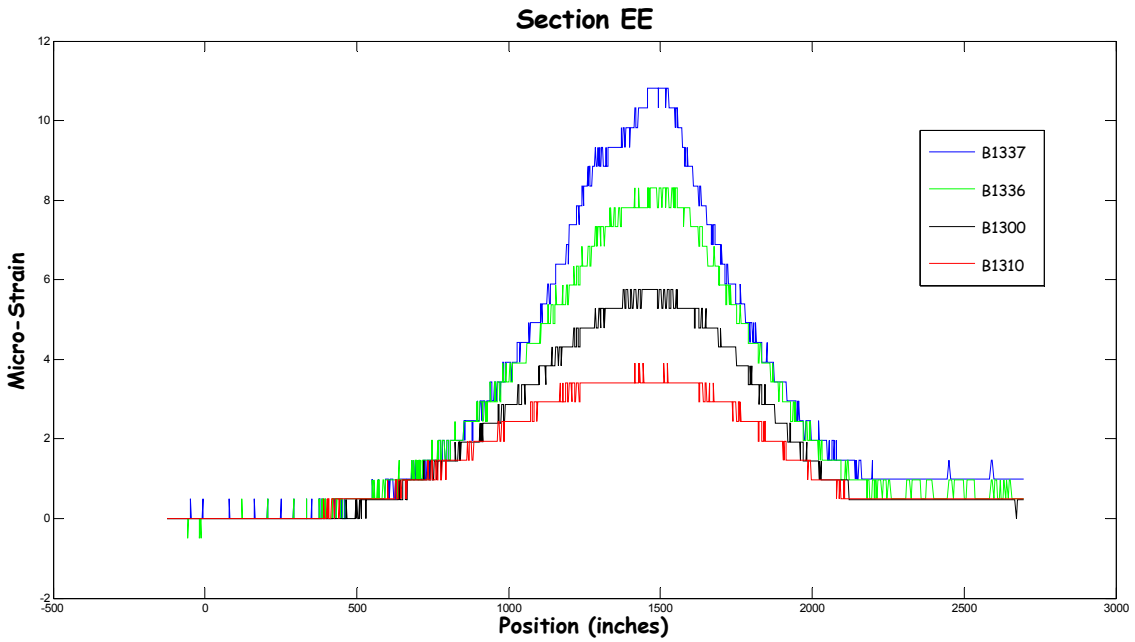

Fig A.16 Measured strain at Section EE for load path Y1.

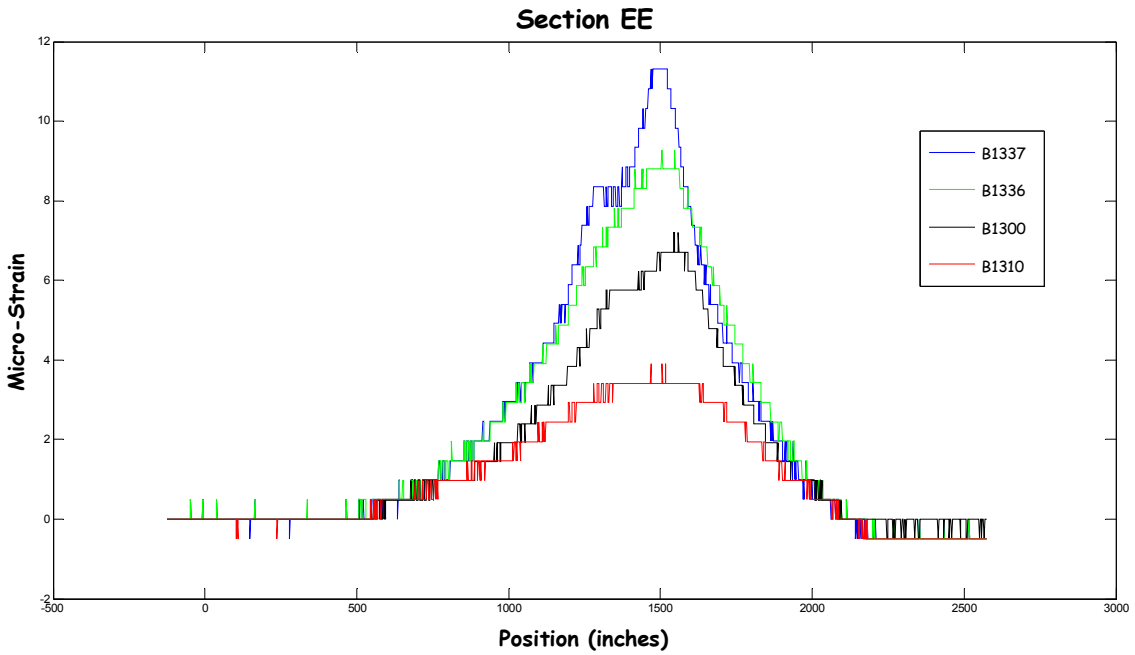

Fig A.17 Measured strain at Section EE for load path Y2.

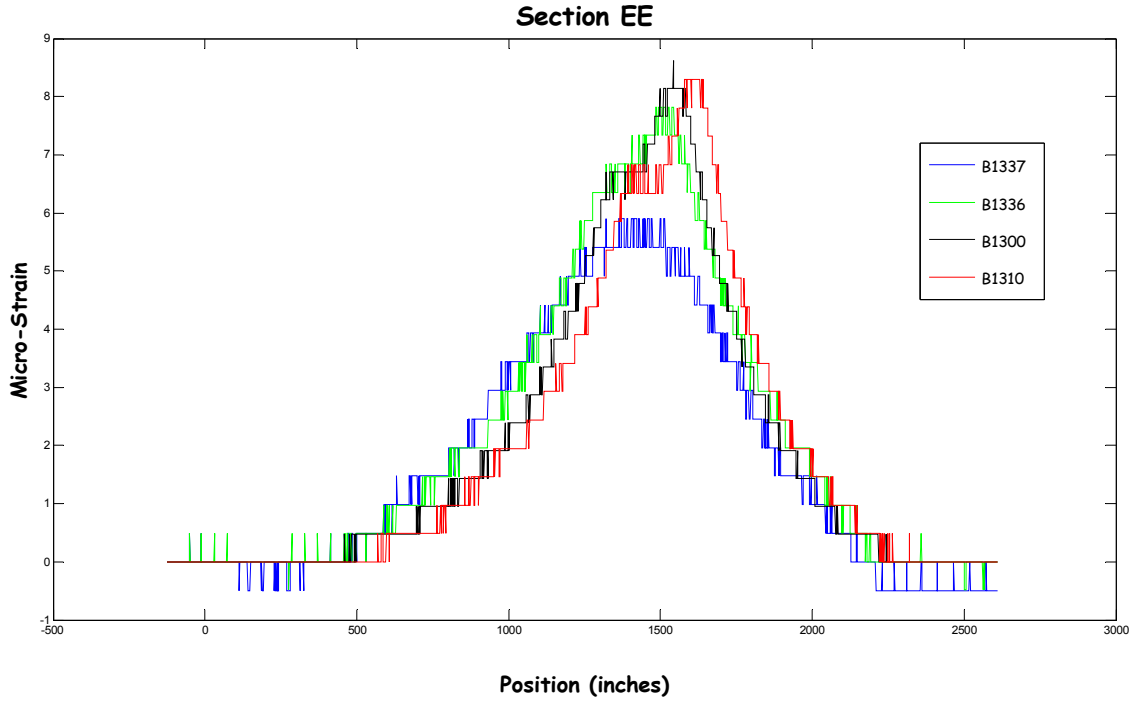

Fig A.18 Measured strain at Section EE for load path Y3.